COOPERATION

Equitable Testing and Evaluation of Marine Energy Extraction Devices in terms of Performance, Cost and Environmental Impact

Grant agreement number: 213380

EquiMar

Deliverable D2.2
Wave and Tidal Resource Characterisation

Deliverable D2.2

Wave and Tidal Resource Characterisation

Vengatesan Venugopal and Thomas Davey
University of Edinburgh, UK

Helen Smith and George Smith
University of Exeter, UK

Brian Holmes and Sean Barrett
University College Cork, Ireland

Marc Prevosto and Christophe Maisondieu
Ifremer, France

Luigi Cavaleri and Luciana Bertotti
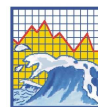*CNR-ISMAR, Italy*

John Lawrence
EMEC, UK

Françoise Girard
Actimar, France

January 2011

Summary

This report gives guidance relevant to the resource assessment of sites considered for the deployment of wave and tidal energy converters. Areas considered include: instrumentation and measurement; techniques and requirements for wave and tidal parameterisation; wave-current interaction; spatial and temporal variation. A number of case studies are also included examining several European sites.

CONTENTS

1   INTRODUCTION

1.1   SCOPE OF THIS REPORT

This report describes and discusses techniques for wave and tidal measurement and analysis for the purposes of resource assessment. Emphasis is given to established techniques and technologies although emerging technologies (and techniques) are also outlined where appropriate.

This report is concerned solely with the measurement and analysis of metocean parameter relevant to ocean energy applications. The performance of Marine Energy Converters is beyond the scope of this report.

1.2   AIMS & OBJECTIVES

o   To describe established methods to characterise the marine environment for the purposes of resource assessment.
o   To highlight the key oceanographic parameters relevant to ocean energy.
o   To describe the principal applications of methods for the development of ocean energy projects.

1.3   RESOURCE ASSESSMENT

Marine energy resource assessments may be conducted to various levels of detail depending on the stage of a project or the end user. In particular assessments may be conducted to identify suitable geographic locations for deployment. Once suitable areas have been identified a detailed assessment will be necessary to characterise a particular site. These processes will be referred to as *Resource Characterisation* and *Site Assessment* in the outcomes of the EquiMar project.

1.3.1 Resource Characterisation

Resource characterisation is normally carried out to establish suitable geographic locations for deployment, and has the following objectives:

o   To ascertain the potential resource for energy production with an explicitly stated degree of uncertainty;
o   To identify constraints on resource harvesting.

1.3.2 Site Assessment

Site assessment is normally carried out prior to deployment, to establish the detailed physical environment for a particular marine energy project, with the following objectives:

o   To assess the energy production throughout the life of the project;
o   To describe metocean conditions;
o   To characterise the bathymetry of the site to an explicitly specified and appropriate bathymetry;
o   To establish extreme (survivability) conditions with a defined return period;
o   To identify potential interference between multiple devices at the site;
o   To ascertain the spatial and temporal variation of the resource with an explicitly stated degree of uncertainty.

2   RESOURCE MEASUREMENT AND INSTRUMENTATION

2.1   DESCRIPTION OF WORK

2.1.1   Need for the information

There are *four* main drivers for measurement of the physical wave, tide and possibly wind, environment.

(i)   *The Energy Resource:* For the purpose of marine renewable energy a primary focus is to ascertain the level of resource, at an appropriate level of confidence, through the development of a project. This information will provide the basis for a specification of power (in time) and the energy to be produced over the length of the project. This information will be necessary to investors, utilities and government (both national and local).

(ii)   *Engineering Design:* Although the major design considerations for any device will be decided it is probable that individual sites may require adaptation of the base design. Certainly, issues of wave and current loading will have to be considered on a site-by-site basis for the design of the moorings. This information will be necessary to designers, constructors, insurers and "classifiers".

(iii)   *Marine Operations*: For a fully operating project the wave/ wind and tidal characteristics are necessary to predict the installation & maintenance strategy which for a large farm in a high energy site will give strong limitations. This information will be necessary to designers, constructors, marine contractors, insurers and "classifiers".

(iv)   *Data for numerical model calculations*: In complex sites, the use and accuracy of any model produced will benefit from "calibration" with measured data.

2.1.2   Level of Measurement

The requirements for physical measurement will depend on the stage in the project development and this may be better met by different instruments and measurement campaigns.

(i)   *Early stage:* When considering a specific site base line information is required to confirm the potential for the specific device. Thus one would wish to have a gross estimate of energy production potential, for example to within 20% of the actual, and to understand those specific physical parameters that would affect the base-line power productions (energy spread in frequency and direction, bathymetry). These would involve the combination of any available data from "nearby" measurement sites along with model information. The start point could be the regional and local maps that have/will be produced.

(ii)   *Project Development:* Once a decision to develop devices to a site has been made, measurements will be necessary to (a) reduce uncertainty (project risk) in energy production estimates (e.g. to 10%) - although the ease of this will depend on the "length of time" that the estimate is required for, (b) refine engineering design further, and (c) develop appropriate O&M plans.

(iii)   *Marine Operations for the farm:* It is probable that, during the operational life of a particular development, some measurement may be necessary to (a) confirm the level of resource for comparison with device production figures, (b) at least in the early farm developments, provide detailed correlation between energy production and resource for machine improvement and development, and (c) produce potentially improved efficiency and survival designs through "real-time" measurement of the "up-wind" energy resource.

2.2   WAVE MEASUREMENT

2.2.1   Types of Wave Data

(i)   *Time Series*

This type of data is gathered and presented in "time order". The basic data are individual measurements of wave motions from which "heave" wave elevations, and in the case of directional measurements, horizontal displacements, are usually produced. These time series can be very important in determining if there are any errors in the wave measurement. Time series are usually recorded over a period of approximately 20 minutes to 1 hour. Thus data records could for example be taken for either 17 minutes out of every hour in one case or else "continuously" over the hour. The time is a compromise between achieving lower error (longer measurement) and the measurement of different wave states which causes error due to "non-stationarity". Time series can be used to measure individual wave heights and periods and were the original method for determining the significant wave height. Time series provide great detail and opportunities for further analysis but have greater data amounts and are not immediately amenable to inexperienced users.

The continuous data is "sampled" in time in order to produce a series of signals separated in time. Typical sample rates will vary for the application, but for wave measurement a digitising frequency of 2Hz (i.e. points sampled every 0.5 seconds) is typical. Higher rates may produce more detailed profiles of the wave surface but will produce a larger data set which may have to be "down-sampled" to produce good resolution spectra. Depending on the instrument transfer function there may be no benefit in sampling at a higher rate.

(ii)   *Parameters*

The detailed time series are often processed to provide summary statistics of the important wave parameters such as significant wave height, zero-crossing period, wave steepness or maximum wave height. This is particularly done on buoy measurements where the smaller data rates required make this analysis attractive. One would thus compile time series of parameters (H_s, T_Z etc.) based on averages over the individual data record.

(iii) *Spectral data*

Spectral data usually consists of the "energy" (mean square variance density) distribution with the frequency of the wave. Spectral processing on buoys again provides a data compression but also allows further processing from computation of spectral parameters from the spectral moments. It is interesting that for most ocean engineering and oceanography applications one deals in true frequency spectra (see Figure 1). In ocean wave energy there are some who would prefer that we use energy plotted against period as this provides a clearer picture of the energy available for transformation by the device.
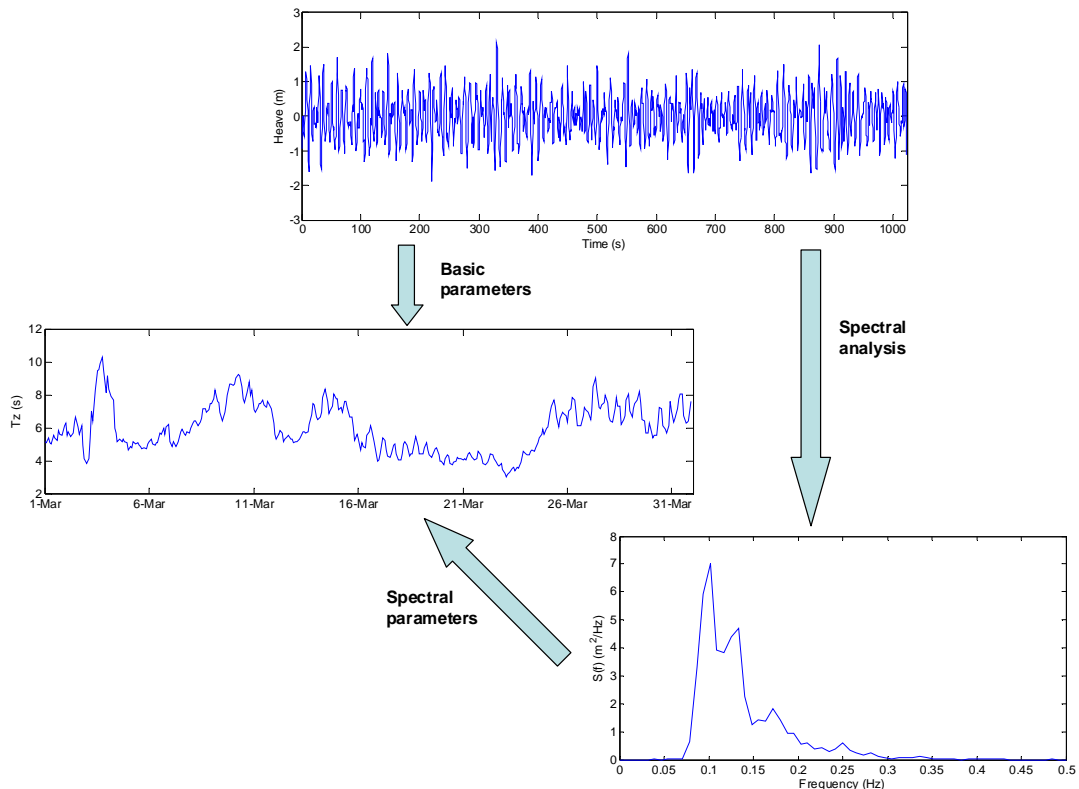
Figure 1 Processing of raw heave time series data from a wave buoy.

(iv)   Directional data

Most modern wave measurement devices have the capacity to measure the horizontal components of the wave motion in addition to the heave. From this data, a directional spectrum can be calculated, which provides both the direction of propagation and a value for the directional spread for each frequency component of the omni-directional spectrum. From these, the mean direction and directional spread of the sea state can be calculated.

2.2.2   *Wave Measurement Devices*

2.2.2.1   Fixed Instruments

Fixed instruments are usually mounted on a structure. The output from these instruments can be recorded and stored on site or sent to shore by cable or telemetry. Stepped-contact staffs, Resistance-wire staffs, Capacitance-wire staffs, Baylor Wave gauges and Laser altimeters are example of fixed instruments. The main disadvantage of this type of instruments is that they need to be mounted a good distance away from the supporting structure to avoid interaction. As a thumb rule 10 diameters away of the supporting structure (Tucker & Pitt, 2001).

2.2.2.2   Sub-surface sensors

Pressure sensors: The modern pressure sensors use strain gauges and are accurate in measuring the dynamic pressure. For most demanding applications Paros Digiquartz pressure sensors are used (Tucker & Pitt, 2001). The pressure signal can be digitised on

the site and data can be sent over a cable. The disadvantage of a pressure sensor is that its response is limited in short period waves. Other sub-surface sensors include an Inverted echo-sounder and Particle velocity meter.

2.2.2.3   Surface following buoys

There are two approaches to directional wave measurement using buoys:

Pitch-roll-heave buoys (PHR) measure the slope of the surface (both its magnitude and direction) and the elevation of the surface.

Particle-following buoys follow the orbits of the water particles at the surface. These buoys divide into two further categories, either sensing the acceleration of the buoy along three axes or measuring the displacement or velocity of the buoy along three axes (using DGPS for example).

Whichever type of buoy is used, the time series data recorded will comprise a triplet of measurements relating to the vertical and horizontal (north and east) movements of the buoy. These are processed into auto- and cross-spectra, from which the variance density spectrum and the directional distribution can be obtained.

Operational considerations

- Compass heading is important for ensuring accuracy in directional measurements
- Calibration of the buoy should be performed both pre-deployment and post-recovery e.g. for maintenance
- Buoy moorings must be designed to provide minimal impedance to the buoy motion
- Buoys will normally need to be recovered every six months to a year to replace batteries, check instrumentation and possibly re-calibrate.

Problems with Buoys

(i)   (Double) Integration of acceleration signals: Although better than the original buoys the processing of acceleration data into displacements is difficult as very low frequencies or offsets are present. The double integration has the effect of amplifying these lower frequencies with the noise superimposed. The application of a high pass filter has the effect, for a particle following buoy, of filtering the second order non-linear part of the waves. This impacts on the measured heights of the wave crests.

(ii)   Low and high frequency noise (see (i) above).

(iii)   Phase shifts

(iv)   Mooring compliance: The normal operation of the buoy requires that it move freely, but must be kept "on station" at the measurement site. The mooring has to be appropriately designed for the water depth, current and wave climate that the buoy will be deployed in.

(v)   Data transmission: Distance and high waves may interrupt transmission.

(vi)   Wave "jumping" in high waves: This problem can bias the measurements in high sea states. The buoy will attempt to "move around" a large wave rather than rise over the crest, thus producing smaller estimates of the higher waves.

(vii)   Non linear effects

(viii)   Interpretation and accuracy of directional measurements

Data recovery

The method to recover data will depend on the budget, location and needs for data. All buoy systems have a combination of on-board storage (which can contain "raw" data, parameters and spectra) and transmission of "hourly" parameters and/ or spectra. Each of these has implications for signal bandwidth and buoy power consumption. Although storing all data on the buoy and manually downloading it on a period basis is a possibility, the need for close to real-time data and the lack of suitable weather windows during winter months means that most buoy systems use some form of data transmission. This can be achieved by one or a combination of the following:

- HF and VHF radio
- GSM (Global System for Mobile Communications)
- GPRS (General Packet Radio Service)
- Satellite communications (ARGOS, INMARSAT, ORBCOMM)
- Cable (relatively unusual

Available buoy wave measurement systems

The three main manufacturers of wave measurement buoys are OCEANOR, Datawell and TRIAXYS. Each produces a range of directional and non-directional buoys for different applications. The key features of their directional wave buoys are described in Table 1.

Table 1: Key features of the directional wave buoys produced by the leading manufacturers (Source: www.datawell.nl, www.oceanor.no, www.axystechnologies.com)

	Diameter	Mass	Digitising frequency	Period response	Accuracy	Transmission options
Datawell Directional Waverider MkIII	0.9m	225kg	3.84Hz	1.6 – 30s	Heave: <0.5% of measurement	HF, IRIDIUM, ARGOS, ORBCOMM, GSM
OCEANOR SEAWATCH MINI II	1.25m	320kg	2Hz	1 – 30s		UHF, ARGOS, INMARSAT-C, GSM
TRIAXYS Directional Wave Buoy	0.91m	197kg		1.6 – 30s	Heave <2% Period <2%	VHF, INMARSAT-D+, IRIDIUM, CDMA, GPRS

2.2.2.4   Acoustic Doppler Profilers (ADPs)

ADPs were originally developed to measure currents in the water column through the Doppler shift of backscattered acoustic signals from 'scatterers', i.e. particulate matter suspended in the water column and moving at the same speed as the water particles. The instruments are versatile and can be deployed in a variety of configurations, including upward-looking from the seabed, downward-looking from the hull of a boat, or side-looking from fixed marine structures.

The technology has subsequently been developed further to enable estimates of the wave spectrum to be made. ADP sensors are generally associated with complementary pressure and distance meter sensors. So, wave spectra can be derived from ADP instruments in one of three ways:

- Pressure record: By recording the dynamic pressure some meters in depth as waves pass overhead, after an inverse filtering (using transfer function between linear elevation and dynamic pressure) a time series of sea surface elevation is obtained which can be processed to produce an omni-directional spectrum. The disadvantage of using pressure sensors to measure wave data is the attenuation of the pressure signal with relative depth (depth to wavelength ratio). To eliminate enhancement of noise, this imposes a high-frequency cut-off which decreases as the depth increases. Unfortunately an optimal cut-off frequency is spectrum dependent.

- Surface tracking: One or more of the ADP beams can operate as an inverted echo-sounder, with the signal reflecting off the surface of the water instead of particles in the water column. This again produces an elevation time series. However, because there is no signal attenuation, this method produces a more accurate record.

- Orbital velocities: Wave orbital velocities are measured in the same way as currents in traditional ADP applications, through the Doppler shift along each beam. Through multiple velocity measurements at various range cells (either separate beams or along one beam), cross-spectra can be used to calculate the directional wave spectrum. Alternatively, where a surface tracking measurement is available, a triplet of vertical motion plus two horizontal velocity components can be processed in the same way as wave buoy measurements to provide directional spectral information.

Operational considerations

- Deployment scenarios: A compromise may be needed between seabed mounting (more secure, but greater water depth and therefore decreased accuracy at high frequencies) and sub-surface buoy mounting (more vulnerable to damage, but operating in shallower depths).

- Mooring: Trawlers are a risk to any bottom-mounted ADP in areas of fishing activity. Anti-trawl mountings are available to reduce the risk of entanglement with nets (see Figure 2).

- Depending on the bottom soil, problems with the device being buried over time could be encountered.

Figure 2: Example of an anti-trawl ADP bottom-mounting.

Problems with ADPs for wave measurement

(i)   Effect of beam spreading on the resolution of the measurement: As the beam diverges from the instrument, the area that contributes to the measurement at the surface is increased and effectively smaller wavelength (higher frequency) waves are not measured. This effectively produces an upper cut-off frequency above which no useful information is derived. This becomes worse as the ADP is deployed into deeper water and lower frequency, higher divergences must be used.

(ii)   Surface effects on reflections: Long, low swell will exhibit predominantly horizontal velocities in the depths where ADPs are likely to be used for measurement, with very little vertical component. The vertical component is unlikely to be resolvable by the ADPs, which could make calculation of the directional spectrum impossible, depending on the method used for the particular instrument. In that case the pressure measurement can be used.

Turbulent water or even schools of marine life can cause bubbles in the water column that will lead to inaccuracies in the measurements

In very clear water, there may be insufficient particles in the water column to produce sufficient backscatter of the signal

Data recovery

There are two options for data recovery from ADPs:

The ADP is recovered periodically to the surface for the data to be downloaded. Modern battery and data capacities enable several months of data to be stored; however difficulties can arise from the need to recover the device in bad weather (operational planning). The device is also recovered through an acoustic link/ release and again this greater complexity can lead to failures. There is also the final problem of ensuring that the ADP is suitably marked for recovery and not "lost".

The data can be sent to a surface buoy where it can be transmitted by radio to a satellite or a shore station in the same manner as a wave buoy. This can provide real-time or almost real-time data, but at the cost of the vulnerability of the surface buoy.

Available ADP wave measurement systems

The two most commonly used ADPs for wave measurement are Teledyne RD Instruments' Workhorse Waves Array and Nortek's AWAC with Acoustic Surface Tracking (AST). The Workhorse Waves Array has four transducers transmitting acoustic beams at 20° from the vertical. The four beams contain 3-5 orbital velocity cells in addition to operating as surface trackers by reflecting the acoustic beam from the surface of the water. The unit also contains a pressure sensor which records the varying water depth as waves pass above the sensor. The primary means of calculating directional spectra are the orbital velocity measurements, with the surface tracking and pressure sensor data available for QA and back-up.

The AWAC comprises three beams at 25° to the vertical, each with one orbital velocity cell, with one dedicated upright beam for surface tracking plus a pressure sensor. In contrast to the Workhorse Waves Array, the inclusion of a dedicated AST beam enables operation with very short pulse widths to provide a sub-centimetre resolution of the sea surface variation. Directional spectra can be calculated in one of two ways. Either a maximum likelihood method (MLM) can be applied to exploit the time-lag between the spatially separated measurements of three velocities and the AST, or a triplet approach using the vertical AST track and two horizontal velocity components, similar to that used for buoy processing, can be utilised. ,

Table 2 provides a comparison between the two systems,

Table 2 Comparison between the RDI and NORTEK ADP wave measurement systems (source: www.rdinstruments.com, www.nortek-as.com)

	Deployment depth	Acoustic frequencies	Low period cut-off (for directional wave measurement)	Accuracy in velocity measurement
RDI Workhorse Waves Array	5m 20m 80m	1200kHz (2.5-14m depth) 600kHz (5-45m) 300kHz (10-80m)	1.8s (at 5m depth) 3.5s (20m) 7.0s (80m)	+/-0.3% +/-0.3cm/s (1200 and 600kHz) +/-0.5% +/-0.5cm/s (300kHz)
NORTEK AWAC	5m 20m 60m	1000kHz (up to 40m depth) 600kHz (up to 60m)	1.5s (5m) 3.1s (20m) 5.5s (60m)	1% +/-0.5cm/s

2.2.2.5 Radar systems

HF radar

HF (high frequency) radar provides a land-based method for measuring sea surfaces over a relatively large area, with a typical operating range of up to 150km. It operates in the frequency range of 3-30 MHz and is capable of measuring both directional wave spectra and surface currents. The system comprises two shoreline transmitters with overlapping transmission regions, located a sufficient distance apart that their radar bearings are as close as possible to 90°. Best accuracy is found at the centre of the field with poorer accuracy as one moves away from the centre. HF radar can provide results with a spatial resolution as low as 300m for short-range systems, increasing to over 3km for longer ranges, with a temporal resolution of as high as 10 minutes.

The system utilises the phenomenon of Bragg scattering of the transmitted waves by ocean waves of exactly half their frequency. A Doppler spectrum is obtained from the frequency change between the transmitted and back-scattered radio waves due to reflection from the ocean waves. The Doppler spectrum contains two discrete peaks whose frequencies can be used to determine the surface currents. Inversion techniques can be used on the side bands to obtain directional wave spectra.

There are two key advantages to HF radar over buoy/ADP systems:

- Spatial coverage: HF radar systems can provide measurements with a resolution of approximately 1km over an area of approximately 40km x 40km, at a temporal resolution of up to 10 minutes.. As the area increases, the spatial resolution decreases. However, this kind of spatial coverage would be impossible with traditional instrumentation.

- Land-based instrumentation: The sitting of the transmitters on the shoreline means that any problems can be resolved without the need for weather windows and vessel time as would be the case for offshore systems

A number of commercial HF radar systems are available. The three most widely used are compared in Table 3.

Table 3 Comparison of commercial HF radar systems for wave measurement (source: www.helzel.com, www.codar.com, www.neptuneradar.net)

System	Operating frequency	Range	Spatial resolution	Temporal resolution
WERA	5-50MHz	65-110 km (8MHz) 30-15 km (16MHz) 15-30 km (30MHz)	Up to 250m for short range applications	15 mins
SeaSonde	4.3-5.4 MHz (long-range) 11.5-14 or 24-27 MHz (standard) 24-27 or 40-45MHz (hi-res)	140-220 km (long-range) 20-75 km (standard) 15-20 km (hi-res)	3-12 km (long-range) 0.5-3 km (standard 0.2-0.5 km (hi-res)	
Pisces	6-40MHz	150km at 10MHz	0.75-20km	5 mins

X-band radar

X-band radar has a similar operational principle utilising Bragg scattering as HF radar. However, instead of using the longer electromagnetic (e.m.) waves of the same order as the ocean wavelengths, X-band radar uses short, 3cm wavelength e.m. waves to interact with the ripples on the sea surface. For this reason, X-band radar can only be used for wave measurement when at least a light wind is present to generate surface ripples.

X-band radar is used world-wide, primarily as a shipping-traffic control and navigational tool. It is installed on almost all offshore structures and larger vessels. However, it is possible to use X-band systems for wave measurement, and systems such as Miros WAVEX, a vessel-based measurement system, and WaMOS II, which can be used on vessels or from land, have been specifically developed for this application. With traditional X-band radar uses, Bragg scattering produces 'sea clutter' noise which is subsequently filtered from the record. However, longer waves modulate the clutter, making them visible in the radar image, allowing the image to be processed using an empirical method of wave spectrum scaling. A disadvantage of this method of wave measurement is the lack of definitive scaling between back scatter radiation and wave height, meaning that some form of calibration measurement such as a wave buoy should be used for the best accuracy.

2.2.2.6   Satellite measurement

Satellite-based wave measurement differs significantly from the previous systems discussed due to the coverage available. Although spatial coverage is extensive, spatial resolution is limited by the satellite's tracks, and temporal resolution is low, with satellites' repeat cycles, i.e. the length of time until they return to a track, having durations of many days in some cases. For this reason, satellite data is less suited to short-term, site-specific nearshore wave resource measurement. However, it is able to provide excellent long-term datasets for the analysis of longer-term temporal variability.

The two types of satellite-borne remote sensors that have been used for wave measurement are the radar altimeter and the synthetic aperture radar (SAR), discussed in more detail below. A number of satellites carrying one or both types of sensor are currently operational, as described in Table 4. An example of satellite tracks for three systems is shown in Figure 3.

Table 4 Summary of the key currently and previously operating satellites carrying radar altimeters and SAR (from Tucker and Pitt).

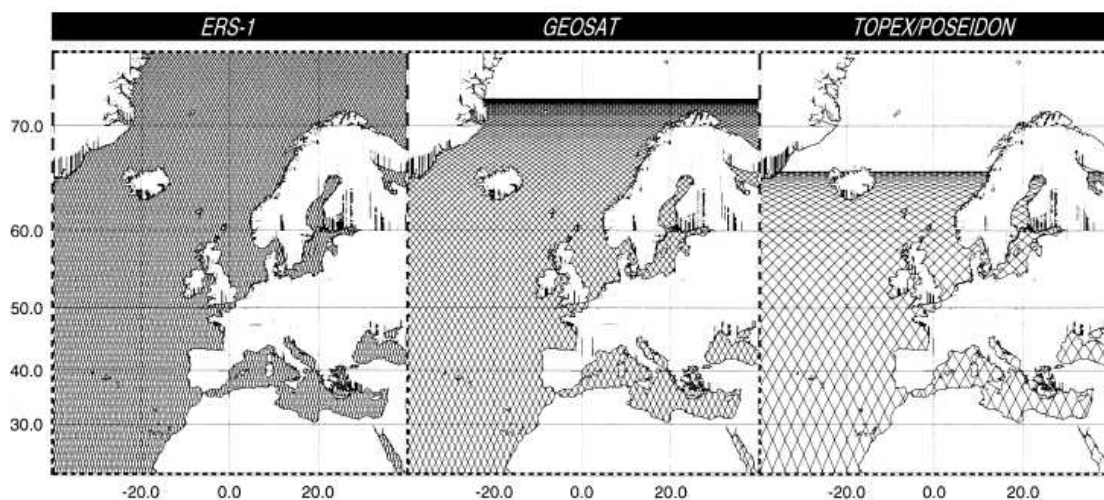|	Launch date	End date	Radar altimeter	SAR
SEASAT	27/06/78	10/10/78	Y	Y
GEOSAT	12/03/85	Nov 99	Y	
TOPEX/POSEIDON	10/08/92		Y	
ERS-1	17/07/91	June 96	Y	Y
ERS-2	21/04/95		Y	Y
RADARSAT-1	04/11/95			Y
RADARSAT-2	14/12/07			Y
JASON-1	07/12/01		Y	
OSTM/JASON-2	15/06/08		Y	
ENVISAT	01/03/02		Y	Y

Figure 3 Satellite tracks for Europe and the eastern Atlantic Ocean. The denser the tracks, the longer the time interval until the satellite next returns to that location (from Krogstad and Barstow, 1999).

Radar altimeter

Radar altimeters emit pulses vertically downward toward the sea surface at a high frequency, e.g. 1000 pulses per second. Echoes are received from both wave crests and troughs, giving a smeared returned pulse with a slowed echo rise time (i.e. the time required for the leading edge of the pulse to rise from one-tenth of its final value to nine-tenths). From the rise time, a value of H_{m0} can be calculated either theoretically or, more accurately, empirically (Tucker and Pitt, 2001). Results are averaged over a large number of returned pulses to eliminate random variations in amplitude, giving an official accuracy in the wave height measurements of approximately +/-0.5m, however higher accuracies are frequently obtained.

The spatial resolution obtained from radar altimeter measurements is generally no better than 7km. Additionally for coastal regions, valid data can only be obtained when the satellite is approaching the land from the sea, or the track is running alongshore. This is because measurements are often missed or are biased when the satellite track first moves from land to sea.

Synthetic aperture radar (SAR)

Synthetic aperture radar (SAR) records images of the sea surface from backscattered radiation over swaths along its tracks. These images can be operated on by a 2-D Fourier transform to produce a directional spectrum. This spectrum must be inverse using the complex nonlinear imaging process of the radar to obtain a wave directional spectrum. It gives waves with periods from approximately 8s to 25s, but much more limited in high frequency in the direction perpendicular to the track of the satellite. This limits in many cases the use of SAR to swell observation This type of spatial resolution is analogous to that produced by global wave models at ocean scales. While a standard swath width might be 100km, some satellites such as RADARSAT carry a SAR which can operate in ScanSAR mode, with a swath 500km wide. Typical spatial resolution for SAR images is ~25m

2.2.3   *Quality Control*

Whichever measurement device(s) is eventually chosen to record the wave or tidal characteristics it is imperative that properly audited quality control measures be put in place to validate the data quality. The data user must satisfy themselves that the data from a secondary source or supplier is not flawed. Poorly QC'd data will lead to errors in the analysis of available resource and the determination of extreme events. When resource assessment is considered then one must remember that adequate quality and quantity of data must be delivered to satisfy the criterion for error limits in the provided parameters/ spectral analysis. *It is considered mandatory that consideration/ description of the data quality control be given in any specific measurement campaign.*

In general the data quality control of wave records is more problematic due to the response characteristics of the measuring devices and the relatively broad-brand form of the data where extremes, although 'unlikely' cannot be automatically assumed to be faulty. Although the general aspects of QC are as important for tidal stream measurements the tests and controls may vary from wave analysis.

There are a variety of tests available which may *indicate* the presence of various faults and errors within wave records. These tests may be carried out on the original wave time series, or often on the resulting frequency spectrum from the time series.

Faulty data can be generated for a variety of reasons from instrument and transmission errors. The most important of these are:

- *Generation of spurious large value (spikes)*: This might arise due to faulty electronics or often within the transmitting process (this in turn will be determined by the transmission power, distance to receiving station and weather conditions). Individual spikes of this kind are often identified through either tests for extreme sensor values (maxima or minima) or statistically through assumptions on the statistical probability of a 'wave' exceeding a specific, unlikely, range. A small number of spikes will have no influence on an analysis but regular large values that are not identified and adjusted will bias the values of record variance for example.

- *Extended constant values:* These can occur from instrument and transmission failure. They are simply tested for by keeping a 'running average' within the time series. Again small runs of constant values will have limited influence on the data and can be compensated by interpolation if it is felt that the constant series is too long. Large data 'drop-out' will lead to the need to reject that data.

- *Instrument noise.* The very nature of wave buoys, involving the 'double integration' of the acceleration signal makes them liable to distortion, particularly in the low frequency range (as these are amplified more by the double integration process). Low frequency noise can often be identified in the resulting energy spectrum, but care has to be taken to ensure that this is not swell. The noise can be removed by filtering in the frequency domain and then re-transforming to the wave surface if this is a necessary quantity. High frequency noise (from poor or old electronics) can be difficult to identify and will have an effect on the calculation of spectral moments (particularly on higher order moments). It is common practice to identify a maximum frequency above which any integration is not performed (typically about (0.3 – 0.4 Hz). This to some extend is dependent on the sea characteristics and the performance curve of the devices.

- *Distortion of the wave form:* Particularly in buoy measurements which involve analogue integration and filtering to be performed there is a danger that poor data be 'disguised' in its subsequent integration and processing. For example instances have been sited where 'spikes' in the data have been convolved with the filtering process to produce seeming 'sensible' large waves. Again, analysis of the frequency of occurrence of these large events will provide an indication of too many "unlikely" events.

- Test for 'sensible' directional variations - mean direction and spread parameter (can detect compass error)
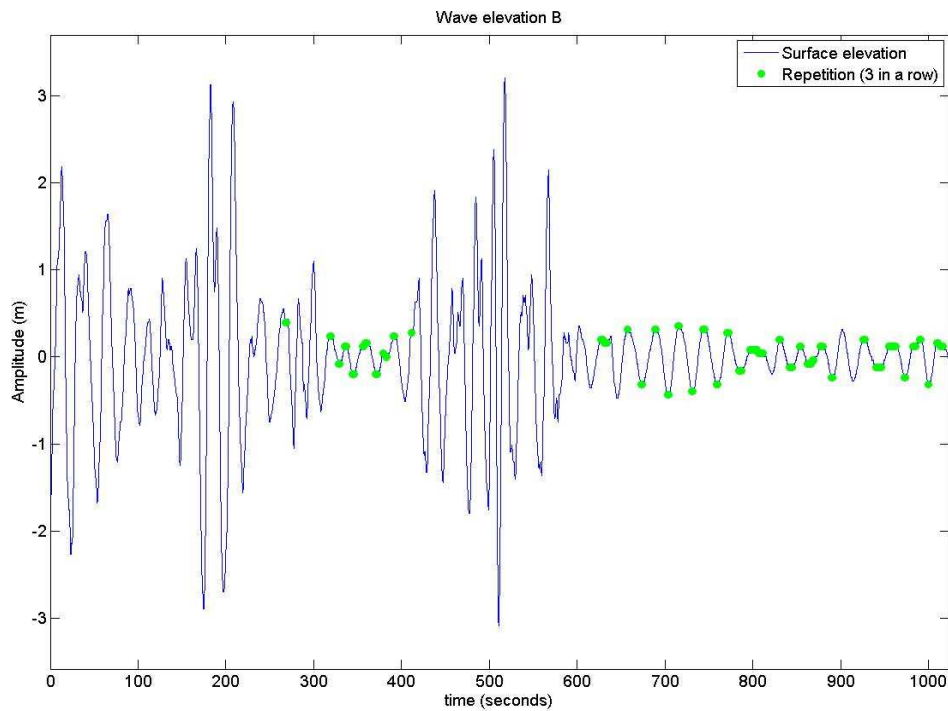
Figure 4: Example of a record showing a significant number of repetitions
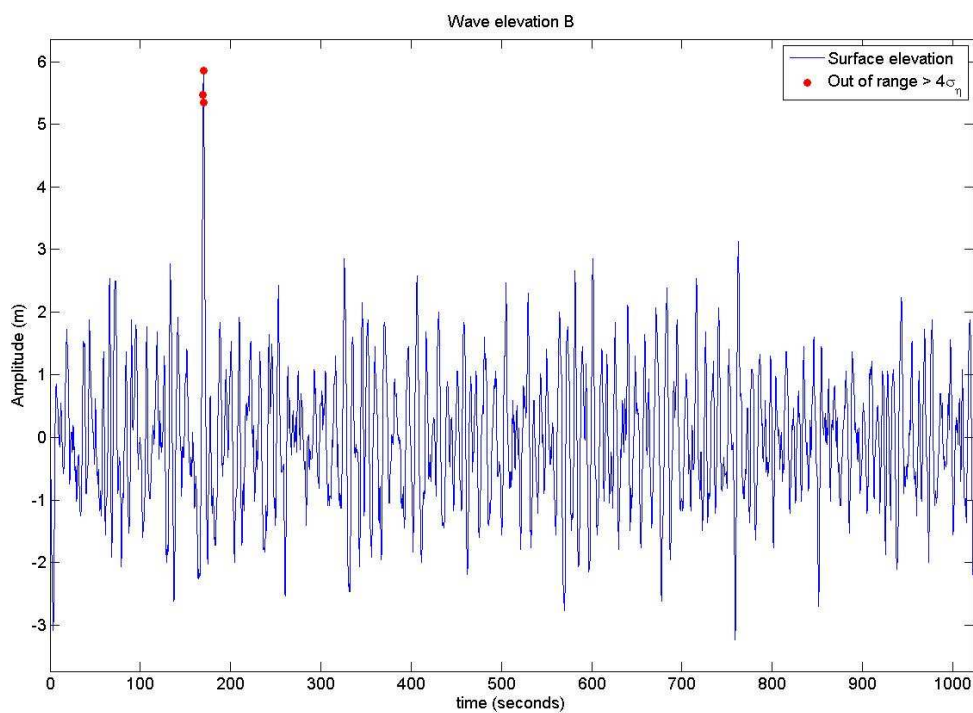
Figure 5: Example of a record with a wave elevation that has a statistically small probability of happening

In the quality control process, extreme care should be taken to ensure that the data is not biased by the very act of quality checking. It is recommended that:

(i)　　　in the first instance errors should only be FLAGGED. These records should be archived to ensure that they may be available if necessary.

(ii)　　　a report on the occurrence and frequency of each flagged error should be provided to give some indication of 'problem' records

(iii) further visual analysis of the time series or spectra may then help to determine the final quality of a particular record. It is recommended that prime parameters (Hs, T, Dp) are inspected visually at the end of each of month when the monthly reprocessing finishes. If there are outliers or suspicious trends then the corresponding time series or spectral files and plots should be reviewed.

Quality control tests can be done on the initial time series (which requires intensive processing for a large number of tests) Further, more detailed, description of the problems of wave analysis in particular is contained in the references by Tucker (1993), Tucker and Pitt (2001) and Mackay et al (???)

The data quality control of wave measurements is an ongoing activity. Those interested in more detail might wish to review the QUARTOD website –

http://nautilus.baruch.sc.edu/twiki/bin/view

or the Coastal Data Information Program website -

http://cdip.ucsd.edu/?nav=documents&sub=index&units=metric&tz=UTC&pub=public&map_stati=1,2,3

2.3   TIDAL MEASUREMENT

2.3.1   Types of Tidal Data

(i) Time Series

This type of data is gathered and presented in "time order". Tidal stream data is usually collected at a number of heights distributed regularly through the water column, depending on the measurement sensor. The typical measurement sensor for this application is the acoustic profiler (see below). The data may be presented as magnitude and direction pairs, or as orthogonal flow components. Orthogonal flows in turn may be presented as (east, north) values, or in beam directions relative to the instrument orientation. The doppler samples 'spot' flow rates, and a series of these should be averaged over a suitable time scale for meaningful results. For initial campaigns an averaging regime of hourly values may be suitable, but for detailed information a sample average of 10 minutes should be used. Attention should be paid to the obtainable accuracy of the measurements with regards to the number of pings averaged. Details should be confirmed in the sensor's technical reference.

Other data sources may be HF or X-band radar systems which can provide information on surface currents is a region.

(ii) Tidal Parameters

The time series data is analysed for the tidal frequency components. These components may be used to predict tidal streams at the future, although such predictions cannot account for changes in flow cause by weather and other non-periodic effects.

2.3.2   Tidal Measurement Devices

2.3.2.1   ADPs

The fundamental principle of operation of the ADP relies on the scatter of acoustic energy from within the water column. The energy is transmitted into the water from transmitter/ detector heads (usually piezo-electric materials). The frequency of the original signal will be shifted according to the   local velocity of small particles suspended in the flow (the Doppler Effect). The frequency shifted (scattered) sound is then detected by the same instrument. The position of the signal in the water is determined by phase/ time of flight mechanisms and is usually averaged over a small volume to give a local measurement along the beams. These cells or bins can be chosen by the user but are typically of the order of 0.5 to 1m. The volume of the cell will depend on the degree to which the beam diverges as it propagates through the water. This is determined by the transmitter head design and bean angles are typically of the order of 4 degrees. One may wish to limit the bin size to matches the of the cells with the needs of the measurement or to satisfy the need for a good signal to noise ratio (A larger volume will typically provide more "signal" at the cost of lower spatial resolution).

ADP's are often deployed on the sea bed but can be placed in mid water using subsurface buoys. This allows the use of higher frequency instruments, but care has to be taken to ensure that wave induced motions do not affect the measurements.

Measurements can be made at repetition rates up to several per second.

The range of the beam is dependent on the properties of the water thought which it is moving and the properties of the instrument. Scatter can be heavily affected by suspended sediment that reduces power (range) rapidly. This is dependent on beam frequency with higher frequency beam energy being attenuated faster than low frequency.

This means for example that in shallow water frequencies above 1 MHz can be used. The higher frequency beams can be made to diverge less and give better measurement resolution. In deeper water it is not possible to deploy instruments with enough battery power to support higher frequency beams and one would typically use ADP units with a frequency of the order of 600 MHz. These beams can penetrate further through the water column but will have lower resolution/ accuracy.

2.3.2.2   Radar Systems

HF radar

HF radar system is a shore based remote sensing system using the over the horizon radar technology to monitor ocean surface currents, waves and wind direction [Gurgel et al., 1999]. This long range, high resolution monitoring system operates with radio frequencies between 5 and 50 MHz. A vertical polarized electromagnetic wave is coupled to the conductive ocean surface and follows the curvature of the earth. The rough ocean surface interacts with the radio wave and due to the Bragg effect back-scattered signals can be detected from ranges of more than 200 km. This effect was first described in 1955 by Crombie [Crombie, 1955] and the first radar system using that effect was developed by Barrick et al [Barrick, 1977] at NOAA in 1977.

The Bragg effect describes the coupling of the electromagnetic wave with the ocean wave field. To fulfil the Bragg conditions the electromagnetic wave length needs to have twice the wavelength as the ocean wave, e.g. for a 30 MHz radar signal with Lambda 10 m, the corresponding ocean wave is 5 m. Reflections from waves that fulfil this condition will generate a dominant signature in the received signal spectrum due to in-phase summation of amplitudes.

The accuracy and reliability of ocean current maps has been controlled from an extreme dynamic ocean area off the French coast near Brest. A WERA deployment on the Brittany coast of France, owned by SHOM (Oceanographical and Hydrographical Service of the French Navy) and operated by Actimar, provides data since few years. The radar operates at a centre frequency of 12.38 MHz with a bandwidth of 100 kHz (range cell size of 1.5 km) at 30 Watts rf-power. Over a period of more than 12 months a study was carried out to validate the quality of the provided data by means of a comparison with buoy data [Cochin, 2006]. Furthermore the reliability was qualified by comparing the user's demands for data availability with the resulting data. The accuracy and reliability was studied by SHOM using an ADP and a Wave Rider buoy for ground truthing [Helzel, 2009]. Both instruments were located about 30 km off the coast. **Figure 6** (left) shows a typical current map. The comparison between the measurement data of the ADP and the WERA system is displayed in **Figure 6** (right). The corresponding correlation between the ADP and WERA data, displayed in figure, shows a correlation factor of 0.947. This excellent agreement proves the accuracy of the WERA system to measure ocean surface currents.
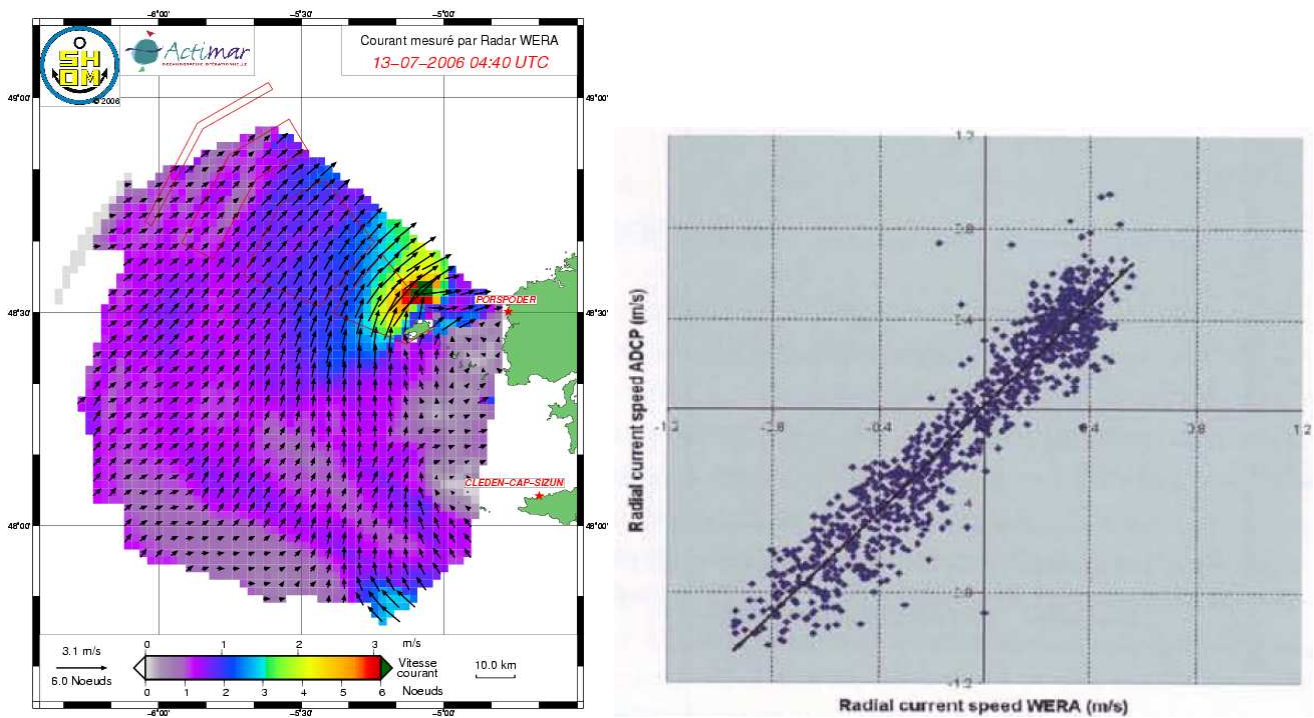
Figure 6 Left: surface current map with averaging time of 12 min and 1.5 km range cell size.
Right: comparison of radial current velocity measured with WERA and ADP, r: = 0.94.

Synthetic aperture radar (SAR)

Quantitative assessment of the Doppler shifts encountered in ENVISAT ASAR WSM observations of the intense and persistent Agulhas Current with variable dominance of shear, convergence and divergence zones yields promising results (http://soprano.cls.fr/L3/L3_currents.html). The greater Agulhas Current makes an ideal natural laboratory for these WSM Doppler shift measurements, as will Doppler shift measurements in the presence of mesoscale eddies. At a spatial (azimuth - range) resolution of 8 km by 4 km a maximum speed near 2 m/s was obtained in the core of the Agulhas Current with an estimated error of 0.2 m/s in Doppler velocity at 40° incidence angle. In contrast the weekly mean surface geostrophic current derived from altimetry reached only 0.6–0.7 m/s.

Advancing the quantitative estimation of surface current dynamics also implies, especially for incidence angles lower than 40°, to have an accurate estimation of local wind speed and direction to properly account for the sea state Doppler shift. The lack of such simultaneous precise wind direction information limits the surface current velocities retrieval in situations when the wind direction is fast changing and therefore atmospheric model a priori is no longer sufficient, such as near atmospheric fronts or rain cells. The ultimate solution would be to have simultaneous scatterometer information available.

In summary, the results are considered promising for strengthening the use of SAR in quantitative studies of the ocean currents. However, for the purpose of tidal resource measurement, satellite data is less suited to short-term, site-specific nearshore tidal measurement because spatial resolution is limited by the satellite's tracks and temporal resolution is low.

Improvements are being made in the use of satellites to observe surface currents. The temporal coverage is , however, rather sparse. It is not feasible to obtain sufficient data for reliable harmonic analysis.

2.3.3   Quality Control

The most likely instrument used to collect a tidal stream data for the time being is the ADP. It is necessary to ensure that the collected data is usable before it is processed. The instrument will report information on the received echo signal as well as the computed stream velocity. Each received data block should be checked to ensure that the echo parameters are within appropriate limits, and that sufficient usable blocks are averaged. Measurements near the surface layer are likely to be compromised by side-lobe reflections of the acoustic beams, which can be identified in the echo data. Another common cause of error is the presence of large, solid objects passing the sensor, causing a spurious echo return. These are commonly identified by a 'fish-finder' routine in the sensor, and can again be identified from echo quality. The existence of these bodies may compromise one or more of the working beams. Also, an assumption of the ADP method is that the flow is notionally laminar. By comparing velocity estimates from each acoustic beam, an 'error' velocity may also be determined. This quantity should also be inspected, to validate the laminar assumption.

3   WAVE PARAMETERISATION

3.1   REQUIREMENTS

3.1.1   Overview

The requirements for wave parameterisation and characterisation have been produced with primarily with regard to Wave Energy Converter (WEC) applications. The influence of waves on Tidal Energy Converters (TECs) is not explicitly considered. The methods and parameters described are likely, however, to be of relevance to the tidal energy community.

It is recognised that the information for resource assessment may be obtained from a number of sources. Physical measurements (e.g. from a wave buoy) usually, but not always, record the elevation time series at some particular point in space. These raw measurements will not always be available, especially when studying archived data. It is probably a more common scenario that only spectral information is available. This will almost certainly be the case when examining data from numerical models. Numerical models suitable for resource assessment purposes examine the transfer of energy in the frequency domain (i.e. spectral information). With the high expense and durations required for extensive physical measurement campaigns it is highly likely that numerical models will play an ever increasing role in resource assessment. Efforts have therefore been concentrated on understanding parameters that can be extracted from spectral analysis.

The potential data sources and their role in resource assessment are illustrated in Figure 7.
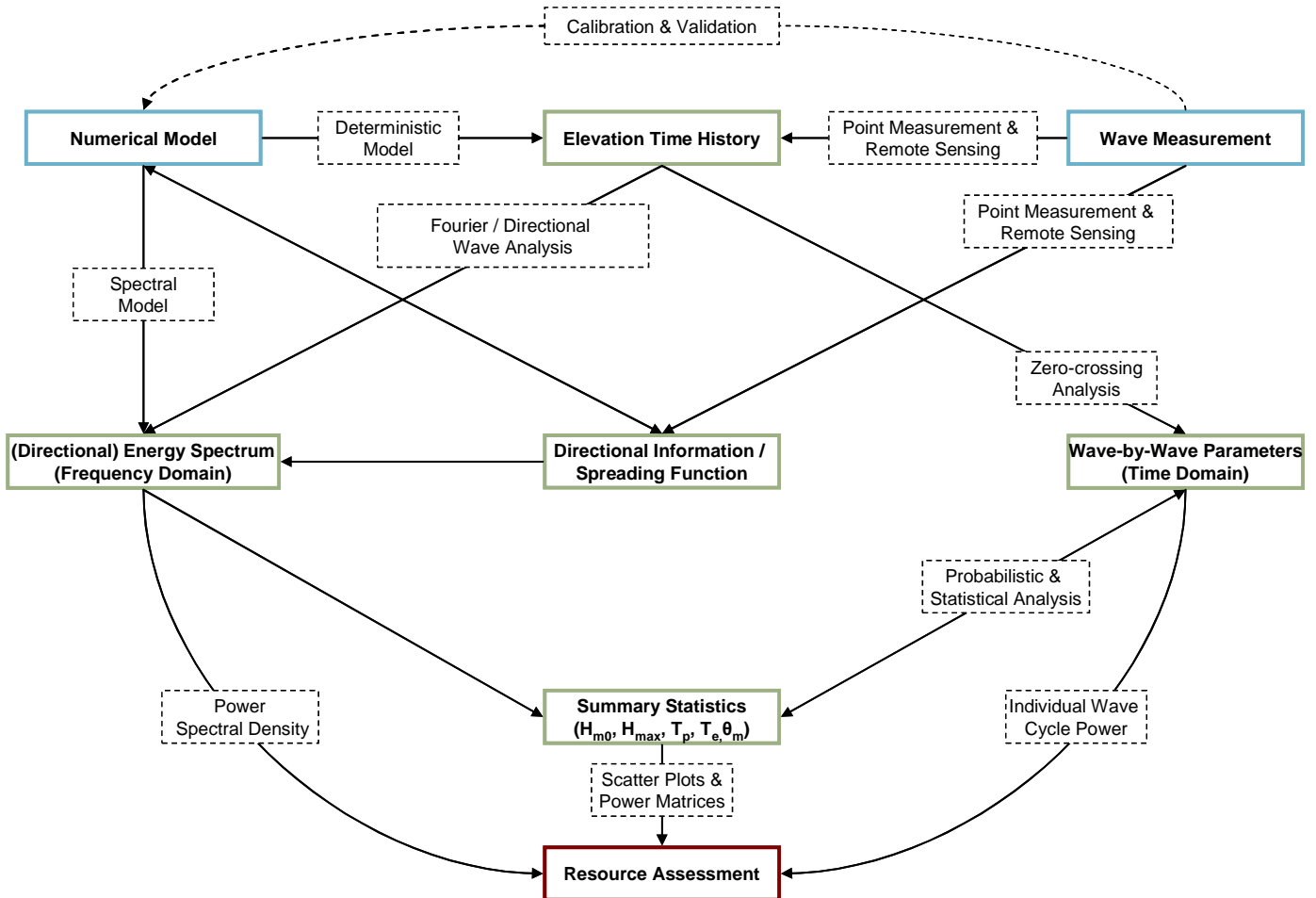
Figure 7 Data sources and analysis methods for wave resource assessment

3.1.2   Wave and Sea Characterisation

In order to supply sufficient information for a thorough wave resource analysis the characterisation of a particular site should provide the following:

1. An estimate of the global parameters (i.e. H_{m0}, T_p, T_e).

2. Provide an estimate of the dominant spectral form, its component seas (e.g. wind seas and swell) and directional characteristics.

3. Provide statistics on selected parameters obtained through wave by wave analysis (i.e. parameters characterising individual waves and crests).

4. Identify potential for significant spatial variation and quantify the variation through measurements (or modelling results) where possible.

5. Provide measurements or modelling results over a duration which allows analysis of seasonal and annual variations.

3.2 *WAVE PARAMETERS FOR RESOURCE ASSESSMENT*

3.2.1 Wave Parameter Calculation

A number of wave parameters are of relevance to the characterisation of the wave resource. These methods are derived either directly from the time-series (wave-by-wave analysis) or through analysis conducted in the frequency domain (spectral analysis). Some of these parameters may be inferred through numerical modelling, in particular those derived from spectral analysis.

3.2.2 Selected Wave Parameters

3.2.2.1 Energy Spectrum

The energy spectrum is the basis for majority of global wave parameters (e.g. H_{m0}, T_e, T_p). The wave spectrum describes the relationship between *Spectral Density* (m^2s) and frequency (Hz). Wave spectra may be defined into two categories:

1. **Discrete Spectra:** Obtained from a recorded elevation time series through Fourier analysis, the spectral density is described at discrete frequencies. Some form of smoothing is usually applied (e.g. "windowing") to allow meaningful interpretation of the noisy raw spectrum.

2. **Parametric Spectra:** Described as a function of global parameters, usually H_{m0} and T_p (along with others) a parametric spectrum describes the spectral density as a function of frequency. Parametric spectra have several applications. These include: providing an estimate of the spectrum where only global parameter statistics are available; where the fit to the measured discrete spectra is acceptable, parametric spectra are an effective method for the characterisation of a particular site or region.

The energy spectrum may be provided in directional and non-directional forms. The established convention is to describe the spectrum in non-directional form *(S(f))* which is expanded by a *directional distribution (D(f,θ))* to give the directional spectrum *(E(f,θ))* as,

$$E(f,\theta) = S(f) \cdot D(f,\theta) \qquad (1)$$

The directional distribution may be given as a set of discrete values over a range of frequencies and directions but this is relatively rare. It is more common for measurements to be given as a set of Fourier coefficients over the range of discrete frequency values.

Where detailed directional information is unavailable or where a parametric approximation of distribution is desirable, the directional characteristics may be described using a spreading function. The most commonly applied spreading function is the $\cos^{2s}$ description and distributions obtained from Maximum Entropy Method (MEM) which allows for multimodal distributions. See §3.3.1.3 for more information.

3.2.2.2 Spectral Moments

The spectral moments are keystone of frequency domain analysis. The most commonly required moments are m_{-1}, m_0, m_1, m_2 and m_4. The zeroth moment (m_0) is equivalent to the variance of the elevation time series. Caution must be exercised when calculating the higher order moments as they may be unrealistically dominated by high frequency components of the energy spectrum. This issue may be mitigated by applying an appropriate cutoff frequency limiting the range of the spectrum.

The nth spectral moment is defined as:

$$m_n = \int_0^\infty f^n \cdot S(f) df \qquad (2)$$

When examining discrete spectra, or where the spectral function cannot be solved analytically, the following approximation may be applied to calculate the spectral moments:

$$m_n = \sum_{i=1}^N f_i^n \cdot S(f_i) \cdot \Delta f_i \qquad (3)$$

Selected spectral moment expressions (expressed as functions of H_{m0}, T_p and other parameters) are given in ITTC 2003 for the commonly applied parametric spectra.

3.2.2.3 Spectral Bandwidth

The bandwidth of a spectrum may be characterised through a number of dimensionless *bandwidth parameters*. The characterisation of bandwidth is of importance for several reasons. Where a WEC's performance is modelled as a function of frequency the application of a bandwidth parameter potentially allows for a high level assessment of a site or region's suitability without recourse to examination of the full spectrum.

The recommended *sea-state bandwidth parameter*, as also adopted by the MRDF *Preliminary Wave Energy Device Performance Protocol* is defined:

$$\nu = \left[\frac{m_0 \cdot m_2}{m_1^2} - 1 \right]^{\frac{1}{2}} \tag{4}$$

The above formulation is recommended as it mitigates issues encounters in other formulations that use higher order moments (e.g. m_4).

3.2.2.4   Significant Wave Height

The term *significant wave height* tends to be somewhat ambiguous. Traditionally this was defined as the average of the 1/3 largest waves in a record, denoted as $H_{1/3}$. An alternative definition is through the standard deviation (σ) of the elevation time series ($H_\sigma = 4\sigma$). These are both time-domain definitions (i.e. calculated from direct analysis of the elevation time series).

H_{m0} is a measure of significant wave height calculated through spectral analysis ($H_{m0} = 4 \cdot m_0^{1/2}$). This parameter is preferred to the time domain based parameters. The notation H_S for significant wave height is ambiguous in terms of its definition and should be avoided.

3.2.2.5   Mean Wave Period

The mean (zero-crossing) wave period (T_z) is strictly defined as the average of the wave periods obtained through a zero-crossing analysis of the measured elevation time series. It is recommended, however, that the mean period is calculated through analysis of the wave spectrum to allow for a consistent approach for different data sources (e.g. wave buoys vs numerical models).

Two common frequency domain estimates of mean period are T_{01} and T_{02}:

$$T_{01} = \frac{m_0}{m_1}; \qquad T_{02} = \sqrt{\frac{m_0}{m_2}} . \tag{5}$$

$T_{0,2}$ provides an approximation of the time-domain zero-crossing period (T_z).

3.2.2.6   Energy Wave Period

A statistic often utilised when characterising the wave resource is the energy period (T_e):

$$T_e = \frac{m_{-1}}{m_0} . \tag{6}$$

The power output of a particular device may be described using a multi-dimensional power matrix. The power matrix will typically be based on H_{m0} and a parametric period. The use of the energy period may be preferable to mean wave period as it less influenced by high frequency energy (particularly when compared to $T_{0,2}$). The energy period has no time-domain equivalent and must be calculated from the spectrum. In cases where only limited summary statistics are available (typically H_{m0}, T_p, T_z) it is necessary to assume a parametric spectrum from which T_e is calculated.

3.2.2.7   Maximum Wave and Crest Heights

The maximum wave height (H_{max}) and crest height (Cr_{max}) are the largest values measured over a defined period of time. These are time domain parameters calculated through zero crossing analysis of the time series (see §3.5).

3.2.2.8   Wave Steepness

Wave steepness (**s**) parameters may characterise a sea (i.e. global parameters) or individual waves. A particular sea state may be characterised by the peak steepness

$$s_p = \frac{H_{m0}}{L_p} \tag{7}$$

Where L_p is the wavelength associated with the peak period (T_p).

3.2.2.9   Wave Power Level

The wave power level is a measure of the power available per unit of crest length in a unidirectional sea. It is expressed as

$$P_w = \rho \cdot g \int S(f) \cdot c_g \, df$$

where c_g is the wavegroup velocity and c_p is the wave phase velocity

$$c_g = \frac{1}{2} c_p \left(1 + \frac{2 \cdot k \cdot h}{\sinh 2 \cdot k \cdot h} \right) \tag{8}$$

$$c_p = \left(\frac{g}{k} \tanh k \cdot h \right)^{1/2} \tag{9}$$

k is the wave number corresponding to the energy period (T_e) where

$$k = \frac{2 \cdot \pi}{L} \tag{10}$$

and

$$L = \frac{g \cdot T^2}{2 \cdot \pi} \cdot \tanh \frac{2 \cdot \pi \cdot h}{L} \tag{11}$$

where h is the water depth.

In deep water the wave power level may be calculated directly from H_{m0} and T_e,

$$P_w = \frac{\rho \cdot g^2}{64 \cdot \pi} H_{m0}^2 \cdot T_e . \tag{12}$$

3.3 WAVE SPECTRA

Wave spectra can be split into two basic categories. Spectra derived through analysis of a particular wave record and parametric spectra calculated as a function of a set of particular parameters (e.g. wind speed, fetch, H_{m0}, T_p etc.).

3.3.1 Spectral Analysis

The raw measurement from a wave buoy or gauge consists of an elevation time series. In order to represent this measurement in the frequency domain (as an energy spectrum) a number of assumptions must be made.

It is assumed that the recorded period may be assumed to be a stationary process. In basic terms this requires that the spectrum is valid throughout the period of measurement (e.g. 20 minutes for typical wave buoy). This assumption will be more valid for shorter time periods, although this will, in turn, reduce confidence in the calculated spectrum.

3.3.1.1 Fourier Analysis Methods

Fourier analysis is relatively straightforward to apply mathematically. The resulting spectrum is, however, very "noisy" as the energy at the discrete frequencies calculated on a limited duration is highly variable. In order to produce a meaningful spectrum some form of smoothing must be applied to the raw Fourier transform. The level of smoothing must be carefully determined to preserve the underlying structure of the spectrum and is a trade-off between the estimation bias and the noise on the spectrum. Over-smoothing of the spectrum may hide features such as multi-modality and change the bandwidth characteristics.

3.3.1.2 Spectral Resolution

Measured spectra are defined along a discrete frequency vector with a minimum and maximum frequency. The upper limit of the resolution is limited by the duration of the elevation time history. The recommended minimum frequency resolution is 0.01 Hz.

The lower cutoff frequency should be in the range 0.025-0.05 Hz. The recommended upper cutoff frequency is 0.5 Hz. There are several reasons for setting consistent cutoff frequencies.

- It is not possible to derive the spectrum for values higher than the Nyquist frequency (f_c). Spectral energy beyond this point is a mirror of the values for $f < f_c$ and thus presents a potential source of significant error, particular when calculating higher order moments. The Nyquist frequency is a function of the measurement systems sampling frequency (f_{samp}):

$$f_c = \frac{1}{2 \cdot \Delta t} = \frac{1}{2} f_{samp} \tag{13}$$

- The measurement device will have a range over which it will operate effectively. A wave buoy may not, for example, be capable of accurately analysing high frequency elements of the spectrum. Wave buoys may also have difficulty resolving low frequency energy due to the resulting low accelerations.

- The "long tail" of spectra with high cutoff frequencies will have a disproportionably large influence on the higher order spectral moments (e.g. m_2, m_4). These higher order moments are used in some measures of wave period ($T_{0,2}$) and spectral bandwidth. Given that different measurement devices (e.g. buoys vs. wave staff) will have different capabilities in resolving these high frequency components it is important to apply a consistent approach in order to produce comparable results.

A certain amount of energy will be discarded from the analysis by applying cutoff frequencies. While the level of discarded energy will vary depending on the spectral form the setting of consistent limits allows this effect to be understood better. In reality, the energy discarded by the imposition of a cutoff frequency will be small. The influence of cutoff frequencies may be studied

theoretically through analysis of the JONSWAP spectrum, as illustrated below in Figure 8 (upper cutoff) and Figure 9 (lower cutoff). In this example the cutoff frequency has been expressed as a ratio to the peak frequency (i.e. f_{cutoff} / f_p).

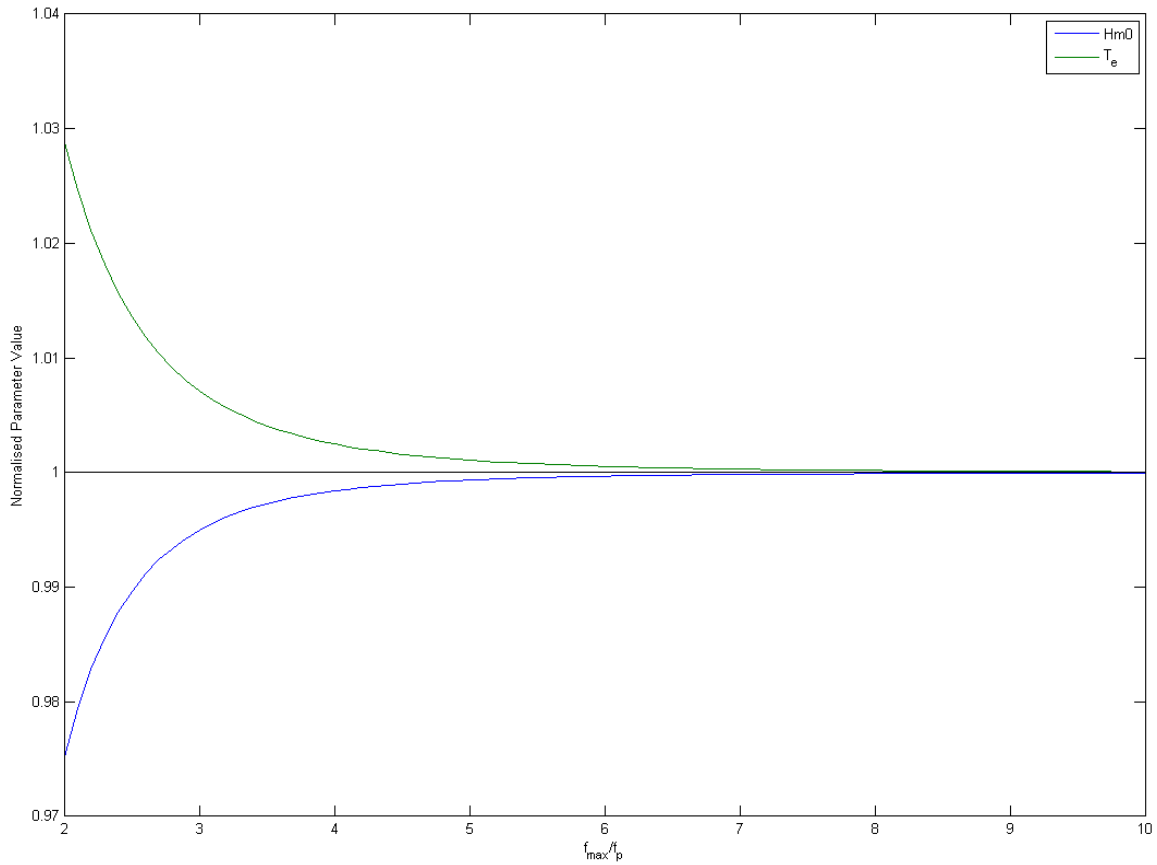**Figure 8** Relative change in H_{m0} and T_e with changing upper cutoff frequency (JONSWAP spectrum with $\gamma = 3.3$)
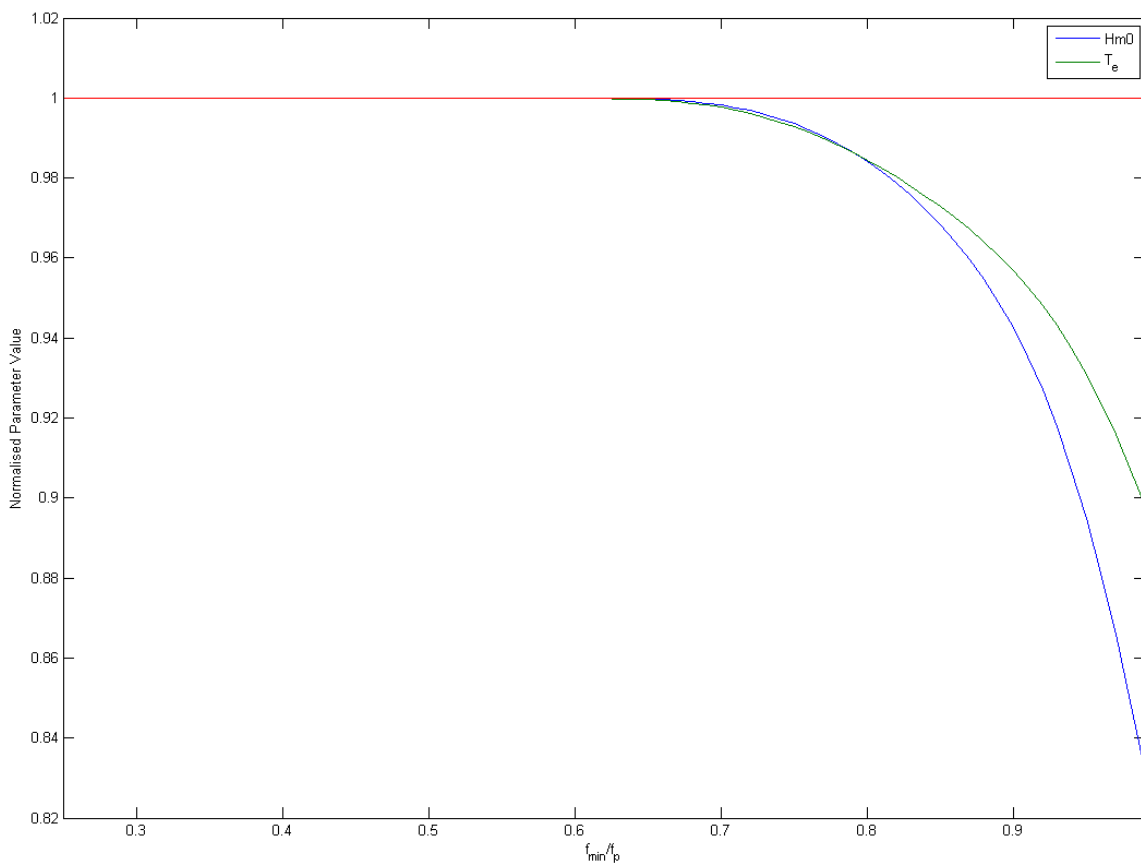

Figure 9 Relative change in H_{m0} and T_e with changing lower cutoff frequency (JONSWAP spectrum with $\gamma = 3.3$)

It is observed in the above analysis that the upper cutoff frequency produces a variation in Hm0 and Te in the order of 3% at low cutoff frequencies. In reality the relative upper cutoff frequency (fmax / fp) will have a value in the order to 4-6. At these levels the error in Hm0 and Te is less than 0.5%. Similarly small variations are seen in the analysis of the lower cutoff frequency.

3.3.1.3 Directional Distributions

The energy spectrum describes the mean energy available at a certain frequency. The direction of energy propagation at a certain frequency is described through the application of a directional distribution, $D(f,\theta)$.

The directional distribution allows the proportion of energy propagating over a directional range to be described for a given frequency of the spectrum. This distribution may be defined as a matrix describing discrete values over the range of frequencies and directions. It is more common, however, for the distribution to be described as a Fourier series for a particular frequency:

$$\hat{D}(f,\theta) = \frac{1}{2\cdot\pi} + \frac{1}{\pi}\sum_{n=1}^{N}\left[a_n \cdot \cos(n\cdot\theta) + b_n \cdot \sin(n\cdot\theta)\right] \tag{14}$$

In the majority of cases (e.g. from a buoy or other single point measurement) only four Fourier coefficients will be available (i.e. a_1, b_1, a_2, b_2). The a_0 coefficient is not usually explicitly included as it is equal to unity by definition.
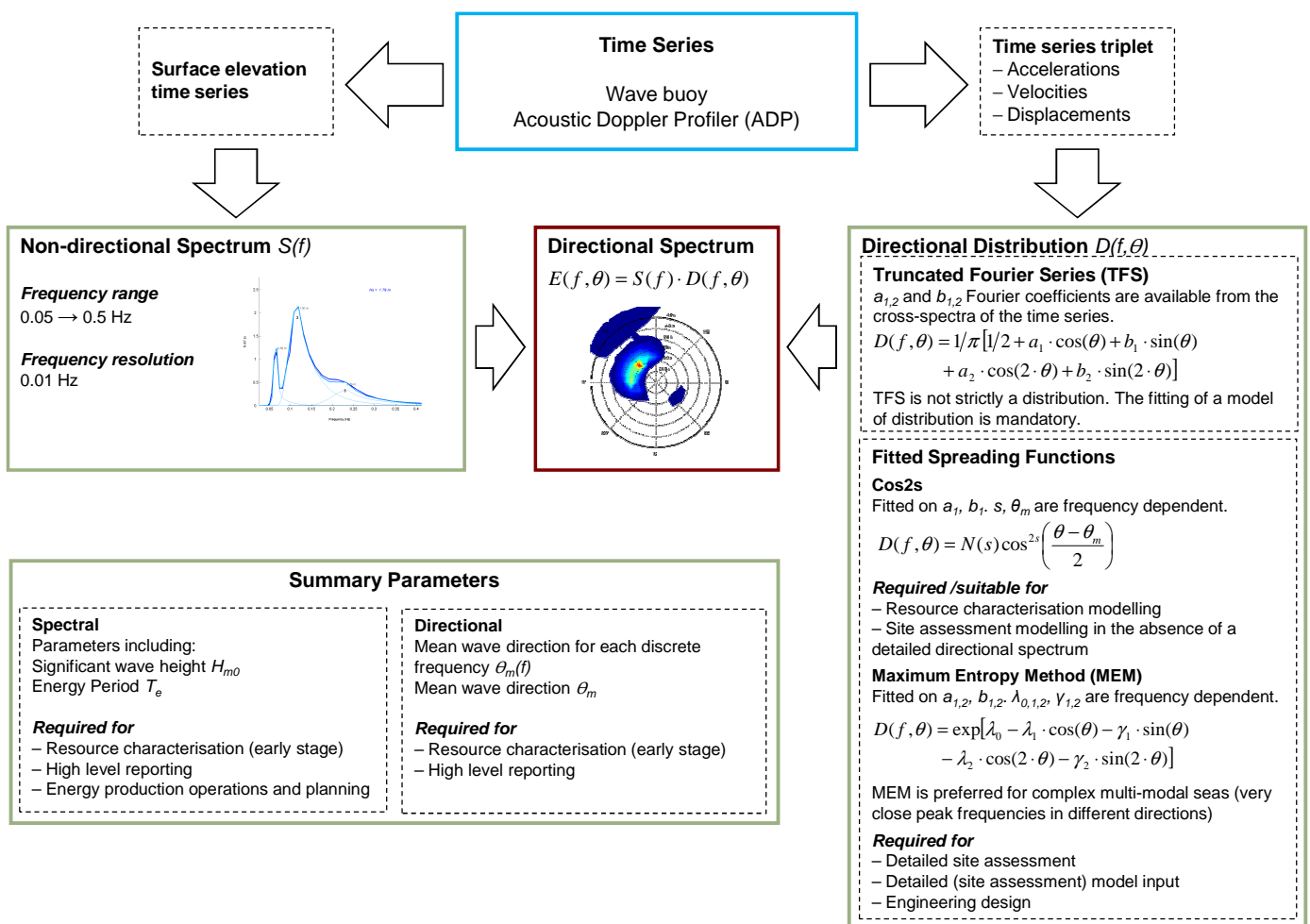

Figure 10 Calculation of the directional spectrum from the raw time series data

The Directional Distribution Function or Directional Spreading Function (DSF), $D(f,\theta)$ can be estimated from measured data by various methods [Benoit et al., 1997]

   a.   Fourier Series decomposition method
        (i) Truncated Fourier Series decomposition method
        (ii) Weighted Fourier Series decomposition method
   b.   Parametrical methods
        (i) Direct fitting to parametrical models
        (ii) Statistical fitting to unimodal parametrical models
   c.   Maximum Likelihood methods
        (i) Maximum Likelihood Method (MLM)
        (ii) Iterative Maximum Likelihood Methods (IMLM)
        (iii) Eigenvector methods
        (iv) Long-Hasselmann method
        (v) Maximum Entropy Method
        (vi) Extended Maximum Entropy Principle
        (vii) Bayesian Directional Method
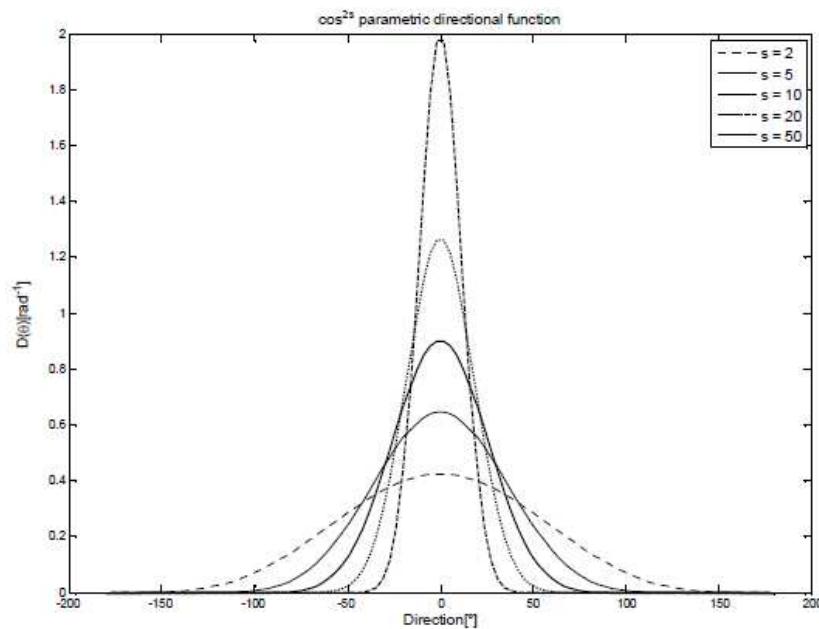
Figure 11 $\cos^{2S}$ parametric directional function for various spreading values (s)

In the absence of measured directional distribution functions, a theoretical function can be used. The popular models are

   (a) Cos-2s model (Longuet-Higgins et al, 1963, Mitsuaysu et al, 1975, Hasselmann et al, 1980):

$$D(f,\theta) = \frac{2^{2s-1}}{\pi} \frac{\Gamma^2(s+1)}{\Gamma(2s+1)} \cos^{2s}\left(\frac{(\theta-\theta_0)}{2}\right) \tag{15}$$

where, $\Gamma(.)$ is the Gamma function and 's' is a function of the wave frequency, θ is the wave direction and θ_0 is the mean wave direction. For practical purposes the value of 's' corresponding to the peak of the spectrum is used [Tucker & Pitt, 2001].

Mitsuaysu et al, 1975 proposed values for 's',

$$s = \begin{cases} s_p \left(\dfrac{f}{f_p}\right)^5 & f < f_p \\[3mm] s_p \left(\dfrac{f}{f_p}\right)^{-2.5} & f \geq f_p \end{cases} \tag{16}$$

where s_p is the value of 's' at the spectral peak, f_p and is given by

$$s_p = 11.5 \left(\frac{U_{10}}{c_p} \right)^{-2.5} \tag{17}$$

Where U_{10} is the wind speed at 10m above sea level and $c_p = g / 2\pi f$, is the deepwater phase speed at the spectral peak.

From North Sea project JONSWAP, Hasselmann et al, 1980, proposed,

$$s = \begin{cases} 6.97 \left(\dfrac{f}{f_p} \right)^{4.06} & f < 1.05 f_p \\[3mm] 9.77 \left(\dfrac{f}{f_p} \right)^{\mu} & f \geq 1.05 f_p \end{cases} \tag{18}$$

Where, μ is related with wave age by

$$\mu = -2.33 - 1.45 \left(\frac{U_{10}}{c_p} - 1.17 \right) \tag{19}$$

(b) The Wrapped-Normal distribution

$$D(f, \theta) = \frac{1}{\sigma \sqrt{2\pi}} \exp \left(\frac{(\theta - \theta_0)^2}{2\sigma^2} \right) \tag{20}$$

where, σ is the 'rms' angular spread and is a function of frequency.

(c) Cos^n model (Longuet-Higgins et al, 1963, Mitsuaysu et al, 1975, Hasselmann et al, 1980):

$$D(f, \theta) = \begin{cases} \dfrac{\Gamma \left(1 + \dfrac{n}{2} \right)}{\sqrt{\pi} \, \Gamma \left(\dfrac{1}{2} + \dfrac{n}{2} \right)} \cos^n (\theta - \theta_0) & for \; -\pi/2 < \theta - \theta_0 < +\pi/2 \\[3mm] 0 \quad elsewhere \end{cases} \tag{21}$$

where, $\Gamma(.)$ is the Gamma function. Typical values of 'n' for wind sea are n= 2 to 4 and for swell $n \geq 4$

3.3.2   Parametric Spectra

A parametric spectrum is defined as a function of a number of oceanographic parameters. Traditionally they are functions of geographical and meteorological parameters (e.g. fetch and wind speed at a defined altitude). For engineering purposes it is more useful to define the spectra in terms of the global parameters (i.e. H_{m0}, T_p etc.).

The most common formulations encountered are the Pierson-Moskowitz (P-M) and JONSWAP spectra.

3.3.2.1   Pierson-Moskowitz Spectrum

The P-M spectrum is based upon the assumption of fully developed seas with effectively infinite fetch. It is given by

$$S(f) = \alpha g^2 (2\pi)^{-4} f^{-5} \exp \left[-\frac{5}{4} \left(\frac{f}{f_p} \right)^{-4} \right] \tag{22}$$

where, $f_p =$ peak frequency of the spectrum, $\alpha =$ Philips constant $= 0.0081$

3.3.2.2   JONSWAP Spectrum

The JONSWAP spectrum is an empirical spectrum borne out of measurements made in the North Sea (Hasselmann *et al.*, 1973) to take into account the limited fetch and non-saturated seas. The JONSWAP spectrum is a function of H_{m0}, T_p and γ (the Peak Enhancement Factor) where $1 \leq \gamma \leq 7$. The spectrum becomes progressively more narrow banded with increasing γ. The spectrum may be regarded as a modified P-M formula. The JONSWAP spectrum is expressed as

$$S(f) = \alpha g^2 (2\pi)^{-4} f^{-5} \exp\left[-\frac{5}{4}\left(\frac{f}{f_p}\right)^{-4}\right] \gamma^{\exp\left(\frac{-\left(f-f_p\right)^2}{2\sigma^2 f_p^2}\right)} \tag{23}$$

where, f_p = peak frequency of the spectrum, α = Philips constant = 0.0081, γ = peak enhancement parameter, which is the ratio of the maximum spectral energy to the maximum of the corresponding Pierson-Moskowitz (PM) spectrum and for this spectrum γ =1.

$$\sigma \quad = \quad \begin{cases} \sigma_a & for \quad f \leq f_p \\ \sigma_b & for \quad f \geq f_p \end{cases} ; \quad \sigma_a \text{ and } \sigma_b \text{ define the left and right side widths of the spectrum.}$$

A mean Jonswap spectrum is defined by $\gamma = 3.3$, $\sigma_a = 0.07$ and $\sigma_b = 0.09$.

3.3.2.3   Spectral Formula Selection and Fitting

Parametric spectra may be used for a variety of purposes which will in turn influence the selection of the formula. Uses include:

To produce a spectra where only limited summary statistics are available (e.g. significant wave height, peak period, mean period etc.). The choice of spectra will influence the calculation of parameters such as the energy period, and other parameters derived from the spectral moment.

To produce a spectral input to a numerical model where a full spectral description is not available (or desirable).

To provide a parametric fit to a measured elevation time history. If a parametric spectrum provides a good fit to the measured spectra it may be used as the basis of a regional model to characterise a particular location.

In deep water with no fetch limitations the P-M spectrum may provide a good approximation for actual spectrum. In cases where the sea states are more complex, however, the JONSWAP spectrum should be considered as the most desirable formulation. This requires some basis for the choice of γ (the peak enhancement factor). A common choice is to use an average value of 3.3.

3.3.3   Spectral Partitioning

The most comprehensive description of a sea-state is provided by its energy spectral density or directional spectrum which characterises the distribution of wave energy as a function of joint frequency and direction (see above). For engineering and design purposes, when using analytical models, spectral densities are usually approximated by mean of parametric functions (JONSWAP, Pierson-Moskowitz, Bretschneider, ITTC etc.), which analytical definition was obtained from statistical analysis of large data bases. These functions are characterised by a set of parameters which can be derived from spectral moments m_n and which can be related to statistical properties of sea-states.

Main parameters are the significant wave height, H_{m0}, which is related to the global energy level of the sea state, a period (either the mean or peak period) and a direction (either mean direction or direction at peak period).

Because of its unimodal form (one single peak and direction), such a parametric representation induces a loss of information. Especially it does not allow an accurate depiction of complex sea-states, superimpositions of two or more wave systems, such as wind-sea and swells. Complex, or multimodal sea-states are more frequent than generally assumed. A unimodal description would lead for instance to an erroneous estimate of the extracted power for an energy converter with a given spectral bandwidth (Kerbiriou 2007). This would be even worse if considering a device with sensitivity to wave directionality.

Methods have been developed (Hanson 2001, Kerbiriou 2007) for partitioning sea-states into wave systems from analysis of directional spectra. Such methods allow splitting the energy between the existing wave systems; each defined by a peak so that the directional spectrum can be described as the summation of parametric unimodal frequency spectra, each associated with a direction and a directional distribution.

Energy distribution as a function of frequency of each wave system is characterized by any of the usual parametric functions (fitting the most appropriate). Energy distribution as a function of direction is also characterized by a parametric function. One of the most widely used is the $\cos^{2S}$ function (Mitsuyatsu, 1975) where s is the directional spreading but other alternative distributions such as Gaussian, Poisson, von Mises can also be applied.

One has to note that in spite of advanced methods such as the Maximum Entropy Method (Lygre and Krogstad 1986, Benoit & al. 1997), it is difficult to provide an accurate estimate of the directional distribution of the wave spectrum. Characterization of directionality of wave systems remains of major importance not only for long term power assessment but also for management of marine operation and survivability studies.

3.4   SEA STATE STATISTICS

3.4.1   Scatter Diagrams

Scatter diagrams allow the presentation and analysis of multiple sea states measured over a period of time at a certain location. These diagrams should plot H_{m0} against a measure of period T^* (T_p, T_{02} or T_e) in tabular form, although other combinations of parameters may be used. Each bin in the table shall represent the relative frequency of occurrence of that particular H_{m0}-T^* combination.

Scatter diagrams illustrating H_{m0} and T_e shall be produced to allow direct calculation of the mean wave power. If records of H_{m0} and T_e are not available due to the historic nature of the dataset this limitation should be noted and alternative scatter diagrams produced using significant wave height ($H_{1/3}$ or H_σ) and mean period ($T_{02,}$ T_z or T_{01}).

Scatter diagrams shall be produced to summarise the annual wave resource. Seasonal diagrams corresponding to *winter* (December, January, February), *spring* (March, April, May), *summer* (June, July, August) and *autumn* (September, October, November) may additionally be presented.

Scatter diagrams shall meet the following requirements:

- Each bin shall display the cumulative occurrences of the H_{m0}-T^* pair. Normalised scatter diagrams may additionally be presented, but the total number of data points used must be stated.
- H_{m0} bins shall be defined in 0.5m intervals over the range 0.5 to 15m
- Wave period (T_e, T_{pc}, T_{02}) bins shall be defined in 0.5s intervals over the range 0.5s to 25s
- Bin boundaries shall be defined by the relationship: *lower limit* $< H_{m0}$, $T_e \leq$ *upper limit*
- The minimum and maximum bins shall have no lower and upper limit respectively. i.e. all H_{m0} observations exceeding 12m shall be contained within the largest bin. This shall be reflected in the axis labels

Scatter diagrams displaying H_{m0}-T_e pairings may be translated into expected gross wave power levels (§3.2.2.9). If the power output of a particular WEC is being considered it is necessary to refer to the *power matrix*. The power matrix gives the expected power output (in kW) for a particular combination of H_{m0} and period (typically T_e), calculated from a combination of tank testing, site testing and numerical modelling.

3.4.2   Power Matrices

Scatter diagrams characterise the sea state and may be used (in the case of H_{m0}-T_e pairings) may be translated into expected gross wave power levels (§3.2.2.9). If the power output of a particular WEC is being considered it is necessary to refer to the *power matrix*. The power matrix gives the expected power output (in kW) for a particular combination of H_{m0} and period (typically T_e). Typically this data will be from a combination of tank testing, site testing and numerical modelling.

While device specific characteristics are outwith the scope of this work, it is recommended that if power matrices are applied they be produced in line with the applicable recommendations for scatter diagrams given above (i.e. limits and resolution of the axes).

It should be noted that it is not likely to be possible to fully express the device power output as function of H_{m0} and T_e. It is important to know the conditions under which the power output is defined so as to make an informed judgement as to its validity at a particular site. For example, the power output for a particular H_{m0}-T_e pair is likely to be predicted using an idealised parametric spectrum (§3.3.2) and simple spreading function. Examination of directional spectra at the deployment site is necessary to understand the validity of these assumptions.

3.5   WAVE BY WAVE ANALYSIS

Wave by wave analysis refers to the process of analysing the elevation time history at a particular site. This analysis may yield both integrated (e.g. significant wave height) and individual wave parameters (e.g. heights and periods). Individual wave forms may be of importance to the assessment of device performance and survivability. Many of these parameters may be expressed probabilistically through the use of parametric probability distributions.

Wave by wave analysis will not usually be required for resource assessment purposes and it is not recommended that this type of analysis is used to obtain integrated parameters. Information describing individual wave forms may, however, be required for some studies and for engineering design purposes.

3.5.1   Zero-Crossing Analysis

3.5.1.1   Zero-Crossing Definitions

The elevation time series is divided into individual waves by similar zero-crossing, either up or down. The choice of up or down crossing makes little or no difference to the global statistics the distinction may be important when examining the largest events. If large, or steep, crest fronts are of importance to device performance it is intuitively more correct to define the wave through zero down-crossing analysis (as the wave will have the trough preceding the crest). The distinction between the zero crossing waves is usually only of importance when examining the wave height, period and steepness. More detailed characterisation of the wave

form involves dividing each crest and trough into two segments, with four segments forming a complete wave. This approach allows for the calculation of a number of parameters, as outlined in §3.5.2 below.
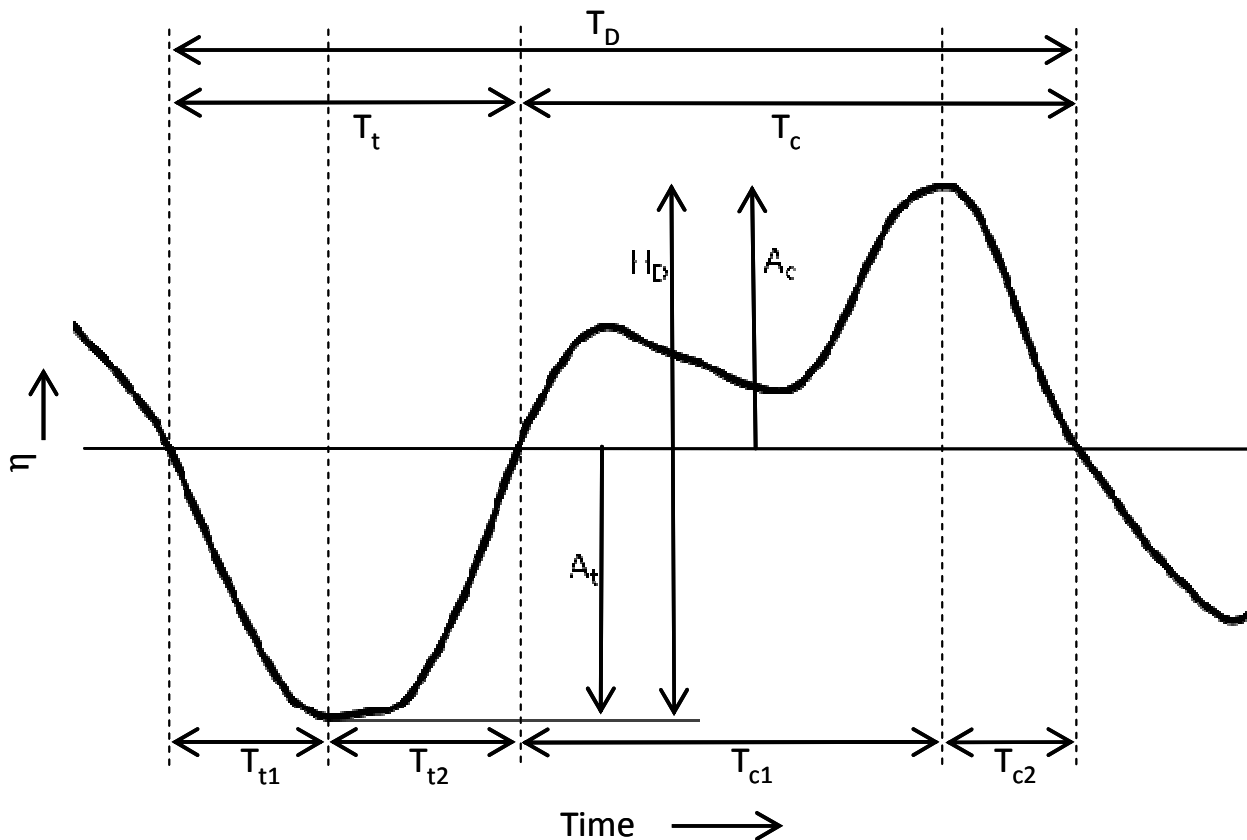

Figure 12 Zero-Crossing Definitions

The definitions of individual wave height and period are described graphically in Figure 12. Also illustrated are the time intervals associated with describing portions of an individual down-crossing wave. The simplest time interval is the zero crossing period. The wave may then be further decomposed into its crest and trough components. The associated durations may are usually referred to as the crest and trough period (T_c and T_t respectively), although the use of term "period" is not strictly correct. The crest and troughs may be further divided into their "front" and "back" sections. Thus a zero down-crossing wave is described by two elevation parameters (A_c and A_t) and four time parameters (denoted here as T_{t1}, T_{t2}, T_{c1}, T_{c2}). The successive wave parameters are denoted as (T'_{t1}, T'_{t2}, T'_{c1}, T'_{c2}).

3.5.1.2   Mean Water Level Correction

In a laboratory setting the zero-crossing points are defined as the point at which the surface elevation passes through the mean level (MWL). Tidal variations make the definition of the SWL more complex for measurements made at sea. In the case of records not exceeding several hours (i.e. less than half a tidal cycle) a parabolic fit to the elevation time history may be used to correct the MWL. This is particularly important for recording devices mounted to a fixed reference point, such a platforms and coastal structures. It is less critical for floating devices such as wave buoys which may not be capable of resolving these very low frequency components.

3.5.1.3   Sampling Rate and Interpolation

An elevation time-series consists of a number of discrete data points, usually logged at a constant frequency. If the sampling rate is high relative to the height and length of the wave the value of the zero-crossing and turning points may be taken as the nearest appropriate data point. This will introduce an inaccuracy when calculating the individual periods and the values of the crest and trough amplitudes will be underestimated. Given that wave buoys commonly archive data at only 1 Hz even quite large waves may be described by relatively few data points (e.g. < 10). It is therefore necessary to apply some form of interpolation and extrapolation to correctly calculate the crossing and turning points.

Goda (2000) recommends a simple linear interpolation for the calculation of the zero crossing point and a parabolic fit (using three data points) for the calculation of the crest and trough amplitude.

$$\eta_{crest/trough} = C - \frac{B^2}{4 \cdot A} \tag{24}$$

where

$$A = \frac{1}{2}\left(\eta_{i-1} - 2 \cdot \eta_i + \eta_{i+1}\right), \tag{25}$$

$$B = \frac{1}{2}\left(\eta_{i+1} - \eta_{i-1}\right) \tag{26}$$

and

$$C = \eta_i. \tag{27}$$

η_i is the largest positive or negative (for crest and trough respectively) discrete elevation measurement lying between two zero-crossing points. The same parabolic relationship may be used to estimate the crest/trough time:

$$t_{max} = t_i - \Delta t \cdot \frac{B}{2 \cdot A} \tag{28}$$

where Δt is the sampling interval.

While the above method is straightforward to apply the linear interpolation is visually incorrect when sample rate is relatively low. Anomalies may also be encountered when the linear interpolation and parabolic fit share the same data points, as may occur with the smallest waves in a record. While these small waves may not be of interest they may introduce practical difficulties when processing large datasets.
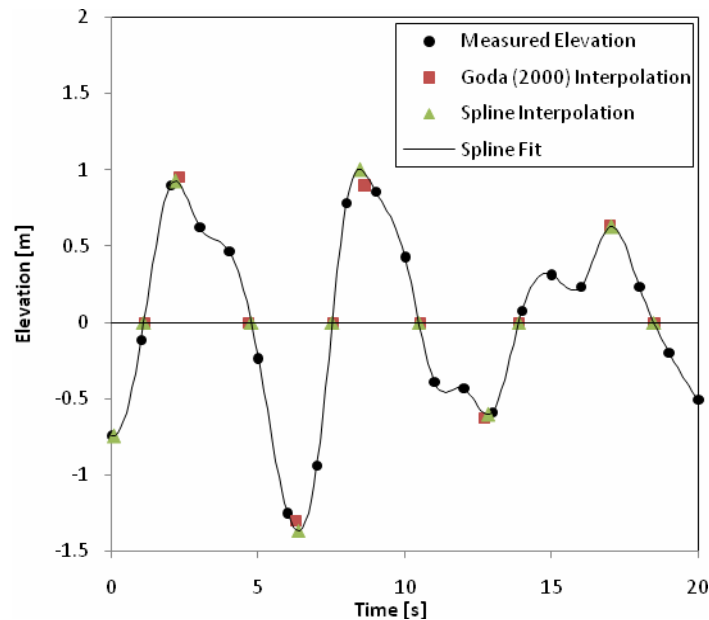

Figure 13 Zero-crossing, crest and troughs interpolated using the method of Goda (2000) and a least-squares fit cubic spline (piecewise polynomial).

The alternative approach explored here is to fit a piecewise polynomial (cubic spline) to the elevation time series using a least-squares method. The region between each data point is described by a degree 4 polynomial, as illustrated in Figure 13. Zero-crossing points may be interpolated by taking the roots of the polynomials crossing the mean water level. Crests and troughs are identified from the derivatives of the polynomials.

3.5.2 Wave Shape Characterisation

Wave height and crest statistics may not always be sufficient to predict a MEC's behaviour at a particular site. It may be the case that both the wave magnitude and its shape are important when assessing the response of the device. The exact nature of this response will be dependent on the design of the individual device. There are, however, a number of parameters which may be used to characterise the shape of an individual wave (or portion of a wave). Details of these parameters are outlined below.

The steepness of an individual wave is the ratio of height to length:

$$s = \frac{H}{L}. \tag{29}$$

The wavelength (L) is calculated from the dispersion relationship

$$L = \frac{g}{2 \cdot \pi} \cdot T^2 \cdot \tanh \frac{2 \cdot \pi \cdot h}{L} , \qquad (30)$$

where h is the water depth. In deep water the relationship reduces to

$$L = \frac{g \cdot T^2}{2 \cdot \pi} . \qquad (31)$$

The steepness (s) is a fairly simple definition of wave shape as it gives no indication on the form of the wave between the crest and the preceding trough. An alternative method (Myrhaug *et al.*, 1986) is the crest front steepness

$$s_{cf} = \frac{A_C}{(g/2 \cdot \pi) \cdot T_D \cdot T_{c1}} . \qquad (32)$$

4   TIDAL PARAMETERISATION
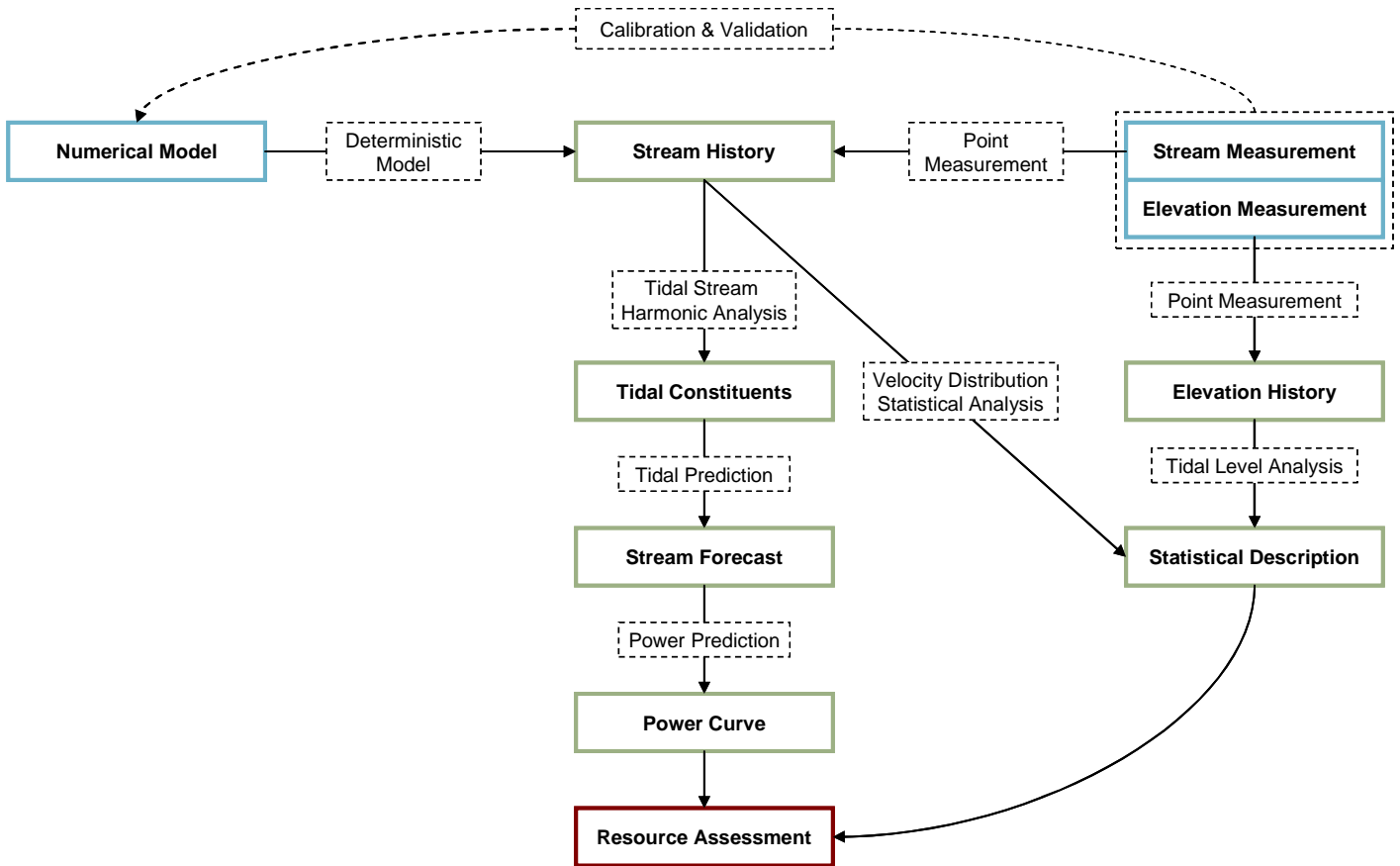
4.1   DESCRIPTION

Figure 14 Data sources and analysis methods for tidal resource assessment

The principal goal is to determine the power generation capability of a tidal flow. The available power in a tidal stream is proportional to the cube of the flow speed. Thus, the total energy available is

$$E_{tot} = \int_t \rho A |u|^3 \, dt \qquad (33)$$

where ρ is the density of the water, u is the flow speed and A is the flow cross-sectional area.

The principal characterisation of the tidal flow is whether a tide is diurnal or semi-diurnal. This is simply whether a site experiences one or two tides per day. More generally, a tidal signal is usually described by the combination of number of signals of different frequencies. The principal tidal signal is usually the moons twice-daily tide. This component follows the moon with a mean rotational period of 12.42 hours. This is commonly known as the M_2 tide. The sun's twice daily tide is commonly known as the S_2 tide, and follows the sun with a period of 12 hours. The timing of high tide in relation to the position of the sun and moon in the sky changes according to location. The interaction of the lunar and solar tides leads to the spring/neap cycle.
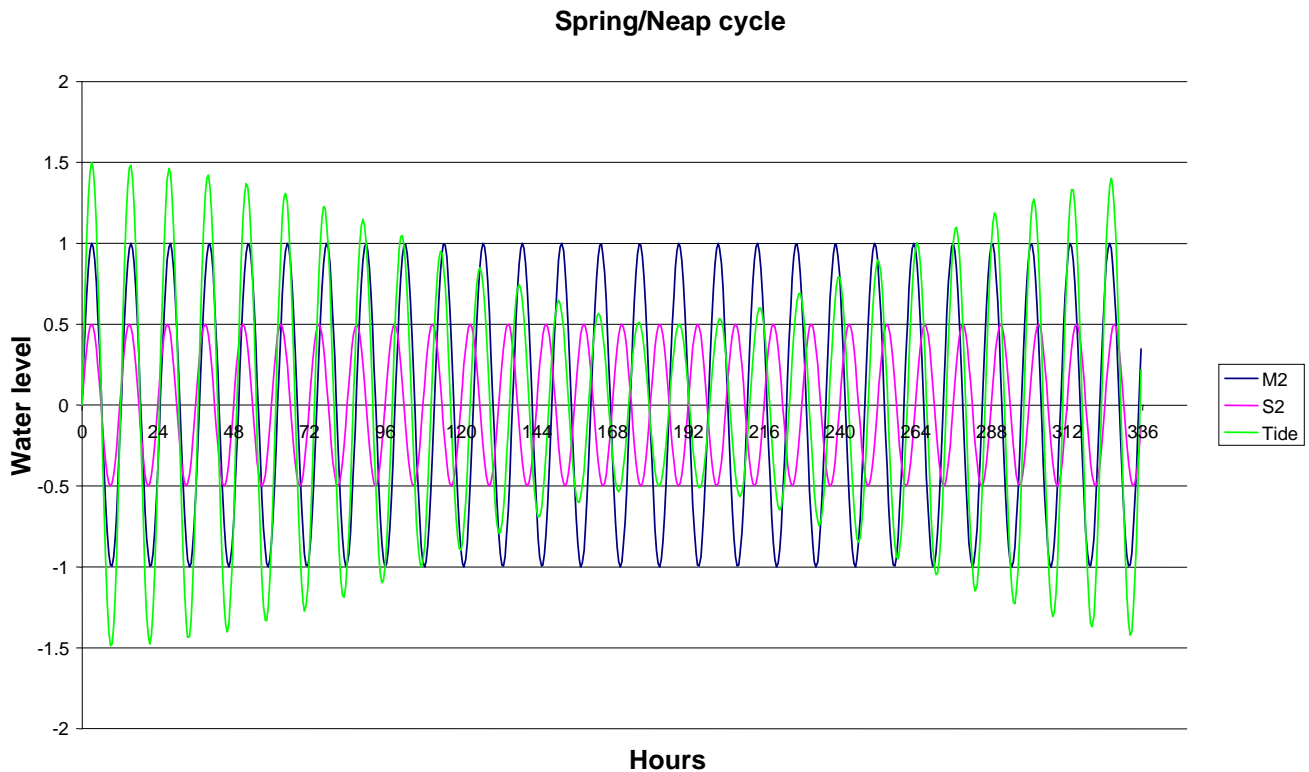
Spring/Neap cycle

Figure 15 (a) : Spring/Neap cycle

When the lunar and solar signals are in phase, the tides are higher, and when the signals are out of phase, they are lower. The principal daily constituents are generally the lunar daily signal, with a period of 25.82 hours, known as O1 and a combined luni-solar signal called the K1 tide, with a period of 23.93 hours. The factor $F = (K_1+O_1)/(M_2+S_2)$ generally distinguishes diurnal (F>3)and semi-diurnal tides(F<0.25), with mixed tides of (0.25<F<3). Analysis of tidal elevations over sufficiently long records shows a large number of components. NOAA typically provide 37 constituents for principal tidal stations.

In shallow water, typical of tidal MECS, higher frequency components such as M_4 and M_6 are known. These change the shape of the tidal curve from a plain sinusoid to some other shape. Statistical properties of the flow may be related to these higher harmonics.

A tidal current in a channel is usually low or zero at times of high and low tidal elevation (slack water), and has a peak flow as the water level passes somewhere near the mean level. This example shows data taken at the EMEC test site.
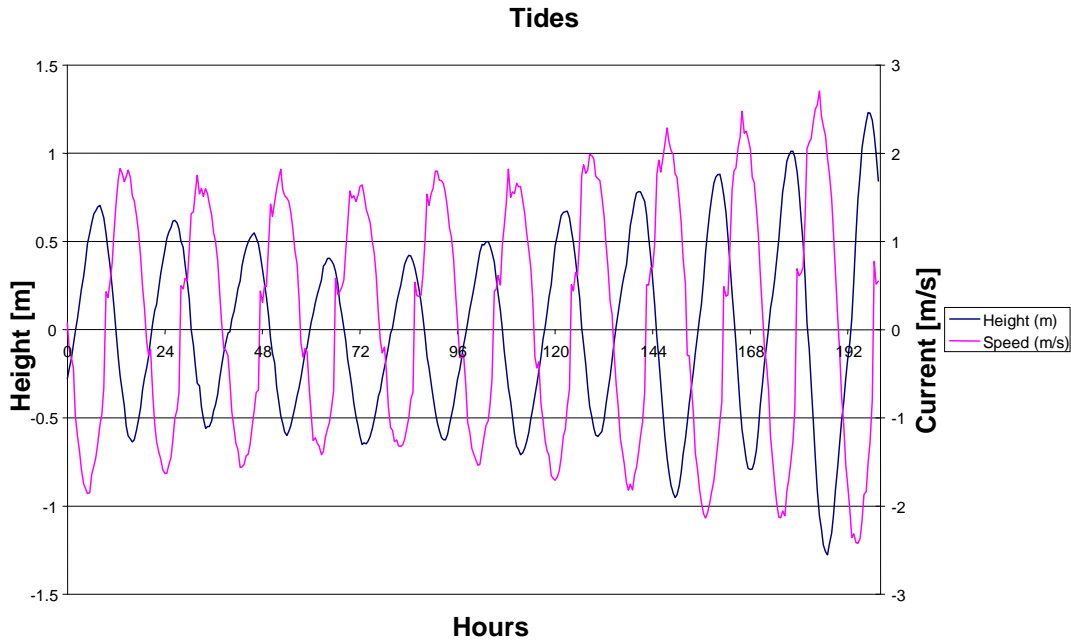
Tides

Figure 16 (b) : Tidal current

The tidal currents can be analysed for harmonic components in the same way as the tidal heights. Parameterisation is performed to describe the general trends of the tidal signal.

Tidal analysis is used to determine the magnitude of the flow over timescales of minutes and hours. Also of interest to the developer are the characteristics of the flow over seconds (usually caused by local waves) and sub-second timescales (generally referred to as turbulence).

The quantification of turbulence is a topic of ongoing research.

4.2   PARAMETERISATION METHODS

4.2.1   Tidal Analysis

4.2.1.1   Harmonic Analysis

The classical method of tidal analysis is the harmonic analysis referred to above. The signal is decomposed into a number of components, and the process may be shown as

$$\eta = \sum_{harm=\{list\}} A_{harm} \cos(\omega_{harm} t - \phi_{harm}), list = \{M_2, S_2, O_1, K_1, P_1, Q_1, N_2, K_2, M_4, ...\}, \text{ where } \omega_{harm} \text{ is the frequency, and } \phi_{harm}$$

is the phase of component *harm.*

The number of components that may be resolved is dependent on the available length of data to analyse, as the frequencies of many of the components are rather close. The process is highly detailed, and reference should be made to a document such as the Admiralty Manual of Tides.

A minimum of 14 days analysis is needed to resolve the M_2 and S_2 tides. The present recommendation from DECC is that 30 days analysis is required to distinguish enough components for TEC power estimation.

Analysis of tidal streams at a series of vertical layers is required establish the vertical profile structure.

4.2.1.2   Fourier analysis

Harmonic analysis only extracts from the observations the astronomical signals in the record. An alternative method is the use of fourier analysis, which decomposes the signal into regularly spaced frequencies.

$$\eta = \sum_{j=1}^{N} A_j \cos(j\omega_0 t - \phi_j) \tag{34}$$

The analysed frequencies no longer correspond to the astronomic components. This method however may reveal non-gravitational influences, and meteorological noise in the signal. This may be of particular benefit to studying storm surges. The principal

drawback in this method is the requirement for long data sets. Generally satisfactory results cannot be obtained for observations shorter than a year.

4.2.1.3   Statistical analysis

The available energy in a flow will vary according to theshape of the tidal signal. To illustrate, consider two following two example tidal flows. These are composed of an M_2 tide of 1m/s and an M_4 tide of 0.5 m/s. The phases of the respective M4 components are however different.

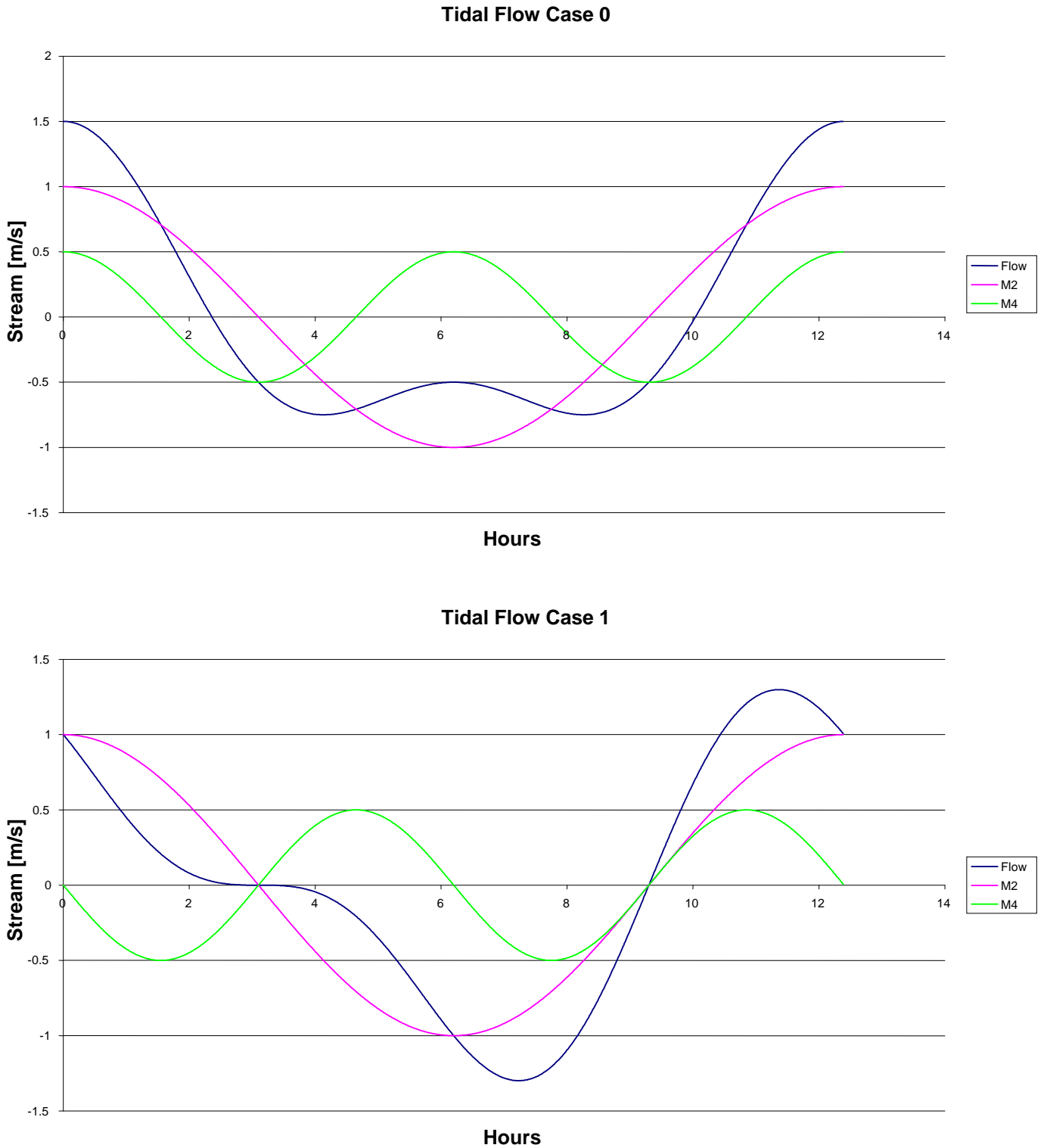**Tidal Flow Case 0**

Tidal Flow Case 1

Figure 17 (c) : Tidal flow

Case 0 has a phase difference of 0 between the two signals. The tidal stream has a maximum flood of 1.5m/s and a maximum ebb of 0.75 m/s. Case 1 has a phase difference of approximately 3.1 hours (in fact, half of the period of M_4) between the two signals,

and has maximum flood and ebb both of 1.30 m/s. The available power density for case 0 is approximately 54.2 m^3/s^2, and the power density for case 1 is approximately 56.1 m^3/s^2.

Plotting the change in power with regard to M_4 lag, it can be seen that case 1 is the maximum power production for a signal compose purely of M_2 and M_4, and case 0 is the minimum.

Power phase comparison
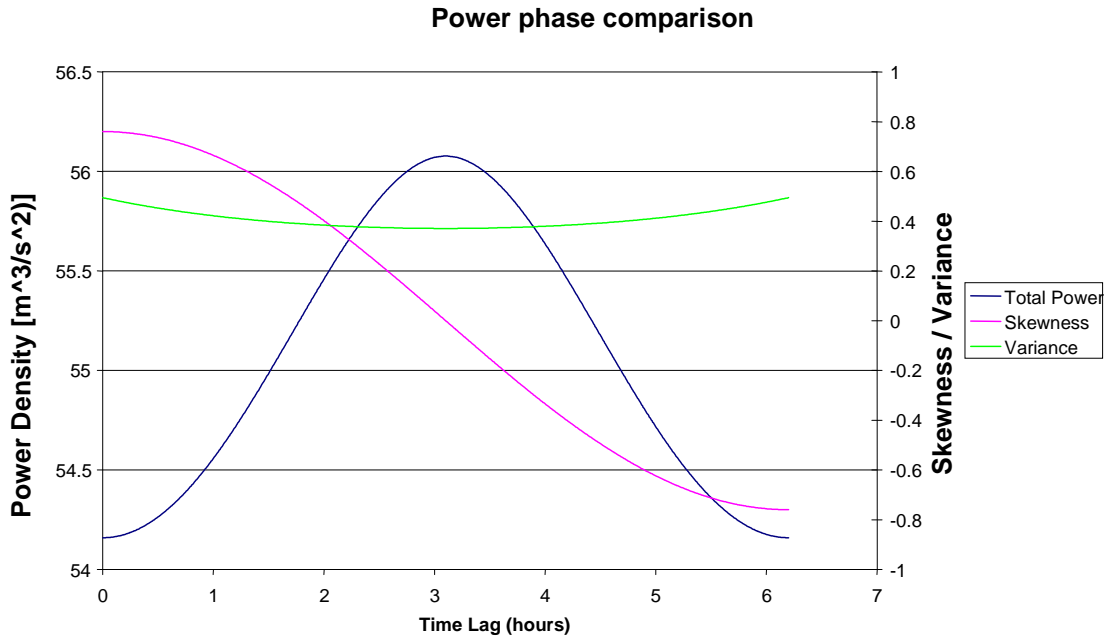
Figure 18 (d) : Tidal power

Also indicated are the statistical skewness and variance for comparison. These are parameterisations of the asymmetric nature of the flow, and hence the 'balance' of power production between ebb and flood.

Comparisons may also be made by the exceedence figure. This illustrates the proportion of time at which a particular power level may be generated. (Typically, a TEC will have a cut in speed, below which there is no generation. This is not reflected here.) It is found for example that with case 0, power production is at 1 m^3/s^3 for only 20% of the cycle, whereas for case 1 this threshold is reached 30% of the time. Considering then the threshold of 2 m^3/s^3 the position is reversed with case 0 generating at or above this point for about 15% of the time compared to case 1 with only 10%.

Power Production Exceedence

Figure 19 (e) : Tidal power exceedence

4.2.2   Turbulence analysis

The measurement of turbulence is important for considerations of blade loading with varying flows. Two measures are presently used, and the topic is still the subject of much research.
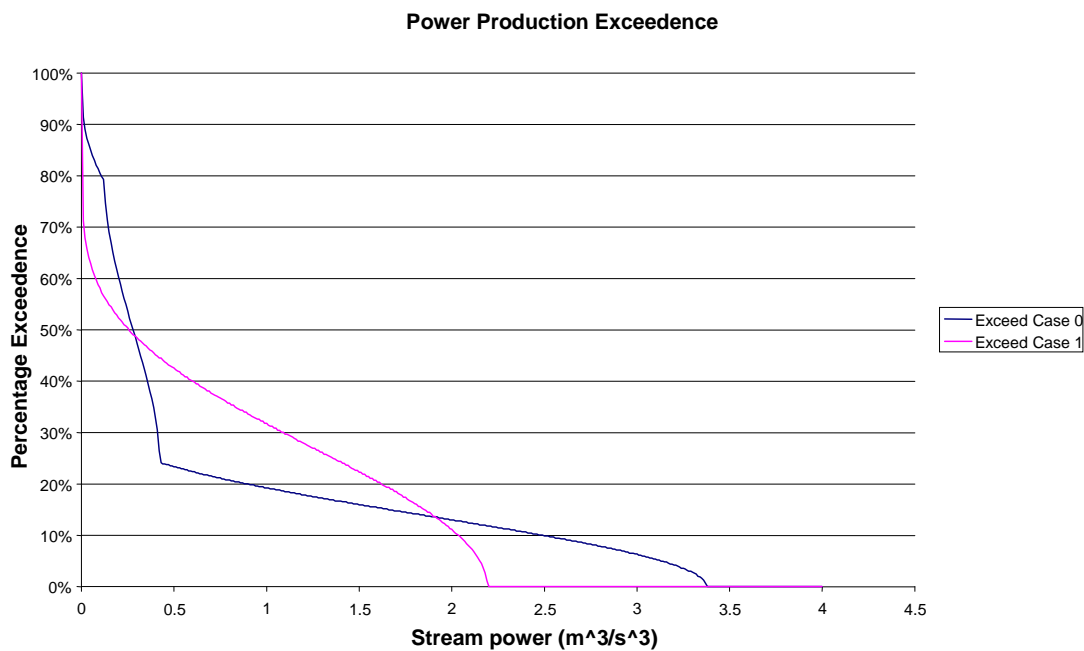
4.2.2.1   Turbulence Intensity

The flow may be characterised by assuming the instantaneous flow U_i is the sum of the mean flow plus the local instantaneous variation.   Thus,

$$U_i = \overline{U} + \hat{u}_i, \quad \overline{U} = \frac{1}{N}\sum_{i=1}^{N} U_i \tag{35}$$

then $\hat{u} = \sqrt{\dfrac{1}{N}\overline{\hat{u}_i}}, TI = \dfrac{\hat{u}}{\overline{U}} \times 100\%$ $\hspace{4cm}$ (36)

The calculated intensity is sensitive to the spatial resolution of the measurement. The averaging length N also needs careful choice to provide a satisfactory smoothing of the mean flow. Turbulence intensity provides no indication of the frequency of the variation, or the spatial scale.

4.2.2.2   Auto spectral density

Fourier analysis of the horizontal and vertical velocities can yield information on the frequency and indirectly the spatial scale of the velocity fluctuations. Results from this analysis are limited however by the measurement technique. As the measuring volume of a typical ADP increases with distance from the sensor, the cut-off frequency of turbulence measurements necessarily reduces.

5   WAVE-CURRENT INTERACTION

5.1   GENERAL

Wave-current interaction is an important issue for modelling of ocean renewable energy converters as all devices can be submitted to the combined waves and currents effects, especially marine current turbines.

Various situations may occur at sea with different waves spectrum and different current profiles and directions. On the shore, the current direction may be perpendicular to the waves direction. In estuaries or in straits, the current direction may be parallel to the waves direction and alternatively following or opposing the waves.

The long waves coming from ocean encounter areas with varying incident currents and varying effects. The bathymetry also influence both the waves and the current and together the wave-current interaction.

In addition, the boundary layers on the sea bottom and on the free surface interacting with wind have a strong influence on the current velocity profiles which may be characterised by the vorticity distribution.

5.2   MODELLING METHODS

5.2.1   Monochromatic first order waves and uniform current

g	gravity acceleration
h	uniform water depth
ω	wave pulsation
k_o	wave number in infinite depth without current
k	wave number in presence of a current and for the given water depth
U	uniform current parallel to the wave direction

The simplest approach under the perfect fluid assumption is to consider the superposition of a uniform current with a sinusoidal Airy wave.

The total potential flow can be described in a reference frame translating at the current velocity.

The dispersion relationship is then (Jonsson, 1990) :

$$\left(\omega \pm \left|U\right|k^{\pm}\right)^{2} = g\,k^{\pm}\tanh\!\left(k^{\pm}h\right) \tag{37}$$

which coincides with the traditional dispersion relation without any current :

$$\omega^{2}=gk\tanh\!\left(kh\right) \qquad \text{or} \qquad k_{o}=k\tanh\!\left(kh\right)$$

In non dimensional form :

$$\left(\sqrt{K_{o}} \pm F_{h}K^{\pm}\right)^{2} = K^{\pm}\tanh K^{\pm} \quad \text{which can be written} \qquad \frac{\left(\sqrt{K_{o}}\pm F_{h}K^{\pm}\right)^{2}}{\tanh K^{\pm}}=K^{\pm} \tag{38}$$

where : $K_{o} = k_{o}h$, $k_{o}=\omega^{2}/g$, $K = kh$

$F_{h} = U/\sqrt{gh}$ is the Froude number based on the water depth.

$\tau = \omega U/g = \sqrt{K_{o}}\,F_{h}$ is the Strouhal number, ratio of the current velocity   to the waves phase velocity in infinite water depth.

Zero indices correspond to the infinite water depth without current.

Two situations may occur :

First, "following current" :

the current velocity is in the same direction as the wave propagation.

$$(\omega - Uk)^2 = gk\tanh(kh) \qquad \text{with} \qquad U>0 \qquad \left(\sqrt{K_o} - F_h K\right)^2 = K\tanh K$$

There is always two solutions K. The lowest one is realistic.

In deep water, when $\tanh K \sim 1$ (as soon as $K>3$).

$$\left(\sqrt{K_o} - F_h K\right)^2 = K \qquad \text{is then equivalent to :} \qquad F_h^2 K^2 - (1+2\tau)K + K_o = 0$$

$$K = \frac{1+2\tau \pm \sqrt{1+4\tau}}{2F_h^2} = \frac{1+2\tau \pm \sqrt{1+4\tau}}{2\tau^2}K_o \qquad \text{practically :} \quad K = \frac{1+2\tau - \sqrt{1+4\tau}}{2\tau^2}K_o$$

In shallow water $\tanh K \sim K$

$$\left(\sqrt{K_o} - F_h K\right)^2 = K^2 \qquad \text{is then equivalent to :} \qquad \left(F_h^2 - 1\right)K^2 - 2\tau K + K_o = 0$$

$$K = \frac{F_h \pm 1}{F_h^2 - 1}\sqrt{K_o} \qquad \text{and :} \qquad K = \frac{1}{F_h + 1}\sqrt{K_o}$$

Second, "opposing current" :
the current velocity is opposite to the wave propagation.

$$(\omega + Uk)^2 = gk\tanh(kh) \qquad \text{with} \qquad U>0 \qquad \left(\sqrt{K_o} + F_h K\right)^2 = K\tanh K$$

There can be up to two solutions K. The lowest one is realistic.
There can be no solution.

On an opposing current, one limit value can be exhibited considering the particular case in deep water when $\tanh K \sim 1$ which is a quite common circumstance as soon as $K>3$.

$$\left(\sqrt{K_o} + F_h K\right)^2 = K \qquad \text{is then equivalent to :} \qquad F_h^2 K^2 - (1-2\tau)K + K_o = 0$$

$$K = \frac{1-2\tau \pm \sqrt{1-4\tau}}{2F_h^2} = \frac{1-2\tau \pm \sqrt{1-4\tau}}{2\tau^2}K_o \qquad \text{practically :} \quad K = \frac{1-2\tau - \sqrt{1-4\tau}}{2\tau^2}K_o$$

A real solution exists if : $\tau < \frac{1}{4}$

Practically, on opposing current, the waves break when reaching this critical value.

For this limiting value : $K = \frac{1}{4F_h^2} = 4K_o$ with $\tau = \sqrt{K_o} F_h = \frac{1}{4}$

In shallow water $\tanh K \sim K$

$$\left(\sqrt{K_o} + F_h K\right)^2 = K^2 \qquad \text{is then equivalent to :} \qquad \left(F_h^2 - 1\right)K^2 + 2\tau K + K_o = 0$$

$$K = \frac{-F_h \pm 1}{F_h^2 - 1}\sqrt{K_o} \text{ and for } F_h < 1 : K = \frac{1}{1 - F_h}\sqrt{K_o}$$

Figure 1 and Table 5 illustrate various situations.

Table 5 gives the wave lengths according to different cases and non dimensional wave numbers appearing on figure 16.

Table 5 Wave length in various situations

Case	Dimensional parameters			Non dimensional parameters		Wave length			
	Wave period	Current velocity	Water depth	τ	F_h	Infinite depth without current	Finite depth without current	Finite depth following current	Finite depth opposing current
	(s)	(m/s)	(m)			(m)	(m)	(m)	(m)
Wave tank situation									
a	1.2	0.25	1.0	0.133	0.080	2.248	2.232	2.768	1.590
b	1.2	0.50	1.0	0.267	0.160	2.248	2.232	3.246	-
c	2.0	0.25	1.0	0.080	0.080	6.245	5.215	5.883	4.478
d	2.0	0.50	1.0	0.160	0.160	6.245	5.215	6.509	3.598
25 m water depth									
a	6.0	1.25	25.0	0.133	0.080	56.21	55.80	69.21	39.75
b	6.0	2.50	25.0	0.267	0.160	56.21	55.80	81.14	-
c	10.0	1.25	25.0	0.080	0.080	156.13	130.38	147.08	111.94
d	10.0	2.50	25.0	0.160	0.160	156.13	130.38	162.73	89.96
50 m water depth									
a	8.49	1.77	50.0	0.133	0.080	112.41	111.61	138.41	79.50
b	8.49	3.56	50.0	0.267	0.160	112.41	111.61	162.28	-
c	14.14	1.77	50.0	0.080	0.080	312.26	260.77	294.16	223.88
d	14.14	3.56	50.0	0.160	0.160	312.26	260.77	325.46	179.92

In the situation of waves propagating on an opposing current, the limit for the existence of a solution is highlighted when the upper curve (red) is tangential to the straight line (black).

Propagation of waves on opposing current is impossible when the Strouhal number is greater than the critical value $\tau=0.25$. This is the case on figure 2.b (T=1.2s , U=0.50cm/s) when the Strouhal number τ equals 0.267 (table 1).

According to the Froude law, figure 1 illustrates the same situations in a 25 m water depth, with waves periods T = 6 and 10 s and current velocity U = 1.25 and 2.5 m/s (table 1).

Practically a 6 s period wave propagation is impeded by a 5 knots opposing current.

According to the Froude law, figure 1 illustrates the same situations in a 50 m water depth, with waves periods T = 8.49 and 14.14 s and current velocity U = 1.77 and 3.56 m/s (table 1).

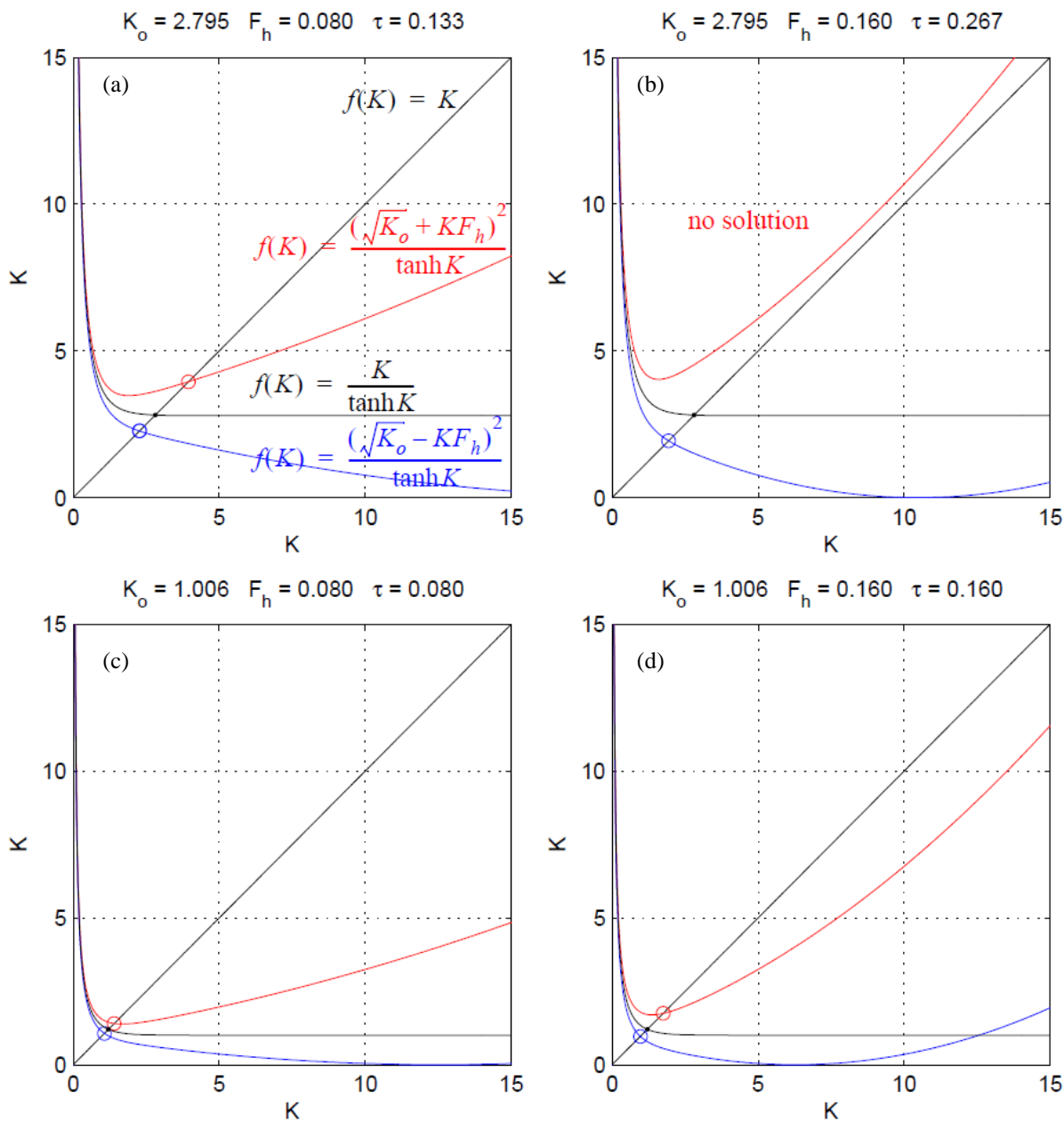Practically a 8.49 s period wave propagation is impeded by a 7 knots opposing current.

Figure 20 Wave number solution in various situations
The titles give some non dimensional values
which illustrate some situations which have been simulated in a wave tank at model scale.
Blue colour stands for current above following waves.
Red colour stands for current above opposing waves.
Black colour stands for waves without current.

Figure 21 (a & b) illustrate the wave number solutions as functions of the infinite depth non dimensional wave number.
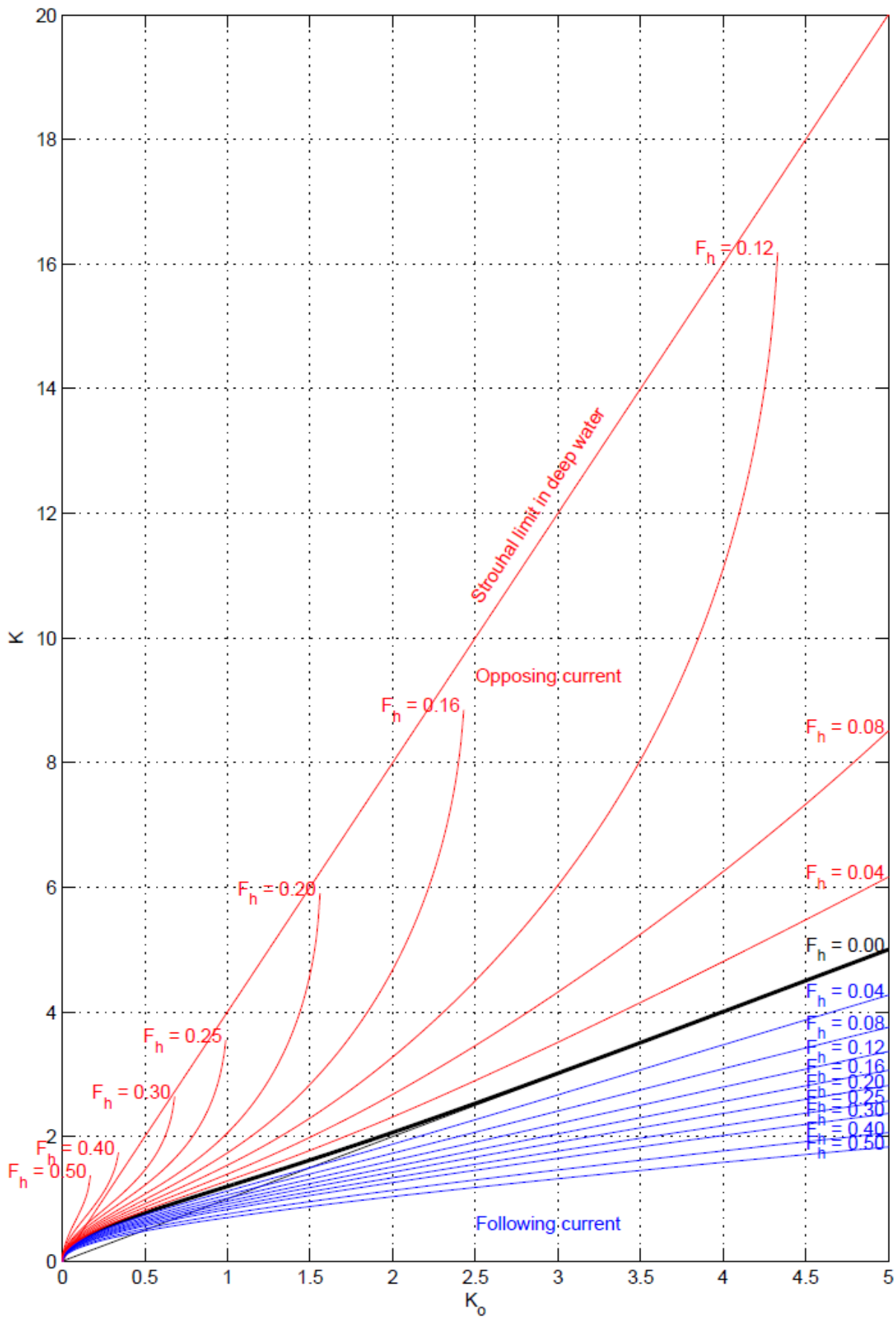
Figure 21a Non dimensional wave numbers on following (blue) and opposing (red) current
Additional parameter is the Froude number (one value per curve).
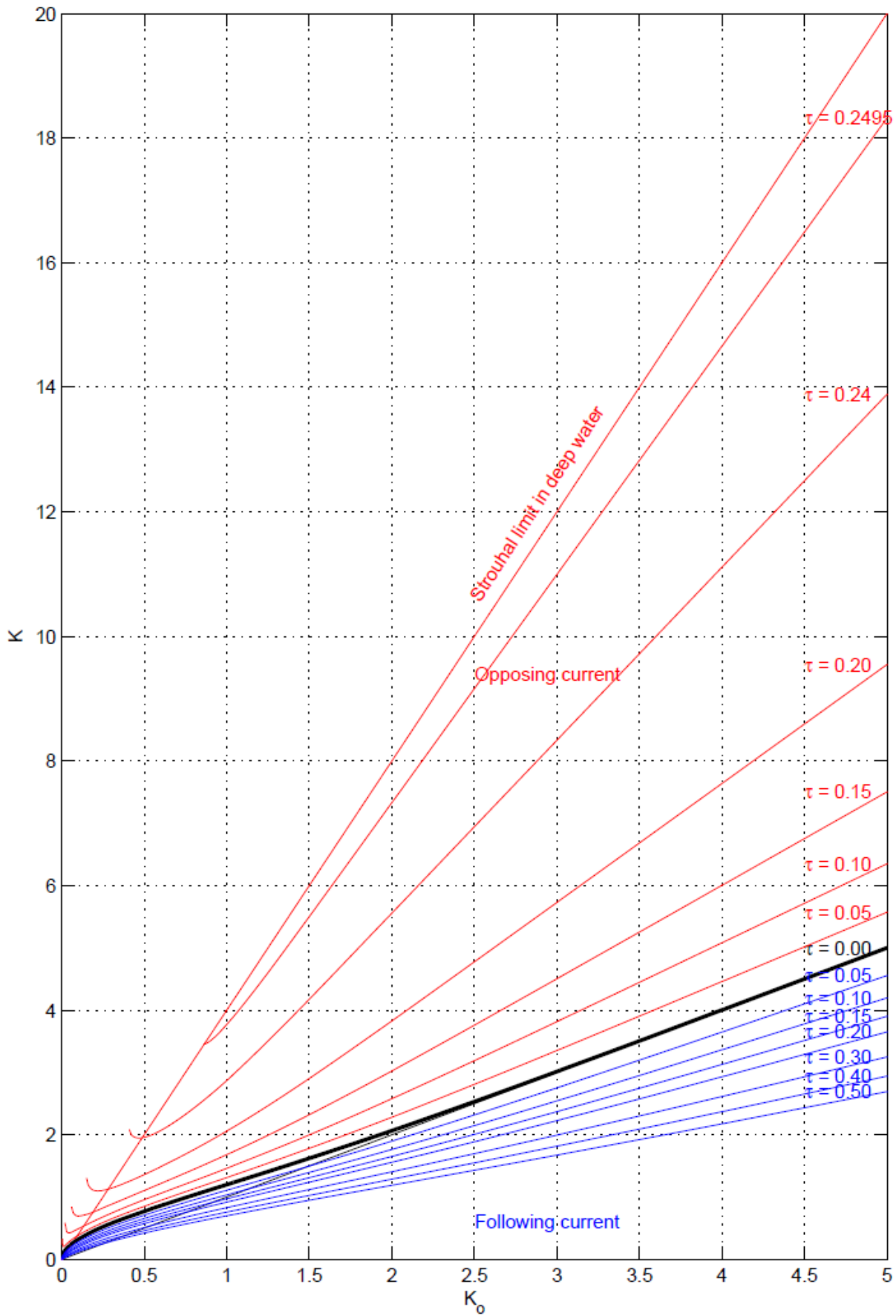
Figure 21b: Non dimensional wave numbers on following (blue) and opposing (red) current
Additional parameter is the Strouhal number (one value per curve).

For a given wave period, the current modifies the wave length without current.

The wave length is shortened on opposing current.

The wave length is lengthened on following current.

A strong opposing current can prevent the propagation of short periods waves.

In the context of small amplitudes waves and a uniform current, an expression of the phase velocity relative to a fixed frame of reference is (Nwogu, 2009) :

$$\frac{c}{c_o}=\tau+\frac{1}{2}\left(1+\sqrt{1+4\,\tau}\right) \qquad \text{with} \qquad c_o=\frac{\omega}{g}$$

and the wave height is modified according to : $\qquad \dfrac{H}{H_o}=\dfrac{c_o}{\sqrt{c^2-U^2}}$

5.2.2　Second order development

Perturbation analysis has been performed by Swan and James (2001) for an arbitrarily sheared week current such that $U(z)/c_o=O(\varepsilon)$, where ε is the wave steepness. One conclusion is that for a weak current, the wave number is modified compared to the zero current solution, but the second order term in the free surface elevation formula remains unchanged.

Skourup et al (2000) developed a second order interaction model between waves, current and a fixed circular cylinder and show that the second order oscillating force are influenced by the current.

5.2.3　Stream Function

Higher order monochromatic waves with current may be described by the Stream Function approach. The general stream function theory issued from he perfect fluid approach was applied to non linear wave modelling by Dean (1965) and Dalrymple (1974).

The method is able to take into account a current varying along the water depth with vorticity.

Starting from the wave period, the wave height, the water depth and the current profile, a set of equations including the non linear free surface condition is build which size depends on an optimised order of approximation. The solution gives the wave length and access to the free surface elevation and internal velocity field. The method is mainly applicable to monochromatic waves or waves with a spatial periodicity.

An applet is available at :

http://www.coastal.udel.edu/faculty/rad/streamless.html

See also :

http://faculty.gg.uwyo.edu/borgman/DSF/dsfwav/dsfwav.html

http://www.civil.soton.ac.uk/hydraulics/download/downloadtable.htm

5.2.4　Boussinesq Model

The Boussinesq approach reduces a three dimensional problem in a two dimensional one by using vertical interpolation with various orders between the sea bottom and the free surface. Then the grid of unknowns reduces to a horizontal space.

High order Boussinesq methods are available (Madsen, 1999, 2006) and can be adapted to the simulation of wave-current interaction (Guinot, 2008) : return current, reflection by bathymetry and wave blocking on opposing current (Figure 3).

5.2.5　Other non linear models

Nwogu (2009) developed a Boundary Element Method to solve for the kinematics of large amplitude waves on a vertically sheared current.

The wave steepness increases in opposing currents and decreases in following currents.

For a given wave height reference without current the resulting wave height decreases on following current and increases on opposing current.

The critical Strouhal number on opposing current is lower (0.2) for the large amplitude waves.

Ryu et al (2003) also developed a Boundary Element Method with similar conclusions. Comparison with a multi-layer Boussinesq model shows good agreement and give information about the kinematics above the mean water level.

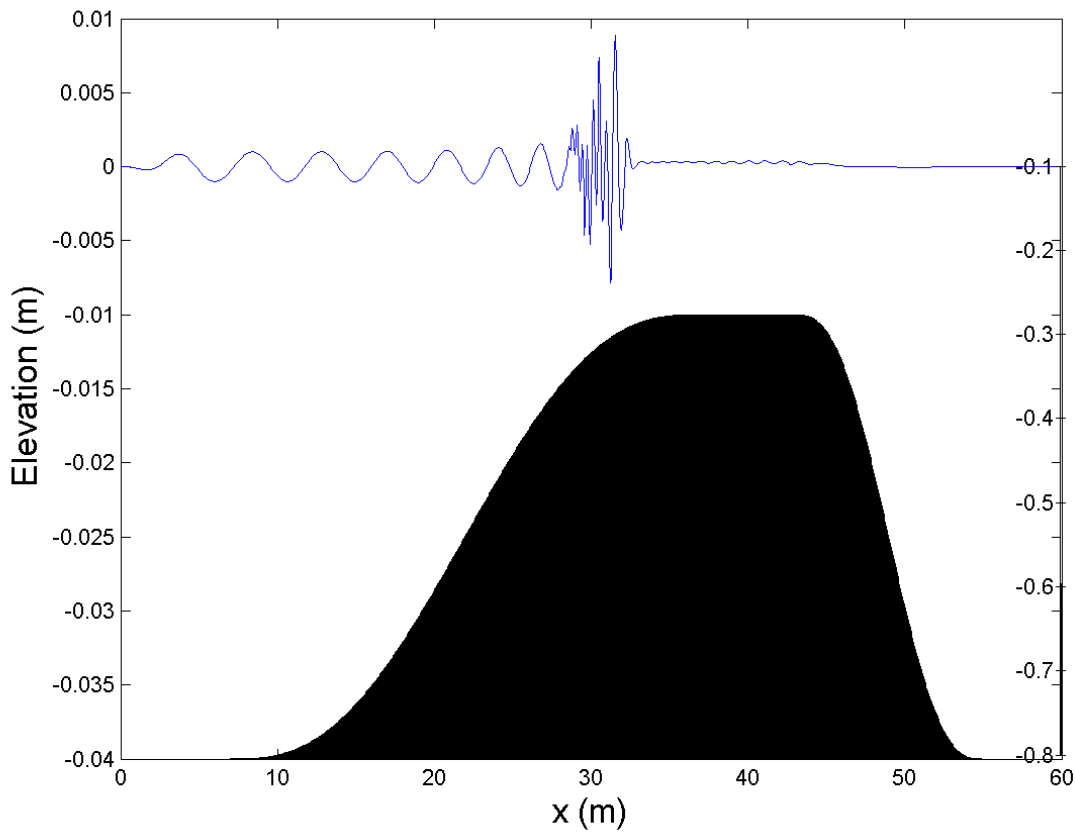**Figure 22:** Wave propagating on an opposing current

Boussinesq method (Guinot, 2008). Wave tank scale.

The waves start to propagate on a uniform water depth on the left side (T=2s, H=0.002m.),

while the current comes from the right side (U = -0.17 m/s).

On the shallower part of the bottom, the current velocity is amplified (U = -0.809 m/s)

and the waves locally experience a Strouhal number larger than 0.25.

6   SPATIAL AND TEMPORAL VARIATION

6.1   DESCRIPTION OF WORK

Definition: That met-ocean information that relates to the geographical region occupied by a group of devices *and* for those regions that may be expected to be affected by the installation and operation of a farm.

The need:

1. To provide a description of a particular site such that more specific detailed and accurate analysis, of the energy production can be undertaken. This will include a local scatter diagram; characteristic spectra (degree of swell/ multimodal seas). Understanding the variability across the site will provide input into energy production models to answer questions on peak power and smoothing over devices. Identification of specific difference from a "general site"; for example effects of coastline/ bathymetry/ prevailing seas and type of sea.

2. To provide detailed information to make engineering decisions specific to the location, fine-tune the installation/ operation of the devices.

Site specific data will (probably) be characterised by shorter measured data sets supported by:

(a) data from adjoining locations

(b)   modelling from a general area model.

Local measurement will be typically from wave buoys or ADP instruments. This could be supported through area measurements from satellites (in some cases) and from coastal radar systems (when finally proven). The need will be to understand the specific temporal and spatial variations that apply to the site. If one has a standard design (wave states/ power production models) for a farm to work from then one would wish to confirm that the assumptions of the general model are met and if there are differences to adapt the model.

The key aim is to produce as robust (and certain) a description as possible with a limited measurement campaign (cost).

6.2   SPATIAL VARIATION OF THE RESOURCE

6.2.1   Wave Resource

6.2.1.1   Overview

The majority of measurements and indeed working theories are based on understanding of time variations at a single point. Time average wave parameters are assumed to be equivalent over a "reasonable" area (and indeed safety factors for loading and response will usually cover any discrepancies). However there are particular reasons why one might wish to understand the spatial/ temporal variation across the site. This will be true both before deployment of the farms *and after* when the devices will produce some complicated (diffraction and radiation) pattern. It should be noted that there is also a need for larger, regional, scale estimation of the wave climate. This would involve scales of the order of 10-100 km and would be needed for understanding of the climatic conditions and their link to the larger scale meteorological conditions to determine the effect of weather front on homogeneity (or lack thereof) of wave fields. See for example (Altnkaynak 2005) who describes a geostatistical method called trigonometric point cumulative semivariograms (TPCSV) to determine the spatial scales from measurements along the US Pacific west coast. Spatial averaging statistical methods are also proposed using correlation analysis (Baxevani et al 2005 and 2009). Again however these analyse the data from Topex Poseidon satellite altimeter where the base area, over which the signal is derived, is 7 by 7 km.

6.2.1.2   Need for this information

(i)   Identification of long term spatial differences across the site for:
     i. Power variation and averaging
     ii. Optimum positioning of devices
     Given that a farm may extend over several square kilometres and "general" assessment of the wave resource will be modified depending on the position and physical properties of the site. The accuracy of the long term predictions will be improved but the fraction of extraction may well be improved through judicious matching of devices in the array to position.

(ii)   *Power performance testing*: when a device output is being compared against a nearby, measured, wave state one must include the factors that will contribute to errors in the assessment These could arise from deterministic effect (instrument miscalibration; a physical difference in the wave field due to bathymetry or current focussing for example) or from statistical variation in the measurements of a random process. Even though the power production can be measured accurately one has to deal with (i) the error bounds of the wave power estimate from the buoy (ii) the statistical spatial variation between the two points. The wave surface is a stochastic process and an average over a certain time at one point

could be different from that at another, *i.e. is the instrument measuring the same thing?* This will come down to averaging time and distance, where a longer averaging time will produce a more stable estimate of the power but also be long enough to account for the spatial variations.

(iii)   Establishing the limits of accuracy for data output for the site.

(iv)   Comparison of "before and after" effects from deployment of an array. The background errors and statistical variability must be quantified in order to understand any variations in the physical environment and whether this is significant. i.e. did the beach change because of natural changes in the wave systems or due to the wave farms. Given the likely small effect of initial installations the question is better posed as "at what level of deployment will any changes be greater than the background?"

Very little experimental work has been done in this area. Most studies have been in terms of instrument inter-comparisons and have taken for granted that the wave fields have been similar, any difference being discussed in terms of random error and instrument errors (see WADIC (Allendar) and WACIS experiments (Krogstad)). There are also studies from "field measurement" systems particularly remote sensing such as HF radar or satellite measurement, but these of course have limited spatial resolution. Below are some suggestions for progress in this area and which are currently the subject of research within EQUIMAR.

6.2.1.3   Analysis techniques and approaches

Short term (inter-record) analysis

Sort-term measurements will use the data within a given sea state (of the order of 20 minutes to 1 hour) to infer the sea-state at a second point. This is fundamentally limited by the statistical accuracy of these short term assessments (of the order of 10-20%) which will mask any smaller differences from deterministic effects (power conversion/ bathymetry, etc.)

Long-term (multi-record) data analysis

The second approach is to use a large amount of longer-term data (seasons to years) to improve the statistical accuracy. This has the negative effect of averaging all the contributing effects to variation and so masking the major contributors. In terms of long-term energy production I do not think this is a problem (we have data that shows that the power measured at the two EMEC buoys produced closer and closer measurements of energy as one moved to a full year's data. However for shorter term assessments this method is flawed. Of course there is the practical aspect of achieving longer term measurements.

Data filtering - to emphasise particular effects

A possible compromise approach is to categorise the larger data sets and then filter to determine the importance of each effect. For example one might take a single year data and only analyse that data with waves coming from a particular range of directions or within the same part of the tidal cycle.

Use (calibration) of models

A final approach is to use standard or modified numerical models of the site. However there has been no clear demonstration that these effects are shown on conventional wave models (again a subject of research within EQUIMAR).

At present several methods have been identified and are currently being tested for sensitivity and power:

(i)   Linear regression of one data set against a second achieved at a second site (with data filtering if necessary);

(ii)   Statistical testing of significant wave height parameters derived form measurements at two sites (See report by Sova on analysing radar measurements);

(iii)   Statistical analysis of spectra between two sites to determine if they come from the same population (see Bendat and Piersol);

(iv)   A method known as triple co-location (See. JANSSEN et al);

(v)   Trigonometric point cumulative semivariogram (TPCSV) concept (see paper by Altunkaynak).

At present we are using two data sets, one supplied by EMEC (two simultaneous buoy measurements) and the second being the "four buoy" data from the Wave hub site, collected over the last four months. Results will be available around Christmas 2010. We are also looking at simulated data, coming from known distributions and known differences to establish the power of each test.

6.2.2   Tidal Resource

6.2.2.1   Overview

The general pattern of topography around a high speed tidal stream induces a number of variations. These may be seen at short spatial scales (and high frequencies) in the form of turbulence, and at large spatial scales in the form of eddy structures and flow reversals. These variations are best studied using a combination of ADP surveys (both fixed and vessel mounted) and a suitable

modelling strategy. Visual observation at an early stage of site assessment will give information on the location of major eddies and gyres. Full understanding of the structures can then inform the choosing of device locations.

6.2.2.2   Vessel Survey

The spatial variation should be examined by a vessel mounted ADP survey. Ideally this is to be carried out at a peak spring tide to understand the flow at its strongest. The aim of this survey is to identify major flow structures such as eddies that may exist in the locality. Individual vessel transects should not last longer than 10 minutes, to obtain flow consistency at each limit of the transect. Also to remove any bias in the measurements from the vessel speed, each transect must be performed in both directions. Transects shall be regularly spaced across the tidal site, approximately perpendicular to the principal flow direction. The ADP should be operated in a high frequency sample rate to understand the turbulence structures.

6.2.2.3   Fixed Survey

A campaign of fixed ADP surveys should also be carried out. Results from this will be used to inform the modelling study. Sufficient ADP locations should be installed to record flow in the principal flow structures in the locality.

6.2.2.4   Modelling

A modelling study should be performed, which is validated against the field survey results. This will give smaller scale information on the behaviour of the local flow structures which is used in the final location decisions.

6.3   TEMPORAL VARIATION OF THE RESOURCE

6.3.1   Wave Resource

6.3.1.1   Overview

An understanding of the variation of the wave resource over time for a specific site can be of importance to wave power developments. The term 'temporal variation' can refer to:

- Time series variations, i.e. the variation of sea surface elevation over the length of an individual record, usually of the order 20mins to one hour. This can influence the control strategies used by devices and may employ methods such as 'wave-ahead-prediction' to tune the power being captured (both for greater power output, but also as a survival mechanism);

- Short-term effects, e.g. daily or weekly variations. This will be important to help define the power that will be provided into any grid for matching and will support the producer in achieving a better price for production;

- Medium-scale effects such as monthly or seasonal variability;

- Long-term inter-annual and decadal variations. Both these last will determine the annual and long term potential for income from generation.

Prediction variations on all time scales will also be important for the definition and practice of the marine operations such as installation, inspection and maintenance (see below).

When assessing the temporal variation of the resource, it is common to consider statistics for wave height and period from which the available power can be calculated. However, an understanding of the variability of other parameters such as bandwidth and directionality will also influence wave power developments and device selection.

6.3.1.2   Need for this information

Knowledge of the temporal variation of the wave resource at a prospective site for a wave power development is crucial to the long-term viability of the project. In general, sites with lower variability will prove more attractive to developers. Devices are designed for optimum performance in sea states with specific characteristics, and although many can be tuned to respond to changing sea states, the rate of tuning will reduce the efficiency of energy generation. Additionally, the issue of device survivability will lead to a preference for sites which only experience infrequent extreme storm conditions. Therefore sites with a more moderate but consistent resource will often be preferable to sites with a notionally more energetic, but less reliable, resource.

1. *Time series analysis*

The variation of the sea surface elevation over a standard record length will provide information relating to the stationarity of the resource over that particular timescale. Although for the purposes of spectral analysis and sea state reporting, it is commonly assumed that sea states are stationary over the period of one record (often for a period of up to three hours), this is not the case in reality and the degree of non-stationarity will have implications for energy extraction.

2. *Short-term effects*

Over short timescales, i.e. hours and days, knowledge of the temporal variability of the sea state will assist with predicting levels of power output variation which will affect issues such as grid integration. The short-term variation in the resource will

also play a role in device selection for a site, influencing issues such as device tuning, i.e. whether there is large variability, making a fast-tuning device preferable, or whether the resource is reasonably consistent. Directionality is also an issue if directionally-dependent devices are to be considered. Another key area where the temporal variation will be important is in the planning of maintenance schedules. Knowledge of the resource variability will assist in the creation of persistence tables, giving the likelihood of a sufficiently calm sea over a particular duration to provide windows for deployment, maintenance and retrieval of devices.

3.   Medium and long-term effects

Medium and longer-term variability will play a key role in site selection. Knowledge of how the available power varies over the course of a year will enable predictions of annual power output, and hence economic viability of a site, to be made. Although seasonal variations are inevitable, with lower energy expected during summer months, too large a degree of monthly or seasonal variation will reduce the viability of projects if sufficient power output levels cannot be maintained year-round.

If longer-term data is available, inter-annual and decadal trends can also be assessed, allowing predictions to be made over the life of the project. Although long-term measured wave datasets are scarce, the availability of wind field data going back to the 1950s or earlier allows the hindcast models of the wave climate to be run, making this type of analysis possible.

The following section will present methods for the analysis of the temporal variation of the sea state over the full range of timescales. A detailed case study for two specific sites will be presented to illustrate both the methodology and potential variations between sites.

6.3.1.3   Analysis techniques and approaches

i. Sea Surface Elevation

Although there is a strict mathematical (statistical) definition for non-stationarity a simple understanding can be based on a measurement of the variation in the *mean* and *variance* of the signal. To be stationary these characteristics in the signal time series must be unchanging in time. So for example a signal with a linear trend is non-stationary, or a wave field in which the size of the waves is growing as a storm develops is non-stationary. This MUST be understood as a time-averaging process. The wave heights will vary from one wave to the next BUT taken over a suitable average a non-stationary wave state will show an unchanging value for its significant wave height for example. (a picture?).

If the level of detail required in the data is such that an assumption of stationarity is invalid, and therefore traditional methods of spectral analysis cannot be applied, specific techniques accounting for non-stationarity must be applied. The analysis of data (time series) which is changing in a statistical sense in time poses some problem for the approach and accuracy of the result. There are techniques both in the 'time domain' and the 'frequency domain' which have either been adapted from conventional methods or indeed developed to fill the need for such analysis.

Much of the methods for the analysis of wave or tidal data are founded on the formation of statistical analyses which assume that the data is either statistically invariant in some sense (wave) or periodic (tidal stream). Thus averaging of data to provide time series of parameters is determined assuming that the mean square wave of the signal is constant over the averaging time (See Bendat and Piersol). It is obvious that with environmental conditions we are dealing with factors that can be changing in time (non-stationarity) or in space (heterogeneous). The many conventional analysis methods then become less appropriate and have to be modified. In conventional offshore technology much of the design work can be based on these averaging assumptions, and this is very much the basis for resource measurement in the marine energy industry. However the need to consider accurate description of time changing effects is stronger. For example any 'tuning system' must be able to respond over the timescales of the change in energy level and frequency. Also, time varying loads become more important for smaller systems whose natural periods are closer to those of the waves. Below is a short review of the types of analysis and techniques that can be used for the analysis of time varying signals in general and more specifically to wave analysis. For general treatments see, for example, Priestly (1988) or Tong (1990). The second difficulty is that conventional analysis does not treat the non-linear events that appear in more extreme data. Almost all conventional analysis of non-linear phenomena depends on the assumption of stationarity. Non-stationary and non-linear processes can have significant consequence for the understanding of wave and energy propagation, wave/wave and wave/current interaction.

Frequency Analysis
Fourier (Spectral) Analysis

Fourier analysis is the conventional method for determining the 'energy'- frequency content of a signal and has been the foundation for the modern methods of describing wave systems. The time series is typically, transformed to provide the energy spectrum which describes the variation of signal variance with frequency. As such all the wave spectral formulae can be related to measured 'wave spectra'. However a fundamental supposition for the development of the Spectral Analysis Methods is *stationarity*. Any departure from this assumption will lead to distortion and errors within the calculated spectrum. It also does not reflect the non-linear nature of the signal and the relation between related wave components. This problem is usually handled by pre-processing of the data which might remove linear o periodic trends in the data. Also the spectrum is calculated based on a time

length over which the data can be considered to be stationary. This is why spectra are defined over periods of 30minues to an hour. There is a balancing act between the need for sufficient data to provide good statistical accuracy and the degrading effects of time varying data. The exact degree of stationarity will of course depend on the local meteorological conditions. Spectral analysis is dealt with in many papers and books. With particular reference to waves (Tucker and Pitt 200

Modified Fourier Analysis

The effects of non-stationarity can be reduced by technique such as short-time Fourier Transform (Cohen 1995) and Adaptive Signal Processing (Windrows et al, 1985). However the accuracy is reduced and the question arises as to the appropriate balance of accuracy and resolution. In effect as one reduces the time window over which the data is transformed one loses information and accuracy about the lower frequency signals. This can be very important when one is considering swell waves.

*Wavelet Analysis (Hubbard 1998 for an interesting introduction)*

Even modified Fourier methods have difficulties with complex time varying, non-linear signals. The very method which allows us to view the distribution of signal variance (magnitude) with frequency destroys out knowledge of local events. For example the spectrum of a step change in voltage does not reveal when that step change occurred, only the frequencies and amplitudes that went to build the step. Thus Fourier techniques lose information about *local* phenomenon. There is also the issue of the effect of a particular part of the signal on the final spectrum. If one has a record which is corrupted at some part then the corresponding spectrum will be in error which is not necessarily readily apparent.
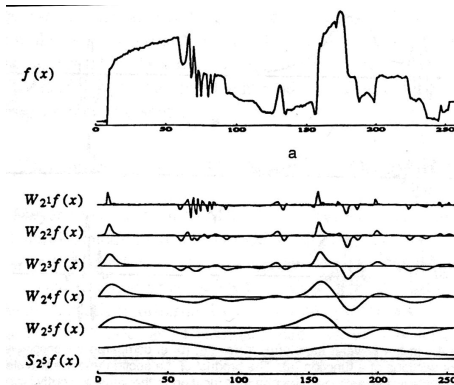
Wavelets have the ability to measure both the large and small scale variations and to show the evolution of the signal over time. The figure below (Hubbard 1998) illustrates this.

a) illustrates the original time varying signal with regions of relative constancy and other with rapid change and sharp discontinuities. B) shows five wavelet components at different time scales. The top is the finest scale and represents the higher frequency variations whilst the lowest is at the lower frequency range an shows the "dc" component of the signal.

Huang (2004). The example below shows wave field using wavelet analysis. Both and the frequency content in time are

Taken from Massel (2000)
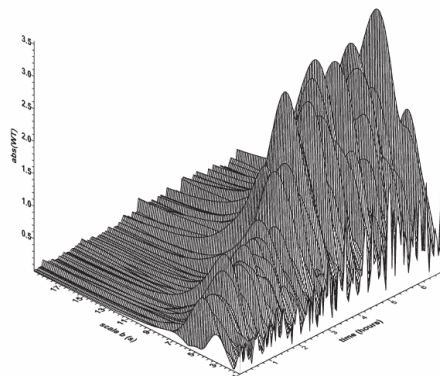
As examples of the use of wavelet analysis, refer to Massel (2001) or the re-construction of a time-varying the variation in the amplitude (energy) readily apparent.

Figure from Massel (2004)

The techniques described above are mostly based on 'convolution techniques' which are fundamentally limited by an 'uncertainty principle': to gain a finer resolution in the frequency domain, the temporal resolution must be reduced and vice versa. Secondly when there are non-linear components in the signal these are manifested in the spectrum as 'spurious' harmonics. This is not true for the HHT as described below. The analysis is *adaptive* to the local behavior of the time series. As such both temporal and frequency resolution can be maintained and the true contribution of non-linear components can be estimated.

Hilbert-Huang Transform

This is relatively new technique which purports to have advantages with regards time/ frequency resolution, accuracy and the ability to resolve non-linear and non-stationary effects (Huang 2005 and 2008). Examples of the use of HHT for wave analysis are given by (Veltcheva 2004), (Schlurmann 2002), (Ortega and Smith 2009). The main difficulty with this approach is that the mathematical and theoretical foundation for the use of this method is weak. It is fundamentally and *empirical* method for which more evidence for its utility is give. Over the past five years this has been happening and great strides have been made in underpinning the practice and defining error and confidence limits, see the papers;   (Wu and Huang 2005), (Sherman 2008) in   (Huang and Shen 2008).

The figure below, taken from Ortega and Smith, shows the evolution of the frequency spectrum (vertical scale) in time (horizontal scale) as two large storm waves pass. This form cannot be achieved using conventional time series analysis and wavelets technique cannot provide the same time/ frequency resolution.
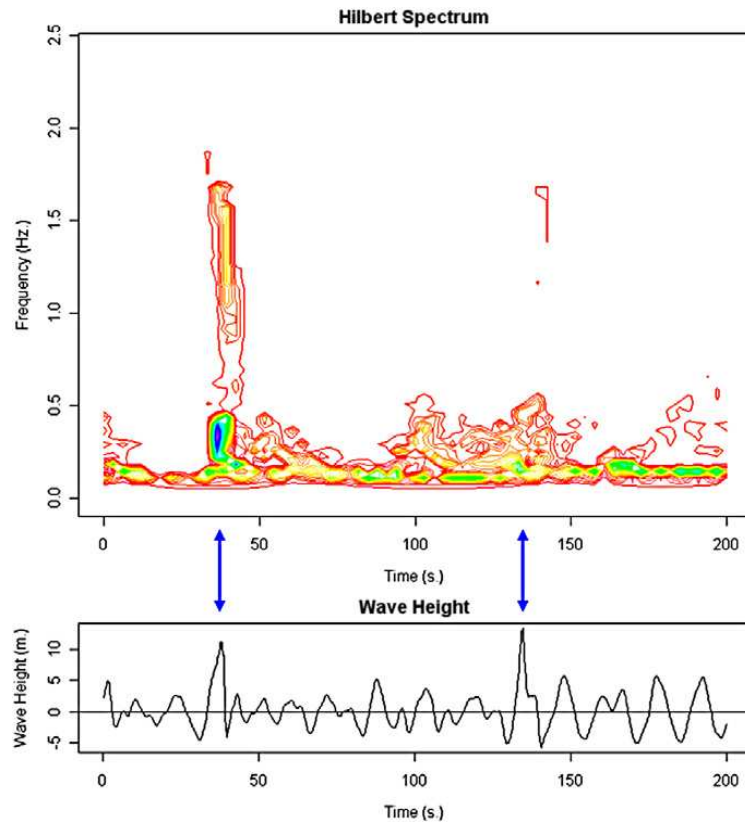

Figure 23 The Evolution of the Wave Spectrum in Time: Taken from Ortega and Smith (2009)

Table 6 Summary of performance of the various frequency methods (taken from Huang, Nii and Attoh-Okine (2005))

Comparison of Fourier, Wavelet and Hilbert-Huang Transforms			
Presentation	Energy-frequency	Energy-time-frequency	Energy-time-frequency
Cope with Non-stationary effects?	No	No	yes
Cope with Non-linear effects?	No	No	yes
Feature Extraction	No	Not in discrete form	yes
Theoretical	Theory complete	Theory complete	Empirical

ii. Averaging techniques

The following techniques can be applied to any sea state parameter (period/ bandwidth etc.) for which an appropriate-length record is held. For the purposes of illustration, examples are provided in terms of significant wave height, H_{m0}.

- Stationary average

One of the simplest representations of the temporal variability of a particular parameter over a specific timescale is to calculate a series of mean values and the corresponding values for the standard deviation. For example over a year, monthly means and standard deviations can be calculated as illustrated in Figure 24.
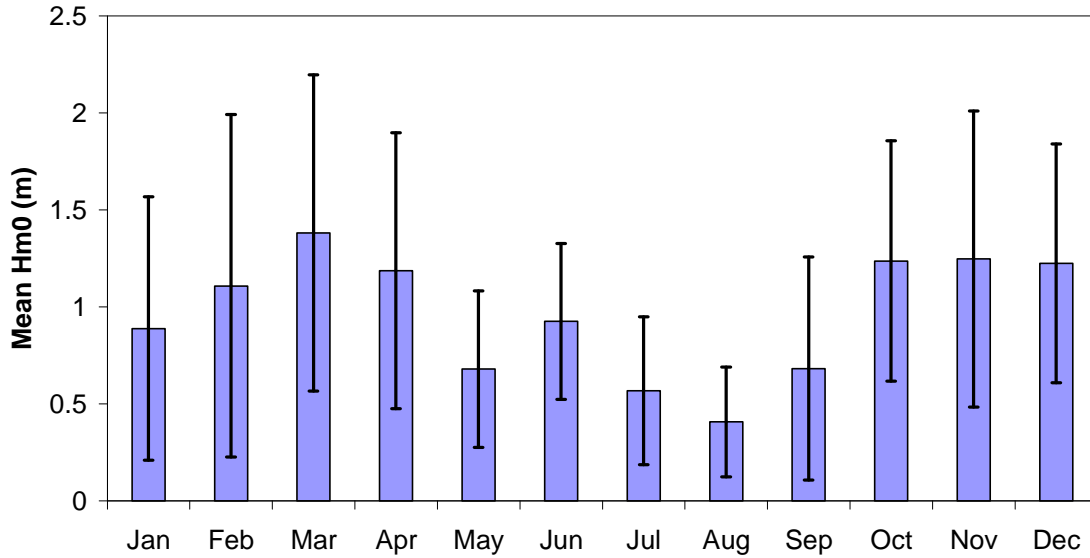
Figure 24 Average monthly values of H_{m0} and the associated standard deviations for one year of data.

- Moving average

Slow variations with time, e.g. over weeks or months, can be analysed by applying a moving average filter

$$H_{m0_{filtered}}(i,k) = \frac{1}{m} \sum_{j=k-\frac{m}{2}}^{k+\frac{m}{2}} H_{m0}(i,j) \tag{39}$$

(e.g. Define et al., 2009), where i is the year, j is the record index within the year, m is the window size in number of data records, and k is the resultant index due to the filter, where

$$k = \frac{24}{h} \times n \times \left(1, 2, 3, ..., \left(\frac{d}{n} - 1\right)\right) \tag{40}$$

h is the interval in hours between successive records, d is the length of the record in days, and n is the increment of the filter window in days.

For example, for a year-long dataset recorded at 3-hrly intervals, $i = 1$, $j = \{1, 2, 3, ..., 2920\}$, $h = 3$ and $d = 365$. To calculate the moving average over 7 days with a window size of four days, values of $m = 32$ (= 4*8 records) and $n = 7$ are required, giving $k = 56 \times (1, 2, 3, ..., 51)$. When datasets for multiple years are held, the mean annual variation can be found by averaging the annual variations from each of the yearly records to give a more accurate representation of the site's seasonal (temporal) variation, i.e.

$$H_{m0_{av}}(k) = \frac{1}{M} \sum_{i=1}^{M} H_{m0_{filtered}}(i,k) \tag{41}$$

where M is the number of years of data held, and k refers to the average value for the particular month for example.

Applying these techniques to a 10-year dataset, Figure 25 illustrates results for the significant wave height from a single year and Figure 26 the 10-year average. It can be seen in the 10-year results that the more extreme values have been eliminated, and a clearer monthly/seasonal trend has emerged. A longer-term averaging of this type will give greater confidence to developers than a single year of data that might be subject to unusually high or low energy events.

This seasonal variation is generally modelled as the superposition of two to four harmonic functions

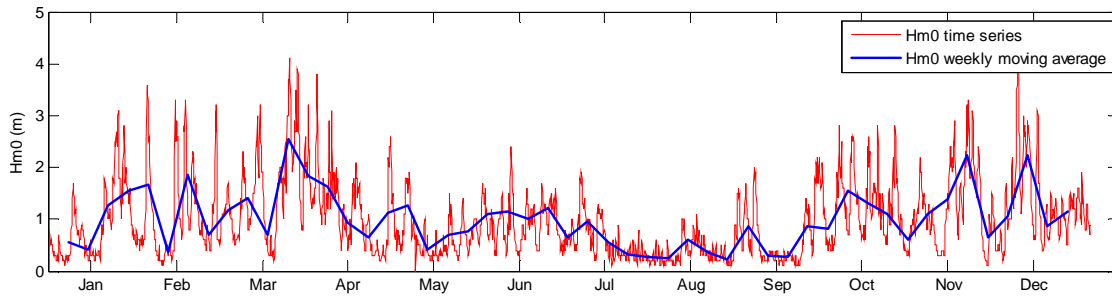Formula H(k)=a0+a1cos(2*pi*(k-1)/M) +a1sin(2*pi*(k-1)/M) +a2cos(2*pi*2*(k-1)/M) +…

Figure 25 Application of the moving average technique to a year-long dataset of H_{m0} (source CNR-ISMAR).
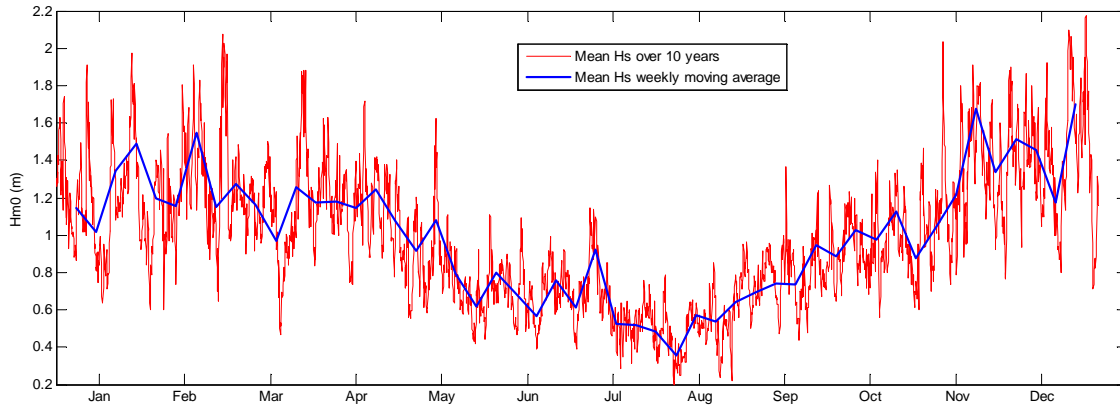

Figure 26 Long-term averaging over 10 years of a weekly moving average for H_{m0} (source: CNR-ISMAR).

- <u>Trends</u>

If longer-term datasets are available, e.g. > 20 years, it is possible to identify trends and analyse variations in the wave climate from year to year. These could be attributed to phenomena such as the North Atlantic Oscillation (NAO), a climatic effect in the North Atlantic which leads to fluctuating atmospheric pressure and consequently wind speeds over decadal timescales, or effects due to climate change. An example of an analysis of this type is a study published by Dodet et al. (2010), who analysed almost 60 years of *modelled* wave data from the north-east Atlantic. Figure 27 illustrates the trend in H_{s90}, the annual mean of the significant wave height values above the annual 90th percentile, for three locations in the north-east Atlantic. The results illustrate a clear upward trend in these largest 10% of waves at the more northerly locations.
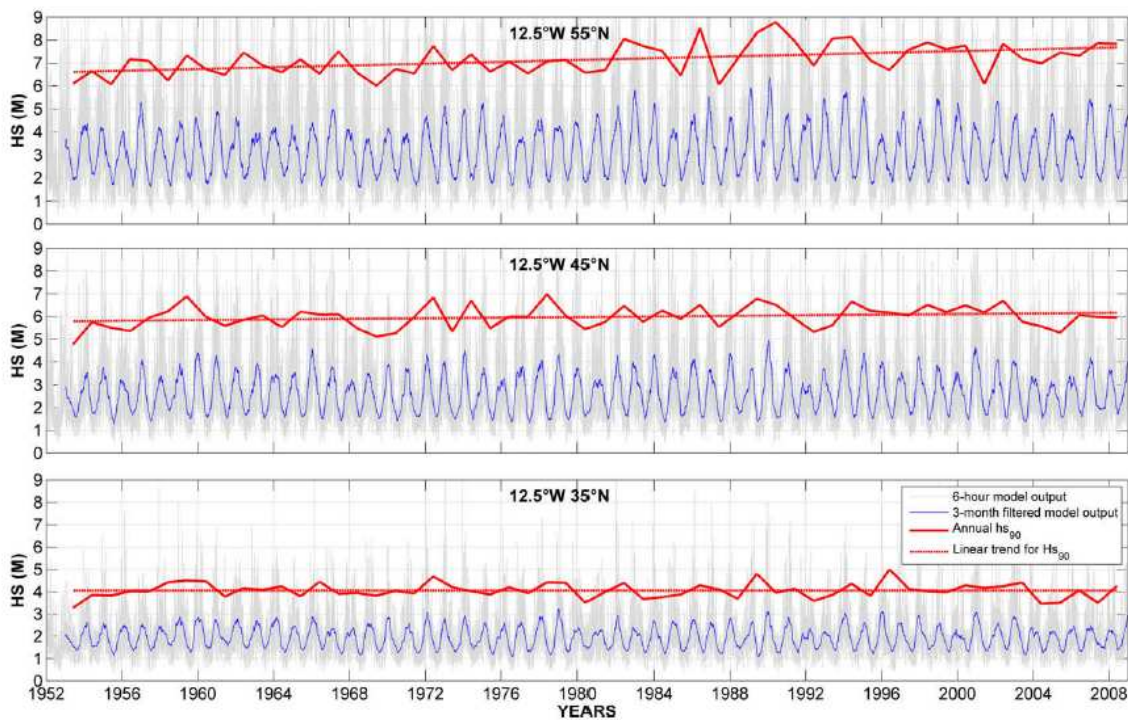
Figure 27 An example of long-term trends in H_s for three locations in the north-east Atlantic. Annual values are calculated for H_{s90}, and a trend line is fitted (source: Dodet *et al.*, 2010).

3. Persistence tables

An important consideration from an analysis of the temporal sea state variation is an understanding of the occurrences of periods of low wave energy during which deployment and maintenance operations can be performed. It is inevitable that the sites with the best wave energy resource will also have fewer significant periods suitable for such operations, but if these are too scarce, maintenance and device repair needs will be delayed, leading to potentially costly device down-time.

One means of assessing the availability of maintenance windows is through the use of persistence tables. These give the probability of occurrence that a particular wave height will be exceeded over a certain length of time.

An example is shown in Figure 28 for a site in the Pacific Ocean, giving the percentage of time for which a particular value of H_s is continually exceeded for a range of durations. For example, if a maintenance period requires the wave height to be below 1m for a period of 3 days, it can be seen in Figure 28 that the percentage occurrence of this height being exceeded for a 72-hr period is 60.95%. There is therefore a 39.25% chance of such a maintenance condition being met at any time.

Hs (m)	Duration (hours)									
	>6	>12	>24	>36	>48	>72	>120	>168	>336	>672
>0.25	100	100	100	100	100	100	100	100	100	100
>0.50	99.472	99.472	99.447	99.447	99.413	99.413	99.413	99.284	99.284	98.372
>0.75	87.526	87.389	86.932	86.559	86.134	85.179	82.475	78.822	70.001	58.57
>1.00	66.527	66.219	65.486	64.485	62.993	60.951	55.493	51.734	43.438	34.46
>1.25	43.751	43.532	42.591	41.436	40.221	37.286	32.817	29.797	21.561	9.845
>1.50	24.107	23.902	23.206	22.074	20.371	18.241	14.639	12.509	5.533	1.554
>1.75	11.733	11.51	10.846	9.833	9.132	7.446	5.21	3.762	0.456	
>2.00	5.179	5.045	4.466	3.967	3.551	2.809	1.782	0.473		
>2.25	2.051	1.979	1.72	1.563	1.452	0.887	0.242			
>2.50	0.947	0.884	0.736	0.57	0.448	0.14				
>2.75	0.419	0.382	0.319	0.268	0.148					
>3.00	0.125	0.106	0.066	0.04						
>3.25	0.057	0.034								
>3.50										
>3.75										

Figure 28 Example persistence table for the planning of deployment and maintenance periods. (source: www.oceanwavedata.com)

4. Statistical analysis

In addition to the more visual representations, statistical measures of the variation in sea state parameters can also be defined to enable comparison between a number of sites or time periods.

- Coefficient of variation (e.g. Cornett, 2008)

The variation in the resource at a particular site and over a specific length of time can be quantified using simple statistical calculations. One such measure is the coefficient of variation (COV), defined as

$$COV(H_{m0}) = \frac{\sigma(H_{m0}(t))}{\mu(H_{m0}(t))} = \frac{\left(\overline{(H_{m0} - \overline{H}_{m0})^2}\right)^{0.5}}{\overline{H}_{m0}} \tag{42}$$

where σ is the standard deviation of the record and μ the mean. The COV can be calculated for any length of dataset, depending on whether the interest is in longer or shorter timescales.

- Seasonal variability index

The seasonal variability index (which can equally be applied as a monthly index) is a measure of the variability of the wave resource with season over a year. It is defined as

$$SV = \frac{H_{m0_{S1}} - H_{m0_{S2}}}{H_{m0_{year}}} \tag{43}$$

where H_{m0s1} is the mean significant wave height for the most energetic season, H_{m0s2} is the mean significant wave height for the least energetic season and H_{m0year} is the mean significant wave height for the year.

6.3.2   Tidal Resource

The nature of a tidal flow is usually predictable with high accuracy over long timescales. The principal temporal variation is the spring neap cycle referred to above. A further variation is provide by the annual solstice/equinox cycle, with higher tidal ranges experienced at the equinox Also, the significant tidal components are approximately periodic over a cycle of 18.6 years as a consequence of the precession of the moon's orbit.

The principal perturbations to the astronomic tides are changes in water flow caused by synoptic weather patterns such as storms, hurricanes or anticyclones. These effects are termed the *storm surge*, where low pressure causes a raising of the oceanic surface (positive surge), and a high atmospheric pressure causes a lowering (negative surge). These can be assessed by long term observations, or by numerical modelling. An associated effect is the *set-up* caused by the mass transport of wave action in a particular direction causing water level to rise on a lee shore. This elevation then creates a balancing current with vertical structure, and can also be assessed by numerical modelling.

7   CASE STUDIES

7.1   WAVE HUB, UK, AND MAZARA DEL VALLO, ITALY

This case study applies some of the techniques described in this section to two datasets from sites with significantly differing wave resources. The first site is the Wave Hub location in the southwest UK. The data is available in spectral form over one year at 2-hourly intervals, initially from a Seawatch Mini and latterly from a Datawell waverider buoy, deployed at 50m water depth. The site is Atlantic facing, and is subject both to Atlantic swells and local wind seas. The second site is Mazara del Vallo, at the southwest tip of Sicily in the Mediterranean Sea. The data is recorded at 50m depth and is available over ten years, but only provides significant wave height, mean period and mean direction. The nature of the resource is very different to that at the Wave Hub site because of the lack of ocean swells; all wave energy is 'locally' generated within the Mediterranean.

The annual variation in significant wave height and mean period, averaged on a monthly basis and with error bars illustrating the standard deviation, can be seen for the two sites in Figure 29a and b. The Wave Hub dataset only contains a partial record for October and no data for November therefore both these months have been excluded from the analysis. For both sites, the average wave heights are larger, and have greater variation as indicated by the standard deviation, in the winter months. This is a typical result, mainly due to the greater severity and duration of winter storms, both locally and in the case of the Wave Hub site, across the northern Atlantic, thus generating large swell events. A similar effect is seen when considering the mean period at the Wave Hub site; the summer wave climate is primarily influenced by local winds and low energy swell, whereas the larger swells that characterise the winter months increase both the mean period and the degree of variability. Although there is a slight reduction in mean wave period at Mazara del Vallo over the summer months, it can be seen that the standard deviation of the periods remains relatively consistent throughout the year, indicating a consistent level of variation in the records.
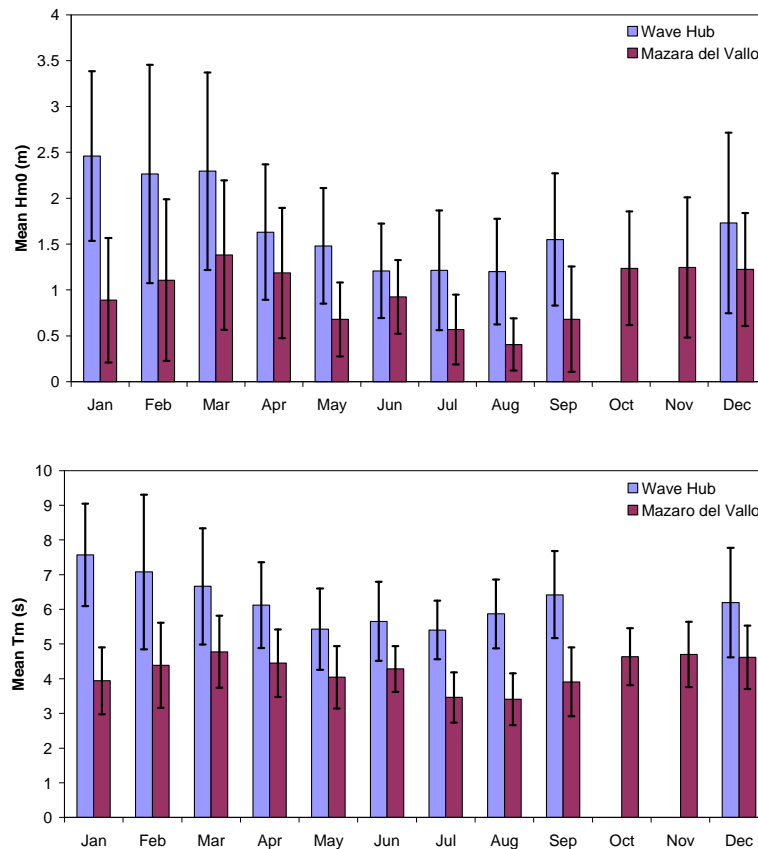

Figure 29 : Monthly mean values of H_{m0} and T_m at the Wave Hub and Mazara del Vallo sites with error bars indicating the standard deviation.

To illustrate in more detail, and also to produce a general trend in the wave heights and periods over a year, a moving average has been applied to data from Mazara del Vallo over a range of timescales from three days to 30 days (Figure 30a and b). The 3-day moving average follows the 3-hrly time series plot relatively closely, producing a realistic overview of the data but eliminating the extremes. As the timescale is increased to seven days, the plot becomes smoother; more of the extremes are ignored but the major increases and decreases can be observed. At an averaging period of 15 days, a smooth plot is achieved which illustrates the general trends in the data over the year. This can be smoothed still further by increasing the timescale to 30 days, although at this point there is a risk that seasonal trends will start to be lost.
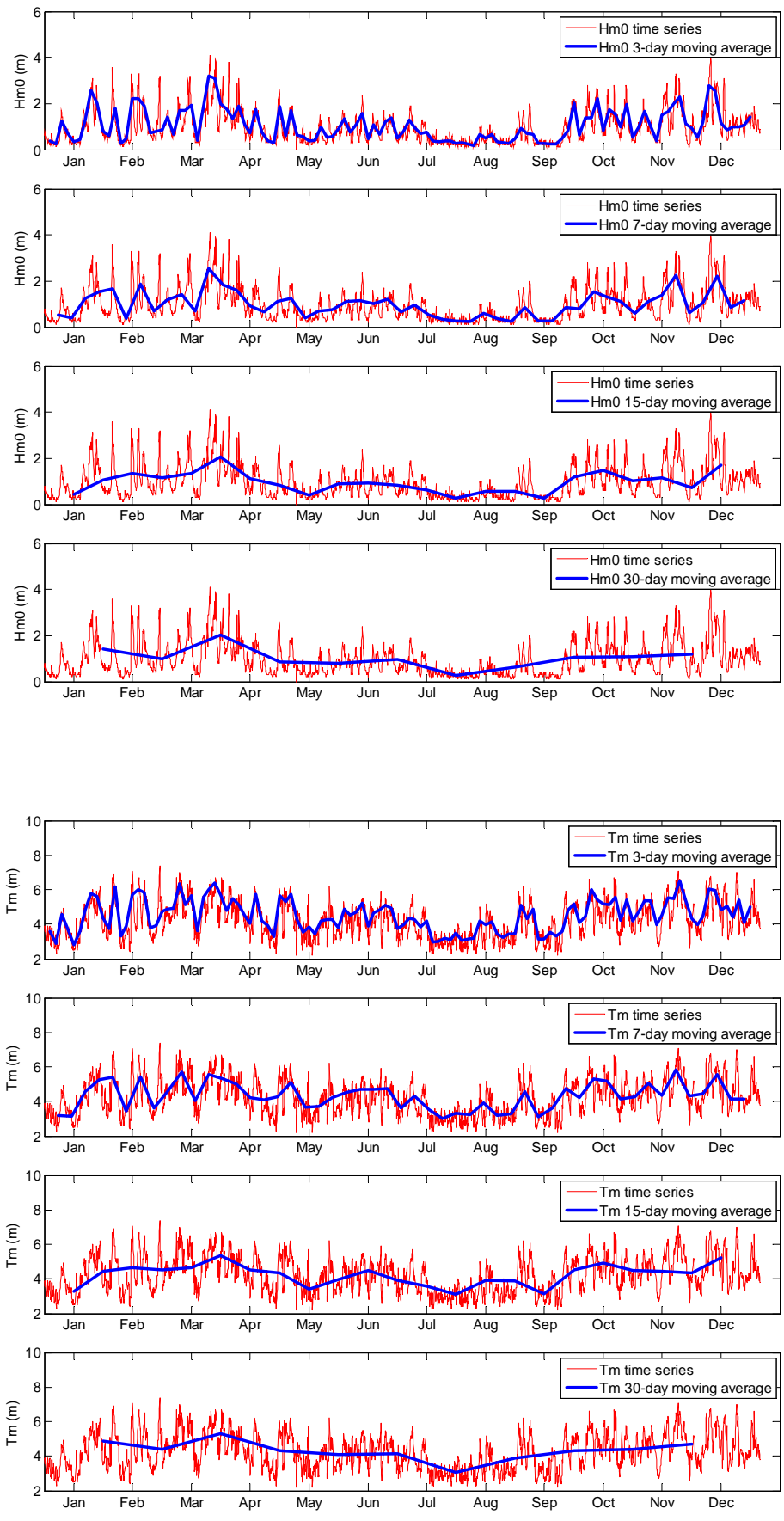
Figure 30a and b: Moving average analysis of the annual dataset of H_{m0} and T_m for Mazara del Vallo. A range of averaging periods have been applied.

For a quantitative comparison between the two sites, statistics for the coefficient of variation (COV) and monthly variability index MV (using the same formulation as for the seasonal variability SV) were calculated, and the results shown in Table 7. The lower the COV value, the less variation there is in the parameter being measured. It can therefore be seen that although the Wave Hub site experiences a more energetic wave climate, its variability (COV = 0.55) is less than that of Mazara del Vallo (COV = 0.73). Both sites experience very similar levels of variation in the mean period, with COVs of 0.24 and 0.25 respectively, despite the apparently greater variability of the mean period at Wave Hub when plotted on the monthly averaged bar chart. The monthly variability indexes show a similar pattern. The availability of spectral data for the Wave Hub site allows the calculation of the energy period T_e and thus the total power available over the year. Repeating the COV calculation for power at Wave Hub gives a value of 1.56. This corresponds well with the value of ~1.5 found by Cornett (2008) for the west coast of Ireland, which experiences a similar wave climate to the Wave Hub site.

Table 7: Statistical measures of the variability of H_{m0} and T_m for Wave Hub and Mazara del Vallo.

	Wave Hub	**Mazara del Vallo**
$\overline{H}_{m0}$ (m)	1.69	0.98
$\sigma_{H_{m0}}$	0.94	0.71
$COV_{H_{m0}}$	0.55	0.73
$MV_{H_{m0}}$	0.74	1.01
$\overline{T}_m$ (s)	6.22	4.23
σ_{T_m}	1.54	1.03
COV_{T_m}	0.25	0.24
MV_{T_m}	0.35	0.33

7.2 ARCH POINT, IRELAND

7.2.1 Measured Seaways

Over eighteen months of sea surface elevation data has been collected by a Datawell non-directional Waverider buoy at Arch Point off of Loop Head (West coast of Ireland) at illustrated in Figure 31. This site is in approximately 50m of water and is exposed to the Atlantic Ocean. This data set includes two consecutive records of six month winter/spring seasons from December to May.

The data buoy recorded the surface elevation with a sampling frequency of 2.56Hz. The receiver at Arch Point used the older Datawell data management system (DIWAR). This resulted in the Arch Point surface elevation having a duration of 20 minutes which is in general logged hourly, however there is a bias towards storm seas due to continuous measurement when the significant wave height exceeded a given threshold. This bias has been removed from the data set.
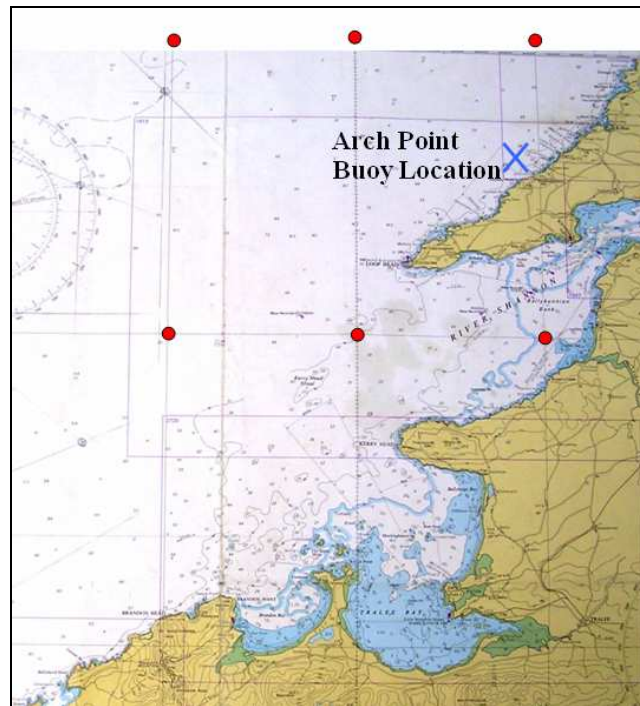
Figure 31. Location map of Arch Point buoy

7.2.2 *Analysis & Seaways*

An FFT routine was conducted on the measured time history surface elevation data to produce individual sea state variance density spectra. Summary statistics such as H_{m0}, T_{02}, T_e and T_p were then derived from the spectrum and used to generate two summary spectral comparison sets:

> *i) Temporal Fidelity*: the significant wave height, H_{m0}, and the average period, T_{02}, were used to produce bi-variate occurrence scatter diagrams at averaged spectra at various time scales ranging from individual days to six month periods.

> *ii) Seaway Fidelity*: By selecting certain combinations of wave height and period in the scatter plot, the average spectral shape of the measured seaway that falls within the selected table element can be compared with a classical shape.

7.2.2.1   Temporal Fidelity

The data analysis flow chart and the comparisons that have been made in this study are depicted in Figure 32. From the Arch Point site, two sets of 6 month data are available for comparison. These cover the winter and spring seasons. From these sets, the percentage occurrence scatter diagrams are produced for different time durations. Average spectra, which are the mean of the spectral ordinates over similar time scales, are produced and compared to a classical Bretschneider profile exhibiting the same summary statistics. The second layer of investigation involves comparing the computed average spectrum of three selected scatter plot elements;

> i.   lines of constant significant wave height,
>
> ii.   average period,
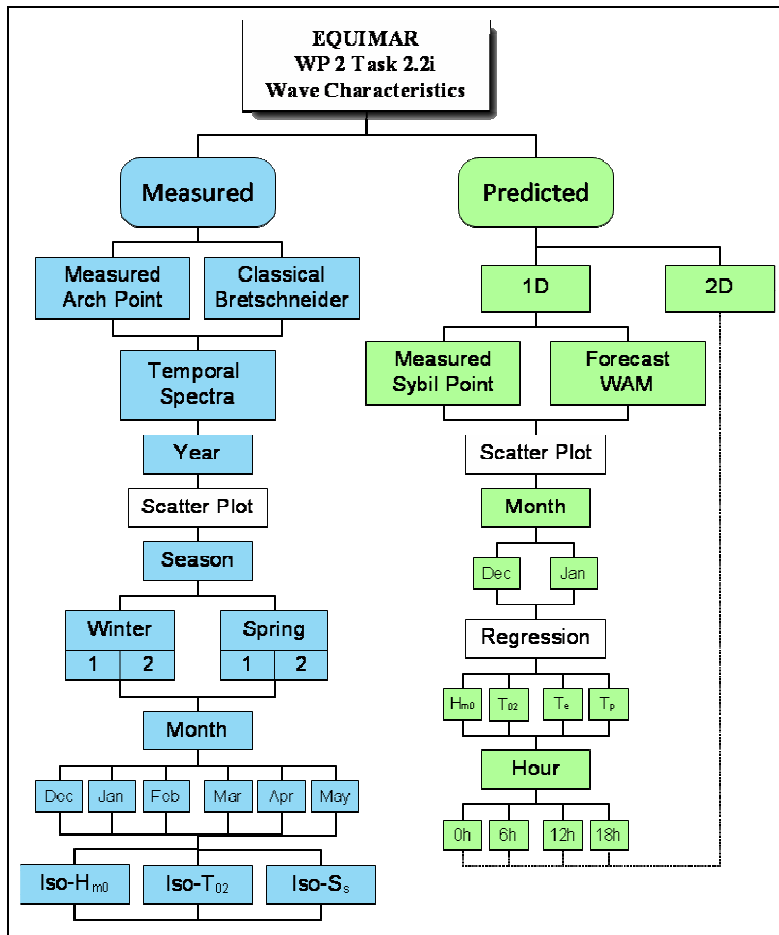>
> iii.   steepness.

These are shown in Figure 33.

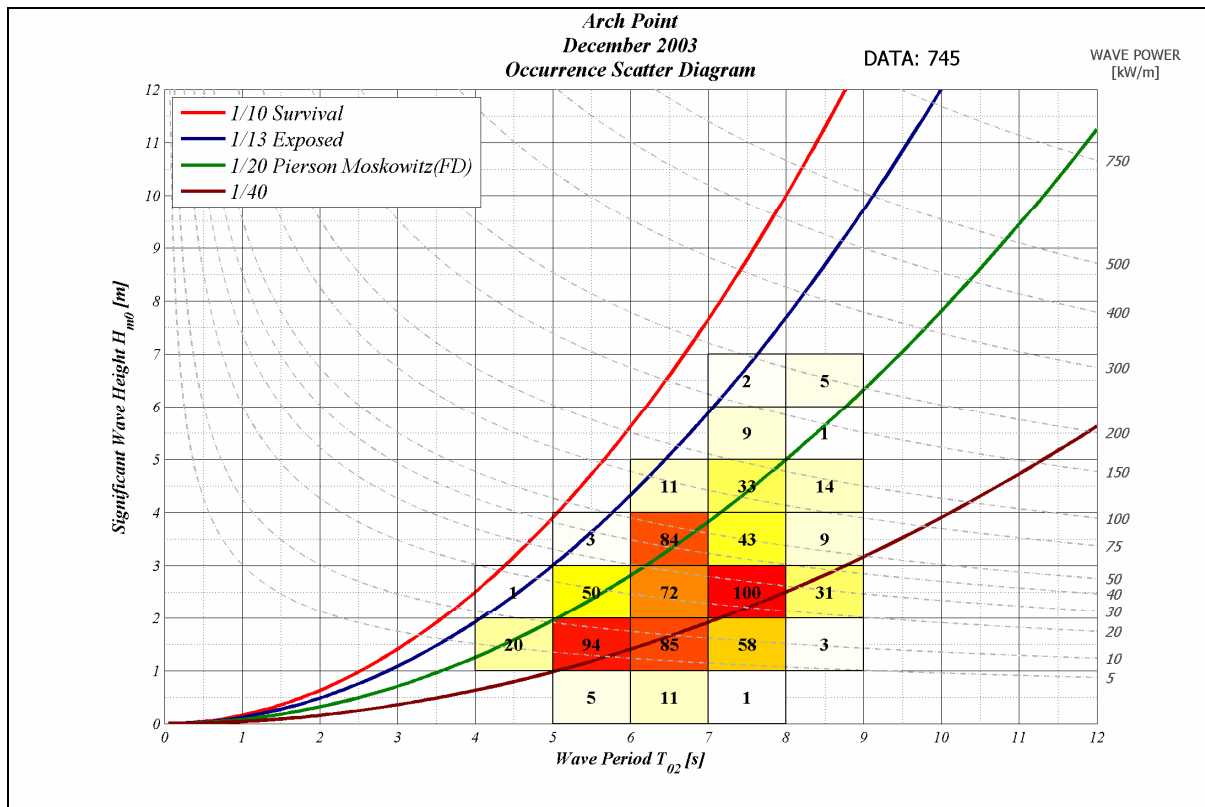**Figure 32. Data comparison flow chart.**

Figure 33. Examples of Grouped Scatter Plot Elements for Analysis.

7.2.3   Measured Spectral Comparison

The surface elevation data provided by a Datawell non-directional Waverider buoy is used to investigate the spectral shape throughout a season and its deviation from the classical empirically derived equations. The vertical acceleration of the Waverider buoy is double integrated to obtain the surface elevation of the sea state. The sampling frequency of the buoy is 2.56Hz and the raw elevation data file comprises 3072 data points which result in a 20 minute time series.

To produce a spectrum that reduces the effects of aliasing and leakage while retaining variance, the 3072 data point time series is segmented into 6 equal divisions of sea surface elevation consisting of 512 data points each. These are Fast Fourier Transformed to produce individual spectral profiles which are then ensemble averaged to calculate the overall variance density spectrum for the elevation record. No taper window is applied to the subseries elevation segments. This method produces a frequency spectrum of 128 equally spaced frequency bins from 0.03Hz to 0.665Hz with a frequency spacing of 0.005Hz. This can be seen graphically in Figure 34.
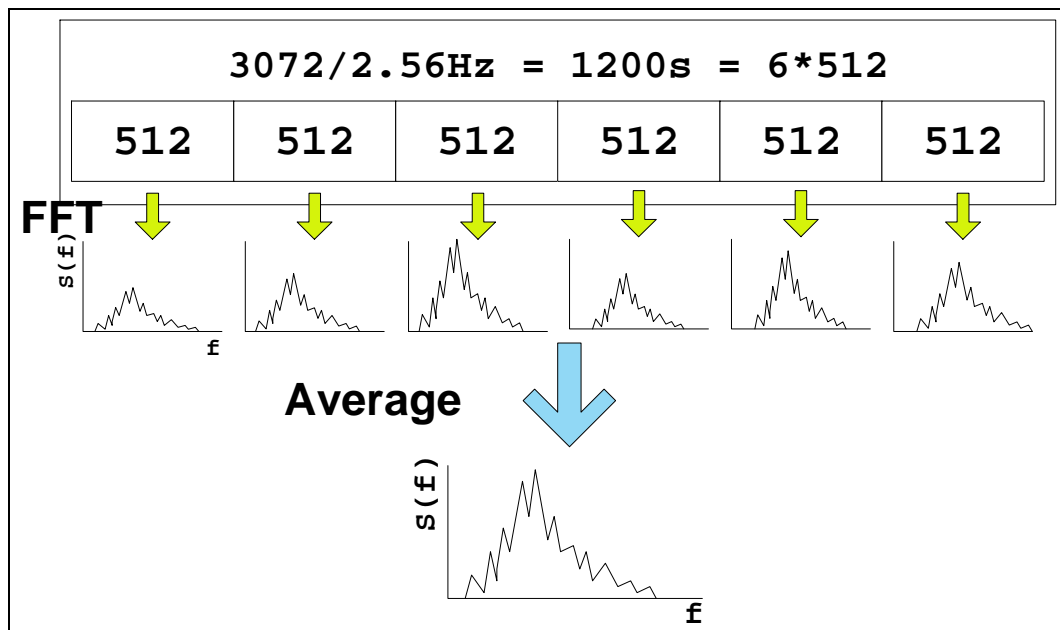

Figure 34. Applied Spectral Analysis Method.

7.2.4   Arch Point December 2003-May 2004

The first portion of the Arch Point data analysed has six months of measured surface elevation over the winter/spring period from December 2003 to the end of May 2004. Initially the data repository contained all data files recorded, which included those extra measurements when the significant wave height exceeded a set threshold level and continuous measurement was instigated automatically. If these additional files were included when calculating the occurrence of the scatter diagram, a bias would exist toward the storm seas. To remove this effect, only files that were recorded in the first twenty minutes of each hour are incorporated into the data set for this study.

7.2.4.1   Scatter Diagrams

Scatter diagram elements of 0.5m by 0.5s were selected as a reasonable size to segregate the data to form the bi-variate scatter diagram as shown in Figure 35. This was taken as the bin size to coincide with current recommendations such as the DECC Protocol. Also plotted on these graphs are lines of constant significant steepness and constant incident wave power on the right hand axis according to the following commonly used equation for wave power:

$$P_{T_{02}} = 0.589 * H_{m0}^2 * T_{02} \text{ [kW/m]}$$

Over 97% of all possible hourly available data for the six months of measurement from December 2003 to May 2004 for the Arch Point location is represented in the scatter plot. Figure 35 shows that the centre of occurrences of sea states has a significant wave height, H_{m0} of 2m ($\pm$0.5m) and zero crossing period, T_{02} of 6s ($\pm$0.5s).
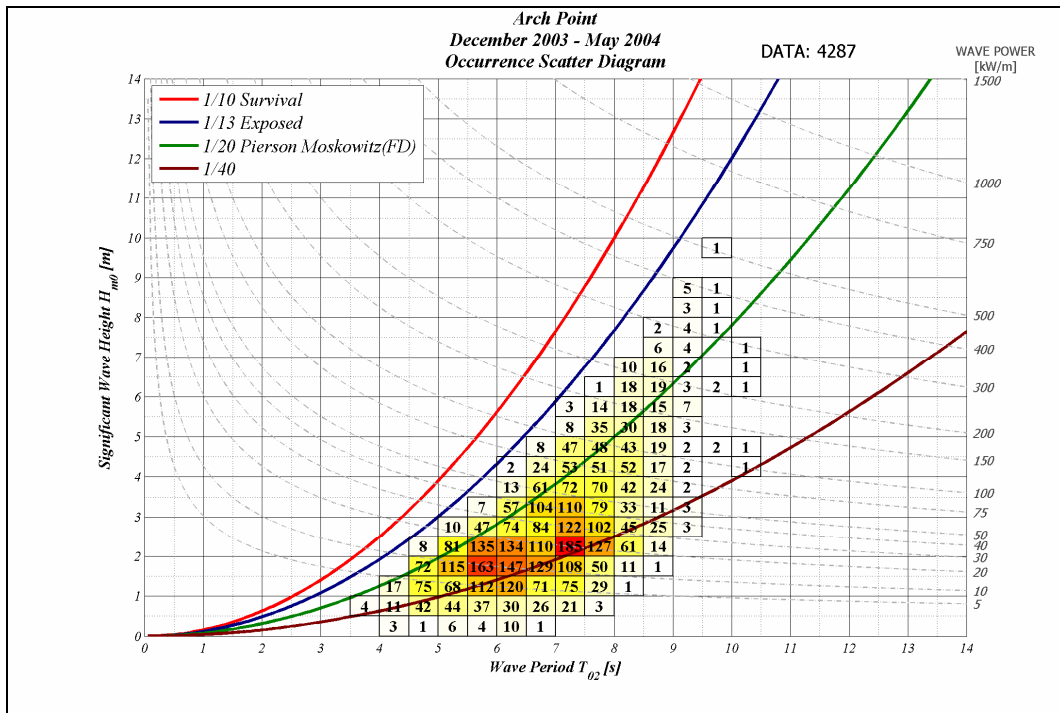
Figure 35. Scatter Diagram of the combined winter and spring seasons of 2003-2004 for Arch Point

7.2.4.2   Spectrum

The average of all the hourly spectra that occurred in this six month period from December 2003 through to May 2004 is shown as the blue plot indicated by circles in Figure 36. This average spectrum is derived by calculating the mean of the spectral ordinates at each frequency for all spectra. There is now the option of fitting an empirical spectral profile to this data. The Bretschneider spectrum is used due to its flexibility and ease of use with only two input parameters, the total variance and the peak frequency. Using the equation shown in Table 1.1, an equivalent Bretschneider spectrum is plotted, with the same summary statistics as those derived from the average spectrum. However, different parameters are available to fit the Bretschneider spectrum to the average spectrum.

Firstly, the total variance of the average spectrum, m_0 represented by the significant wave height, H_{m0} and the peak period, T_p is used as inputs to the Bretschneider equation (*Bret: Matched H_{m0} Tp*). This results in a close approximation to the average spectrum but with a larger magnitude peak.

The Bretschneider spectrum maintains a constant relationship between the various periods, such as the ratio between the average period, T_{02} and the peak period, T_p, which is used as the second method of fitting to the average spectrum ($T_p/T_{02} = 1.406$). In this case, the total variance, m_0 and the average period, T_{02} of the average spectrum are used as the input parameters to the Bretschneider equation. This results in a shift of the fitted empirical spectrum to higher frequencies, clearly shown in Figure 36 (*Bret: Matched H_{m0} T_{02}*). This shift is due to the use of T_{02}, which incorporates the zeroth and second moments in its calculation (See Table 1.1). The second moment, m_2, involves a frequency term raised to the power of two. The average spectrum has a relatively high energy content at frequencies higher than the peak frequency ($f > fp$), in the area indicated by the box and so this results in a shift of the spectrum.

Finally as an alternative to the fitting of the empirical spectrum by using summary statistics, the maximum ordinate of the average spectrum, $S(f_p)$, was used to fit the Bretschneider spectrum (*Bret: Matched $S(f_p)$ Tp*). This fitted spectrum will be similar to the previously fitted Bretschneider (*Bret: Matched H_{m0} T_p*) but to achieve the same $S(f_p)$ as the average spectrum, the overall variance has to be reduced. The effect of this is also evident in the area of the spectral plots identified by the box in Figure 36.

Three methods of fitting the empirical Bretschneider profile to the averaged measured spectrum is presented above and plotted. The initial method of using the total variance, m_0 and the peak period, T_p will continue to be used in further examples in this document, as it retains the overall energy of the target spectrum while it's profile is a closer approximation to the measured spectrum.
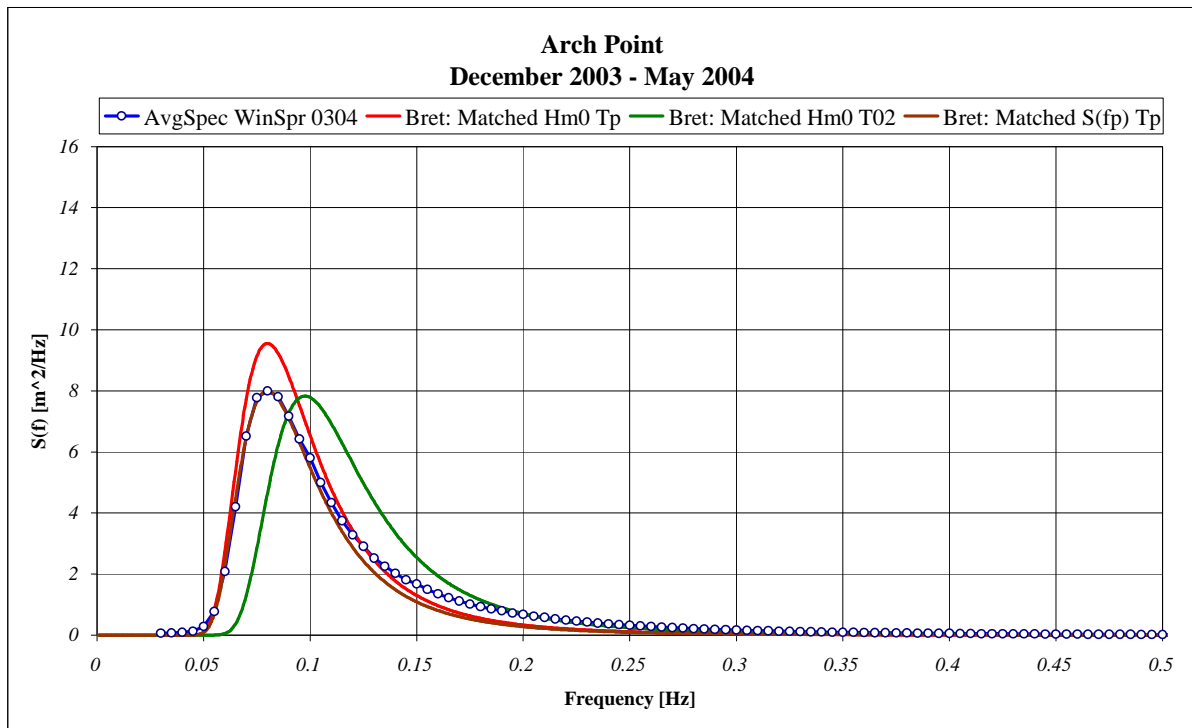
Figure 36. Average spectrum and Bretschneider fit of the combined winter and spring seasons of 2003-2004 for Arch Point.

7.2.5   Arch Point December 2004-May 2005

The same analysis methodology is performed on the second six month data set of the measurements from the Arch Point location for the time frame of December 2004 to May 2005. In this instance, approximately 96% of the possible hourly data is available. The scatter diagram for this period is shown in Figure 37 and the average spectrum for this time period is plotted in Figure 38. Figure 37 shows that this scatter diagram has a similarly located concentration of occurrences as the previous six months of data shown in Figure 35.

The Bretschneider profiles in Figure 38 are plotted using the same methods as applied for Figure 36. This average spectrum shows the same high frequency energy content characteristic, highlighted by the box as in the previous bi-seasonal average spectrum in Figure 36.

From the plots of Figure 36 and Figure 38, it is evident that the closest fit to the averaged spectrum is the Bretschneider profile defined by the total variance, m_0 and the peak period, T_p as it maintains the overall energy of the target spectrum and the peaks coincide at the same frequency. This method will be used in further spectral comparisons.
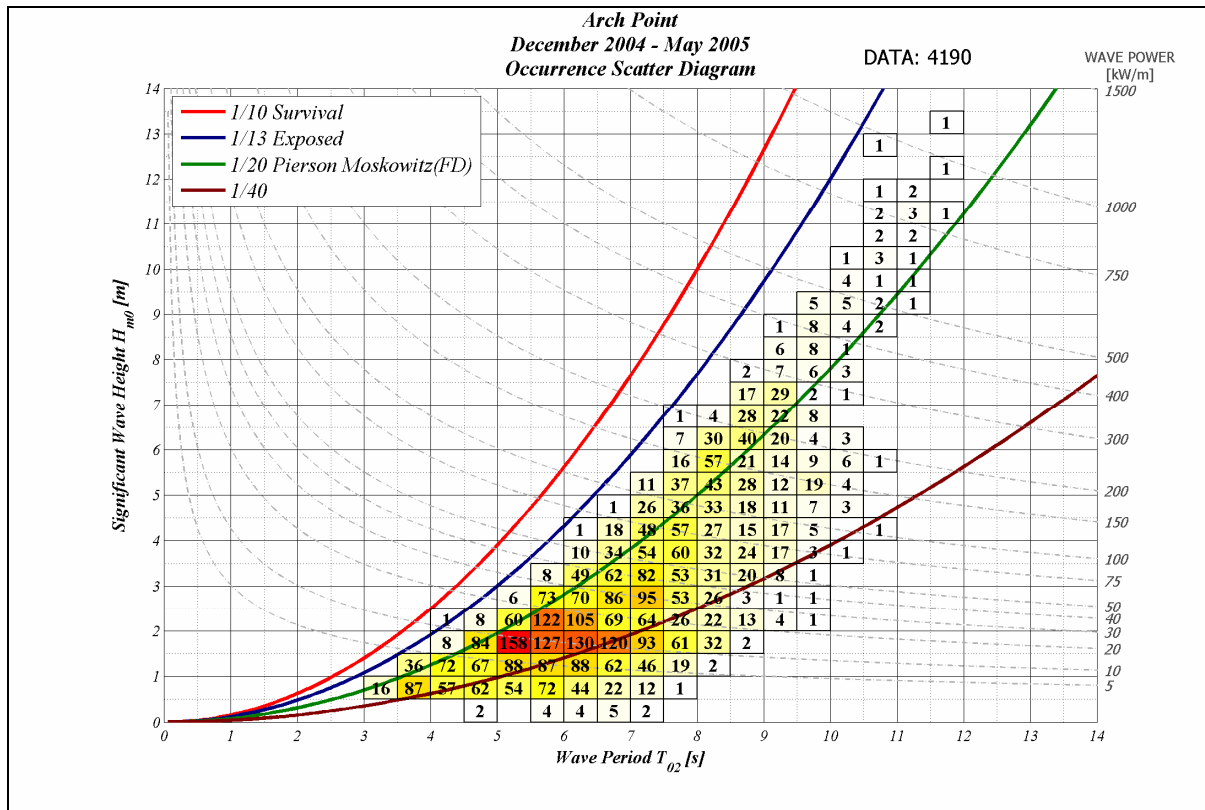
Figure 37. Scatter Diagram for the period December 2004 to May 2005 at the Arch Point location.
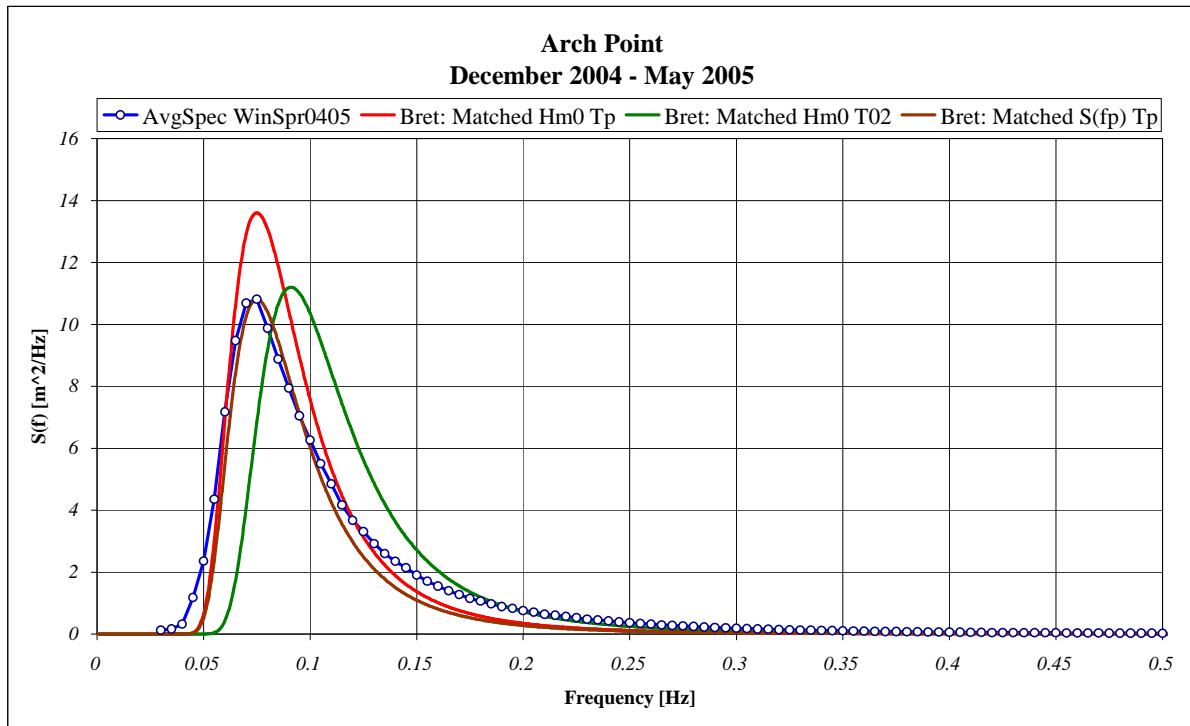

Figure 38. Average spectrum and Bretschneider fit of the combined winter and spring seasons of 2004-2005 for Arch Point.

7.2.6   Temporal Fidelity

The inherent variability of ocean seaways is clearly visible when the bi-variate scatter diagrams of Figure 35 and Figure 37 are compared, since larger sea states are experienced in the second winter/spring seasons. The result is the average spectrum of this data set being larger in overall variance, as shown in Figure 38. The summary statistics of the seasons in question are shown in

Table 8. The two data sets comprised four individual seasons and the summary statistics of the average wave spectrum of each of these seasons are also noted in Table 8.

Data Set	H_{m0}	T_{02}	T_e	T_p	Wave Power (T_e)	Wave Power (T_{02})	% Diff $\underline{P(T_e)}$ $P(T_{02})$
	[m]		[s]			[kW/m]	%
Dec'03-May'04	2.92	7.30	9.96	12.50	41.61	36.66	11.9
Winter *Dec'03-Feb'04*	3.08	7.36	10.03	13.33	46.62	41.12	11.8
Spring *Mar'04-May'04*	2.75	7.22	9.87	11.76	36.57	32.16	12.1
Dec'04-May'05	3.37	7.83	11.00	13.33	61.21	52.38	14.4
Winter *Dec'04-Feb'05*	4.21	8.30	11.50	14.28	99.88	86.65	13.2
Spring *Mar'05-May'05*	2.15	6.49	8.99	11.11	20.36	17.67	13.2

Table 8. Summary statistics of average spectra for Arch Point location.

The summary statistics that are presented in Table 8 are calculated from the spectral moments of the respective averaged spectra of the seasonal data sets. The variability of the seasons is evident from the variation of significant wave height. The extreme winter season of 2004/05 is followed by a low spring season, with the winter and spring of 2003/04 positioned between these in terms of magnitude. There is no large variation of the periods of these average spectra.

The primary wave power equation is derived using the energy period, T_e. The secondary wave power equation, which uses the average period, T_{02}, has a coefficient based on the ratio of these periods when using the Bretschneider empirical equation. The period statistics derived from the average spectra do not conform to the Bretschneider period ratios, therefore there is an inequality in the wave power calculated using both methods. The percentage difference of these figures is also presented in Table 8, which shows that in each case, the wave power calculated from the average period, T_{02} is on average underestimated by 13%.

7.2.6.1   Seasonal Spectral Averages

To quantify the variability of the variance density distribution of all the averaged spectra, a method was required to graph them together. This was achieved by producing a non-dimensional plot of the spectra, both in terms of the variance density and the frequency range. Figure 39 is a log-log graph showing the non-dimensional plots of the average spectra for all four seasons present in the two data sets and the combined two winter/spring seasons. This is not a plot of the variance density distribution, but rather the ratio of each frequency ordinate to the maximum. The thick grey line is the representative Bretschneider spectrum for all the various input variance densities and peak frequencies. The abscissa represents the non-dimensional frequency where the harmonics of the spectrum are divided by the peak frequency. The ordinate axis as described above is the harmonics non-dimensional variance density of the spectrum divided by the maximum value.

When the Bretschneider spectrum is graphed in this way, the non-dimensional Bretschneider profile is the same irrespective of the input variance or peak frequency, as shown in Figure 39. However, this type of graph is only useful to compare the average measured spectrum with the equivalent Bretschneider since inter comparison of the average spectra is not so clear when the ratios between the peaks is not apparent. The actual average spectra and respective Bretschneider fit is shown in Figure 40.
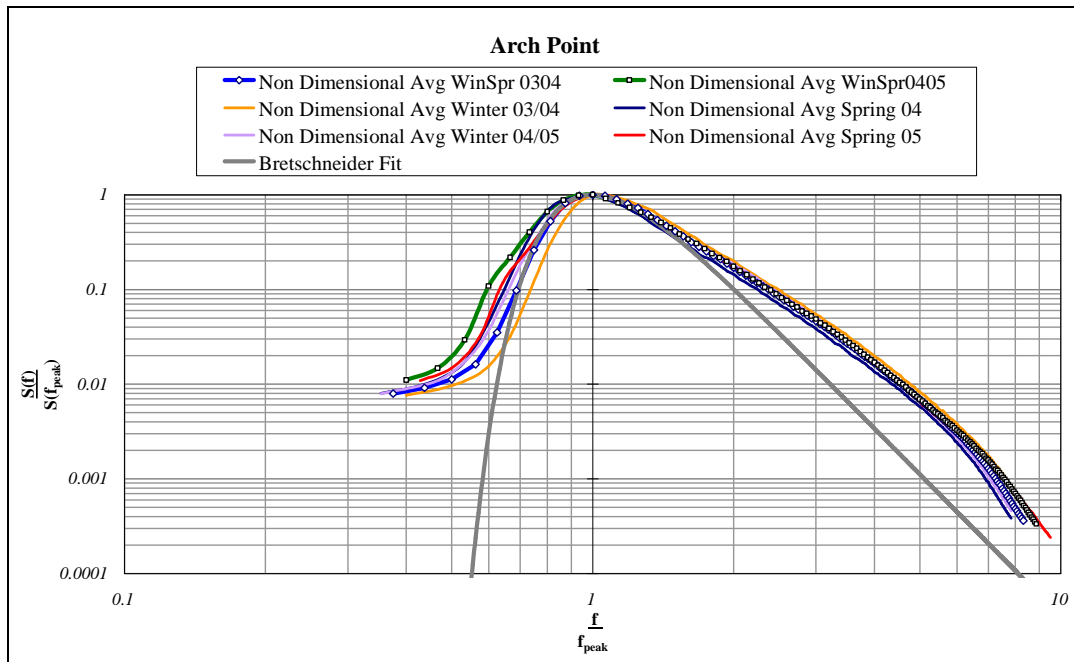
Figure 39. Comparison of non-dimensional spectra.

Examination of Figure 39 leads to the following conclusions. This plot indicates that the ratio of the peak of the spectrum to the ordinates at frequencies higher than the peak frequency ($f>f_p$) i.e. at short periods, is larger than for a Bretschneider spectrum, and that this ratio is similar for all the seasonal averaged spectra depicted in Figure 39. However, the same is not the case at frequencies less than the peak frequency ($f < f_p$) i.e. long periods. In this region of Figure 39, there appears a greater variation in the ratio of spectral ordinate to peak ordinate which may indicate a greater variability in the contribution of long period components to the spectra considered here.
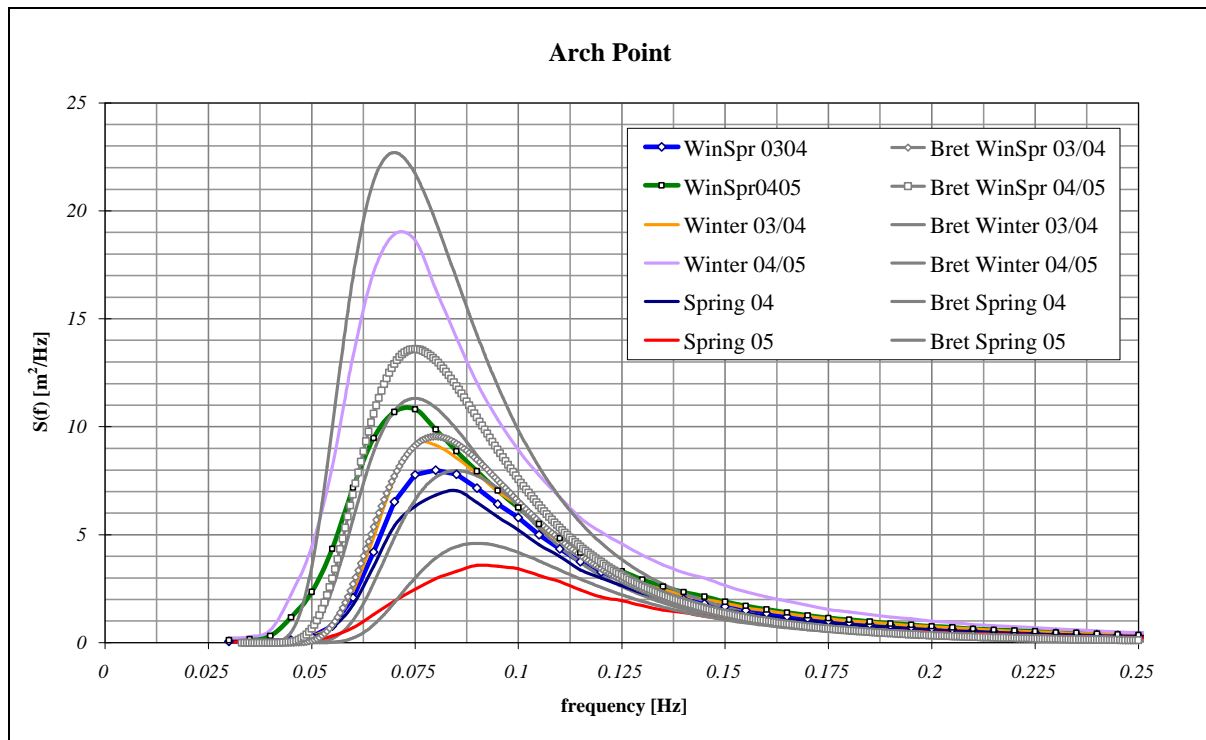
Figure 40. Comparison of Average Spectra and Bretschneider Fit.

The seasonally averaged spectra follow the respective Bretschneider profiles reasonably well but over-estimation of the energy around the peak by the Bretschneider equation in comparison to the averaged spectra is balanced out by the underestimation at frequencies greater than 0.125Hz. The measured spectra and their respective Bretschneider equivalent contain the same energy, depicted by the area under the plot lines in these graphs. It appears that the averaged spectra from the measured data is wider than the empirical counterpart.

By sub-dividing the time scales for further analysis, a greater variation in the distribution of energy in the spectrum becomes apparent. The time scales selected are as follows and ensemble averages of the measured spectra are compared to the classical spectral shape:

- 6 months (Winter & Spring)

- 3 months (Winter)

- 1 month (January)

- 1 Week

- 1 Day

7.2.6.2   Monthly, Weekly & Daily Duration Averages

To assess the variance density distribution of the shorter time span averaged spectra more clearly, they are not plotted together. Figure 41 shows the average spectra and the fitted Bretschneider for the seasonal and monthly time scales. Figure 42 is the same data but now with non-dimensional units as described previously. In general, it can be said that the resultant averaged spectra are closely related to the Bretschneider equation, and that there is very little variation between spectra of the spectral ordinate to spectral peak at either side of the peak frequency.
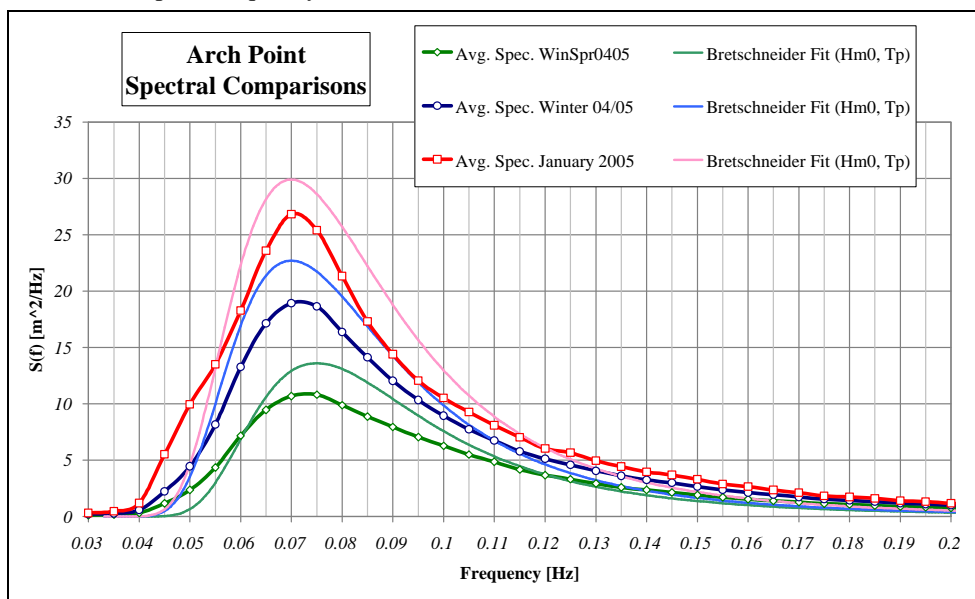

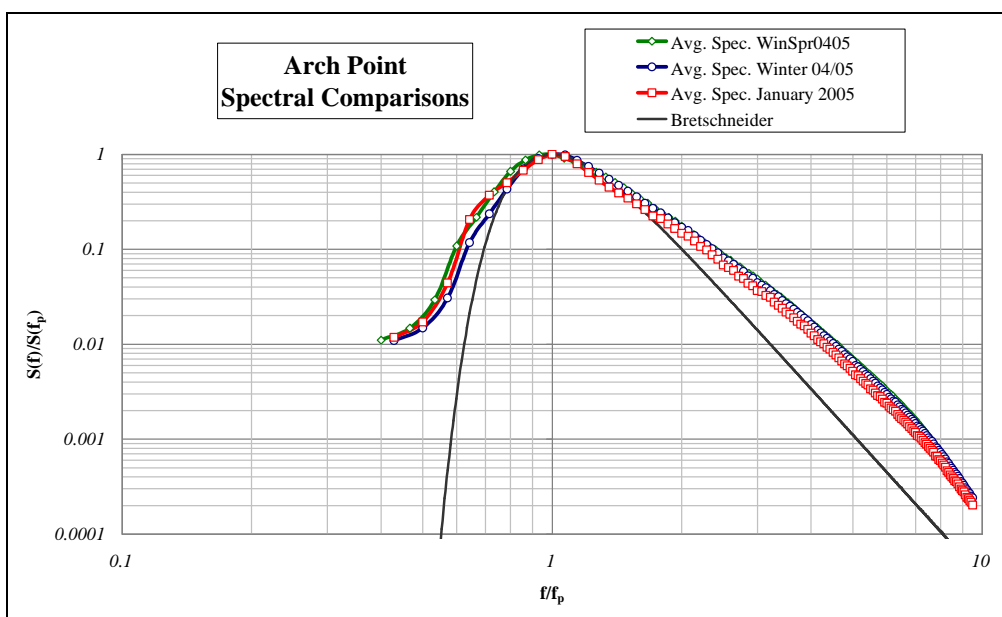**Figure 41. Average spectra and Bretschneider fit for seasons and month time scales.**

Figure 42. Non-dimensional average spectra and Bretschneider fit to compliment Figure 41.

The next time duration determines the average spectra for one week and for two individual days within the selected month. The average spectra of these particular data sets are shown in Figure 43 and in non-dimensional form in Figure 44. It is clear from these plots that there is a greater variation in the average spectra at these time scales. As shown previously in Figure 41, the monthly average closely resembles a Bretschneider spectrum, however the approximation to a Bretschneider spectrum is lost as the time averaging scales are reduced. Even for two consecutive days, there is a marked difference in the overall spectral shape of the average of the hourly measured spectra. This could have important consequences in the rate of measurement and reporting at a potential deployment site.
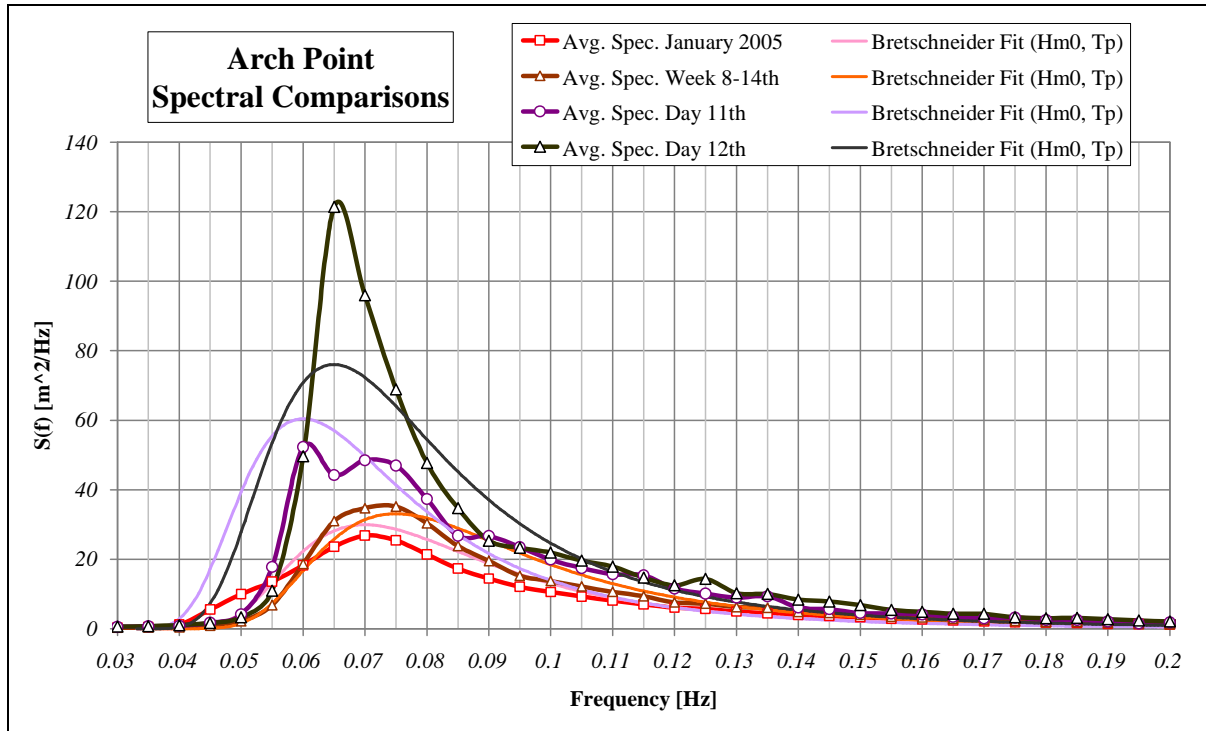

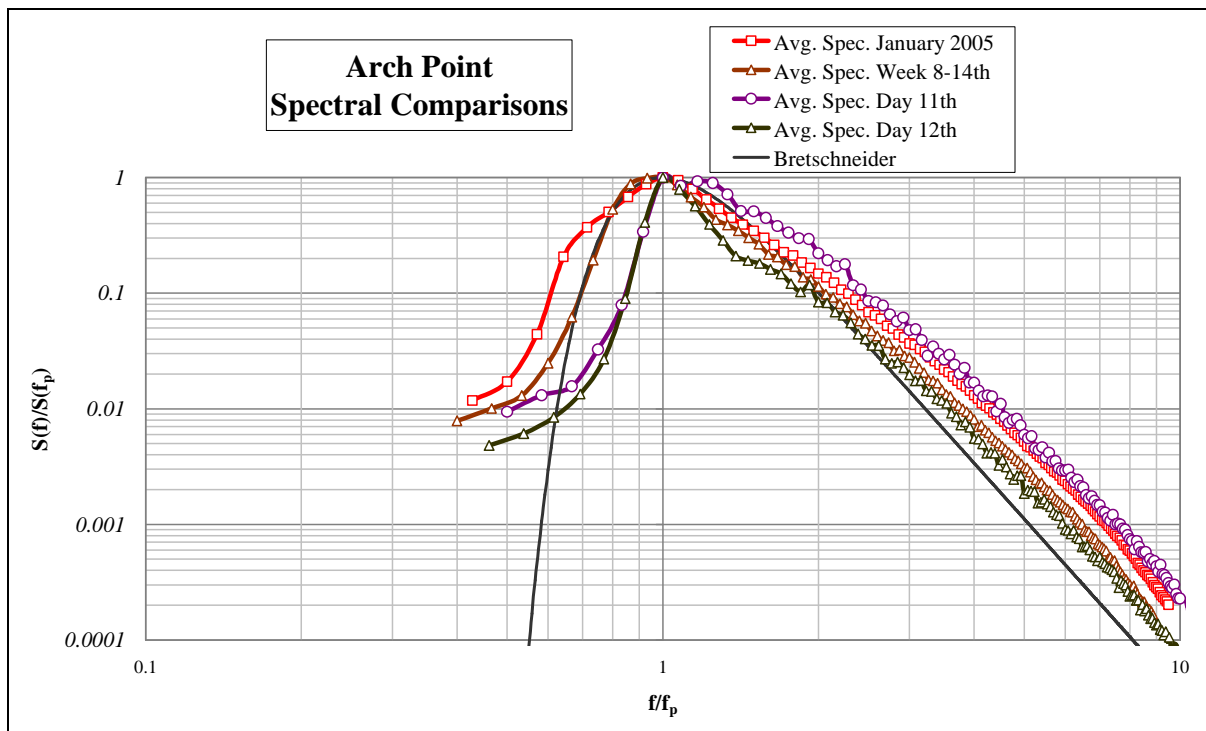**Figure 43. Average spectra and Bretschneider fit for month to day time scales.**

Figure 44. Non-dimensional average spectra and Bretschneider fit to compliment Figure 43.

7.2.6.3   Daily & Hourly Duration Averages

To greater understand the variation in the two daily averaged spectra shown in Figure 43, the individual hourly spectra, daily average spectra and respective Bretschneider fit are plotted in Figure 45. The consequent summary statistics of significant wave height and average wave period for these selected consecutive days are shown in Figure 46 and it is apparent from this plot the difference in average spectral shape for the two days. Day 1 (11th January 2005) has a step change as the significant wave height doubles from below 4m to over 8m. Figure 47 is a plot of the wind speed from a meteorological station positioned at Shannon Airport, the closest met station to the site of interest. This shows an introduction into the measurement area of a generating wind in the second half of Day 1, resulting in two distinctive forms of spectra occurring. However, the declining storm wind speeds during Day 2 (12th January 2005) correspond to the wave height levels as the storm abates, leading to similar forms of spectral shape occurring.
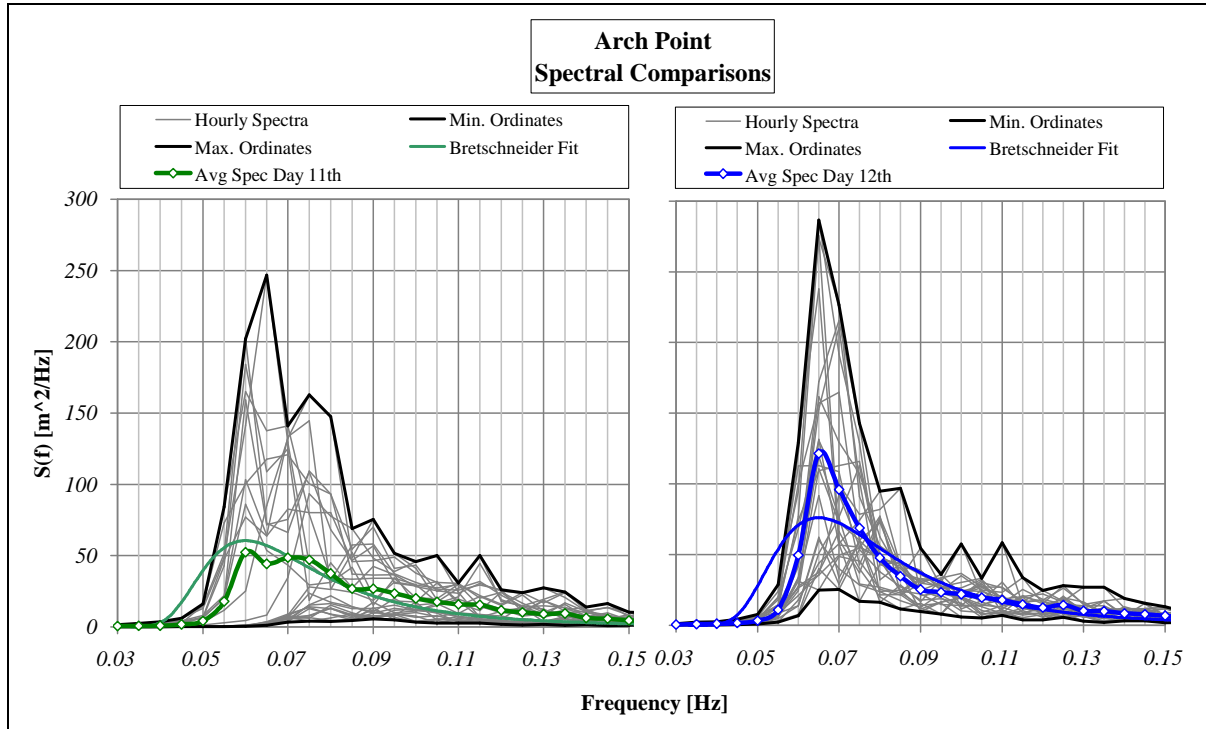

Figure 45. Hourly and average spectra with Bretschneider fit of two consecutive days.
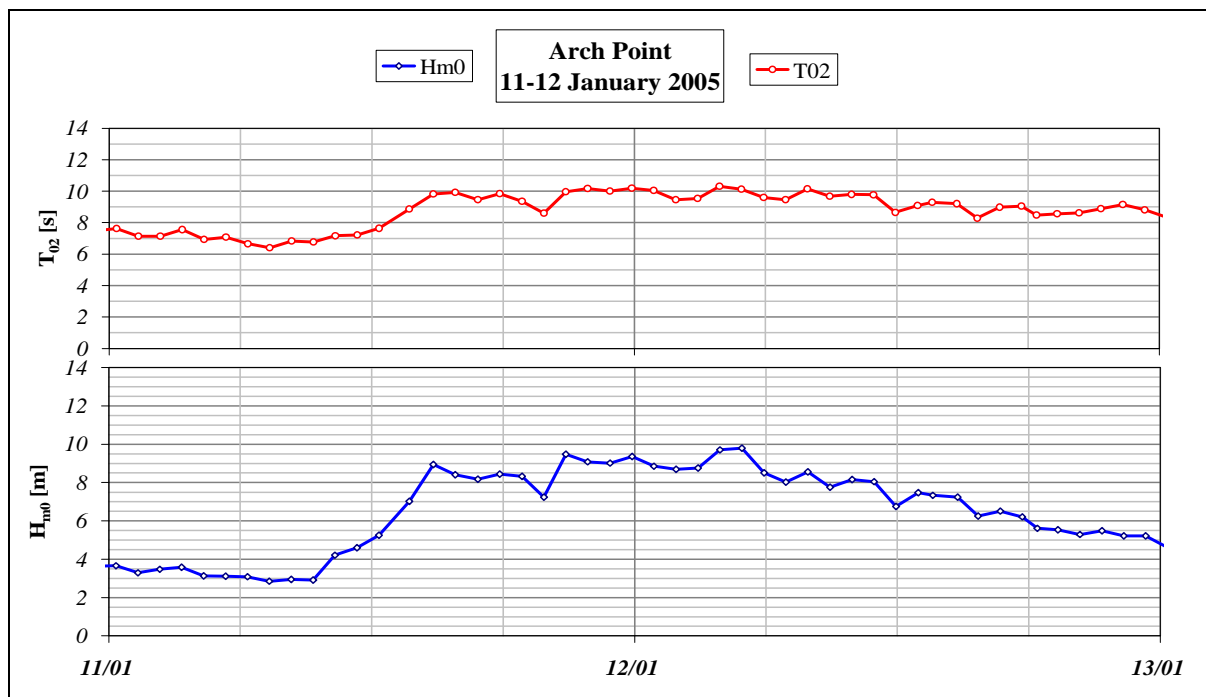

Figure 46. Significant wave height, Hm0, and average wave period, T02 for the selected two consecutive days.
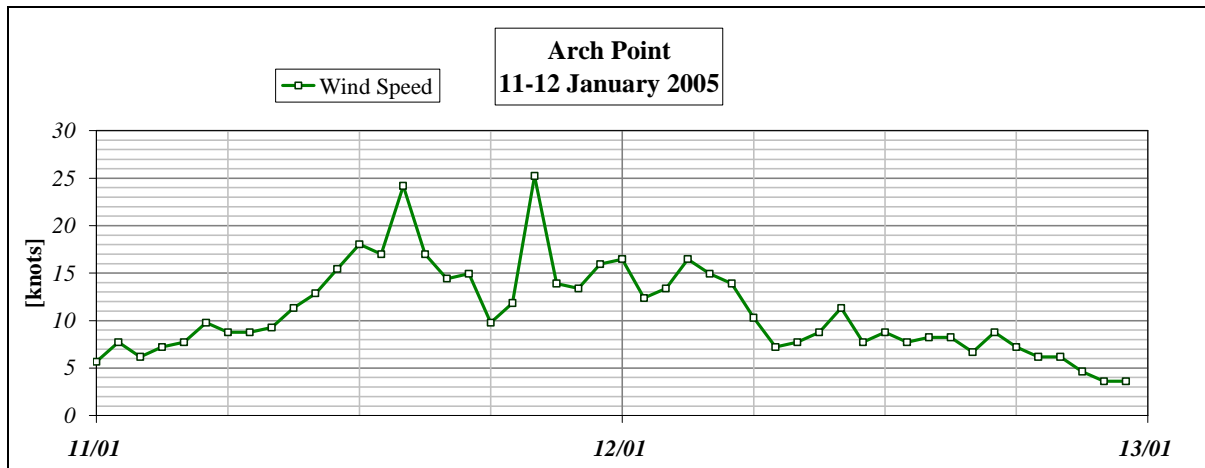
Figure 47. Wind Speed [knots] land station close to Arch Point

7.2.7   Summary Statistic Variations

Having looked at the variation of the spectral shape in terms of time scales, the variation of spectral shape due to changing summary statistics is now investigated. This is conducted by assessing the average spectra within elements of a scatter diagram. Although it was mentioned previously that the recommended scatter diagram elements should be a half meter by half second in size, for this study a 1m by 1s element size bin is used for convenience and to increase the number of spectra residing in a scatter diagram component.

7.2.7.1   Iso-Height & Iso-Period

Figure 48 below shows the bi-variate scatter diagram from the month of December 2003. The scatter elements of iso-height with a range of $2m \leq H_{m0} < 3m$ and iso-period of $7s \leq T_{02} < 8s$ are indicated by the bounding boxes. These were selected as they both incorporate the element of most occurrences (H_{m0}: 2-3m, T_{02}: 7-8s).
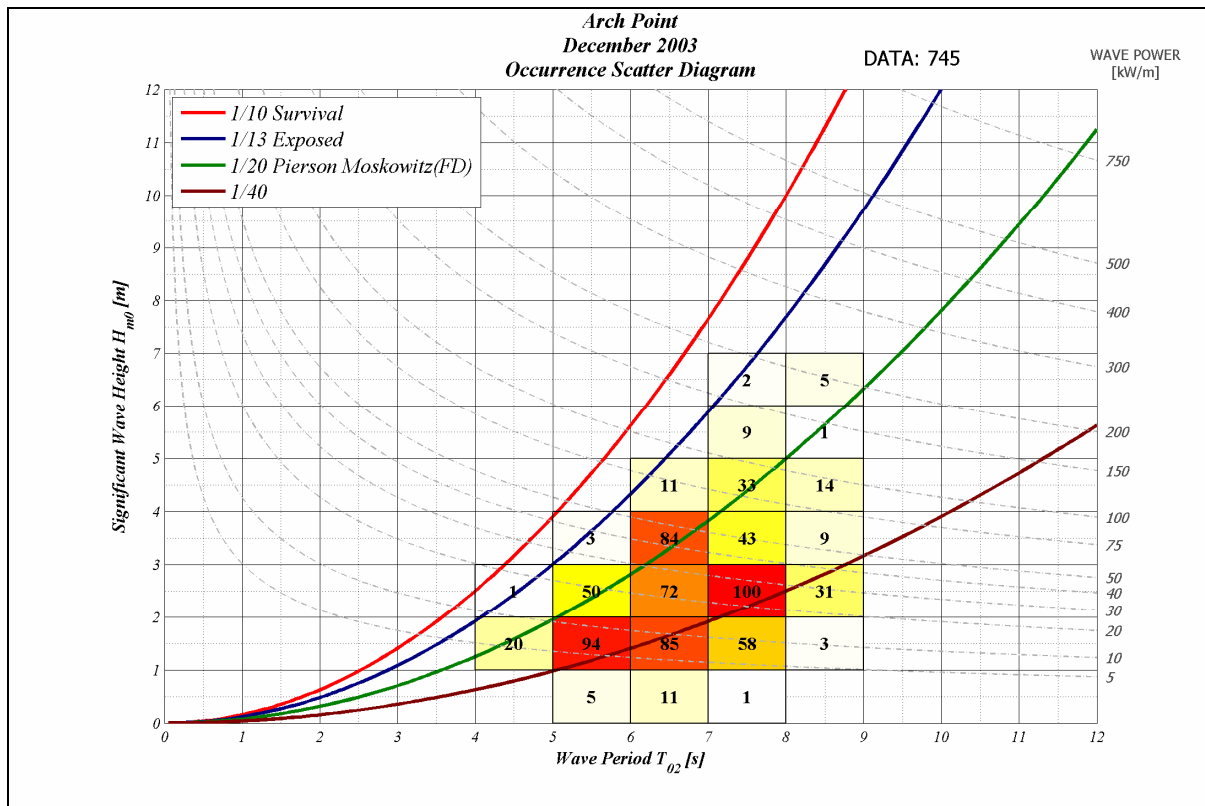

Figure 48. December 2003 bi-variate scatter diagram with selected iso-height and iso-period elements.
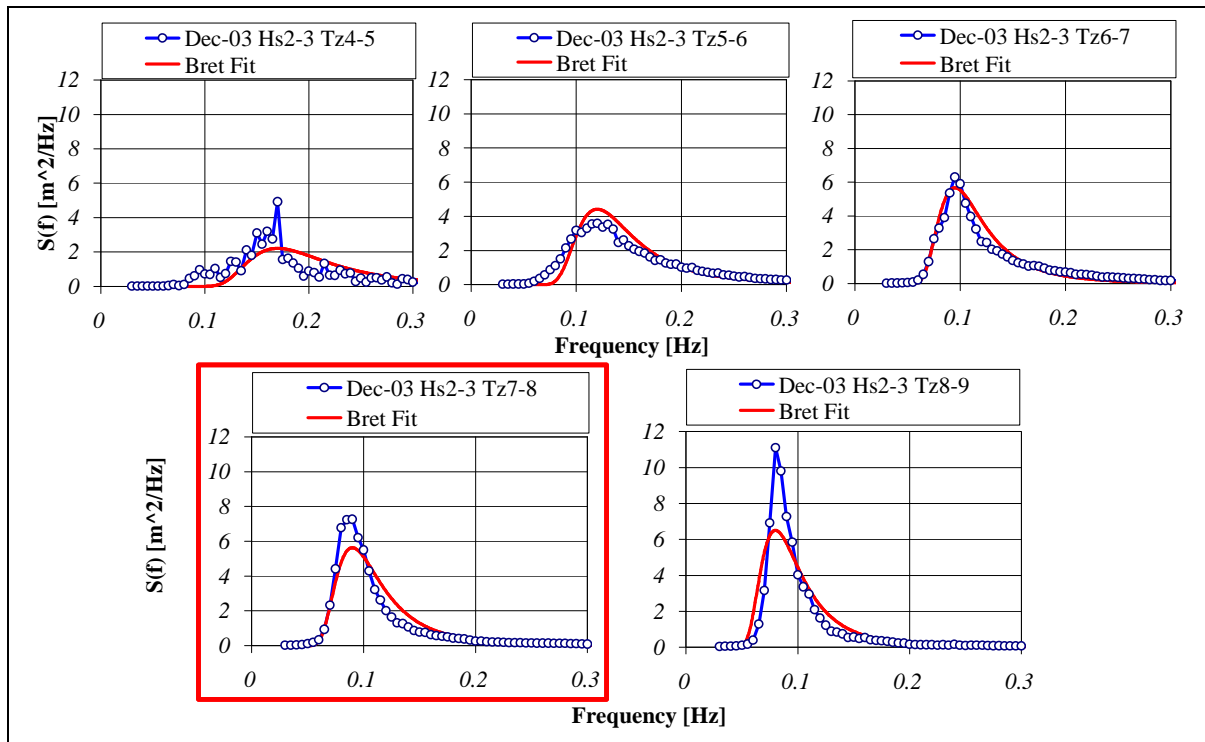
Figure 49. Average spectra and Bretschneider fit for iso-height scatter elements of Figure 48.
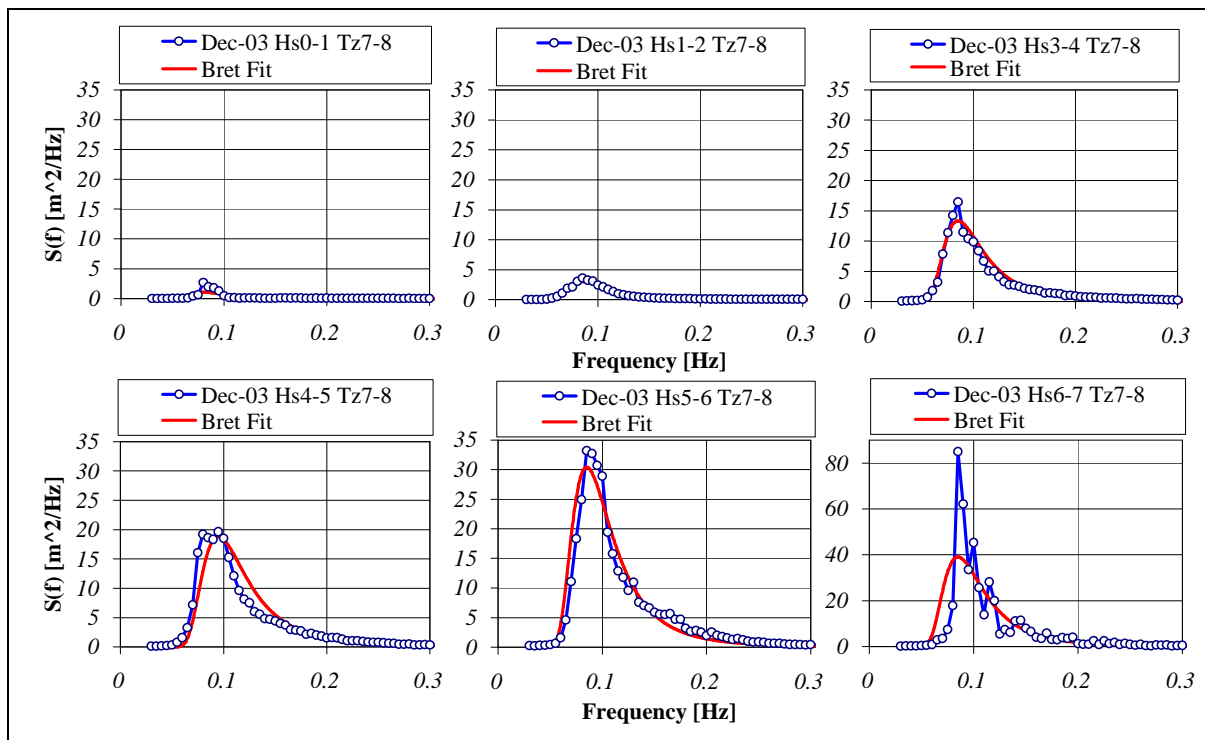

Figure 50. Average spectra and Bretschneider fit for iso-period scatter elements of Figure 48.

Figure 49 shows the average spectra and relevant Bretschneider equivalent for the five elements that are contained within the iso-height band of the scatter diagram of Figure 48. The Bretschneider fit was calculated from the significant wave height and average period of the resultant average spectrum and not the median points of the scatter diagram elements. The plots are truncated at a frequency of 0.3Hz for convenience as the spectral ordinates that reside from 0.3Hz to the upper frequency limit contain very little energy. The goodness of fit of each of the empirical spectra are clearly visible by inspection.

Figure 50 shows the average and Bretschneider spectra for each of the iso-period scatter elements indicated in Figure 48. The common component of H_{m0}: 2-3m, T_{02}: 7-8s to both the iso-period and iso-height is not repeated in Figure 50 but outlined in Figure 49. Also note that for convenience, the ordinates of the last plot of Figure 50 does not have the same scale as the other plots in that figure. From Figure 50 it can be argued that the average spectra of each scatter diagram component is a better fit to

their equivalent Bretschneider spectra except for the element of H_{m0} of 6-7m, T_{02}: 7-8s which is better approximated by a JONSWAP type spectral shape.

7.2.7.2   Iso-Steepness

As a final investigation into the variation of measured spectra, the scatter diagram components that follow the significant steepness line of 1:20 was investigated for the month of January 2005. This month was selected as it incorporated the highest recorded significant wave height in the duration of the measurement scheme. The significant steepness of 1:20 was chosen as it is an approximation of the steepness of a Pierson-Moskowitz empirical spectrum (s_s = 1:19.7), therefore the fitted Bretschneider spectrum to the average spectra would be a close approximation to a P-M spectrum. The positions of the chosen facets of the iso-steepness are indicated in Figure 51 below, the bi-variate scatter diagram for the month of interest. As previously stated, this is the unbiased scatter diagram for the month of January and incorporates 737 (95%) measurements, which results in one measurement per hour for the entirety of the month.
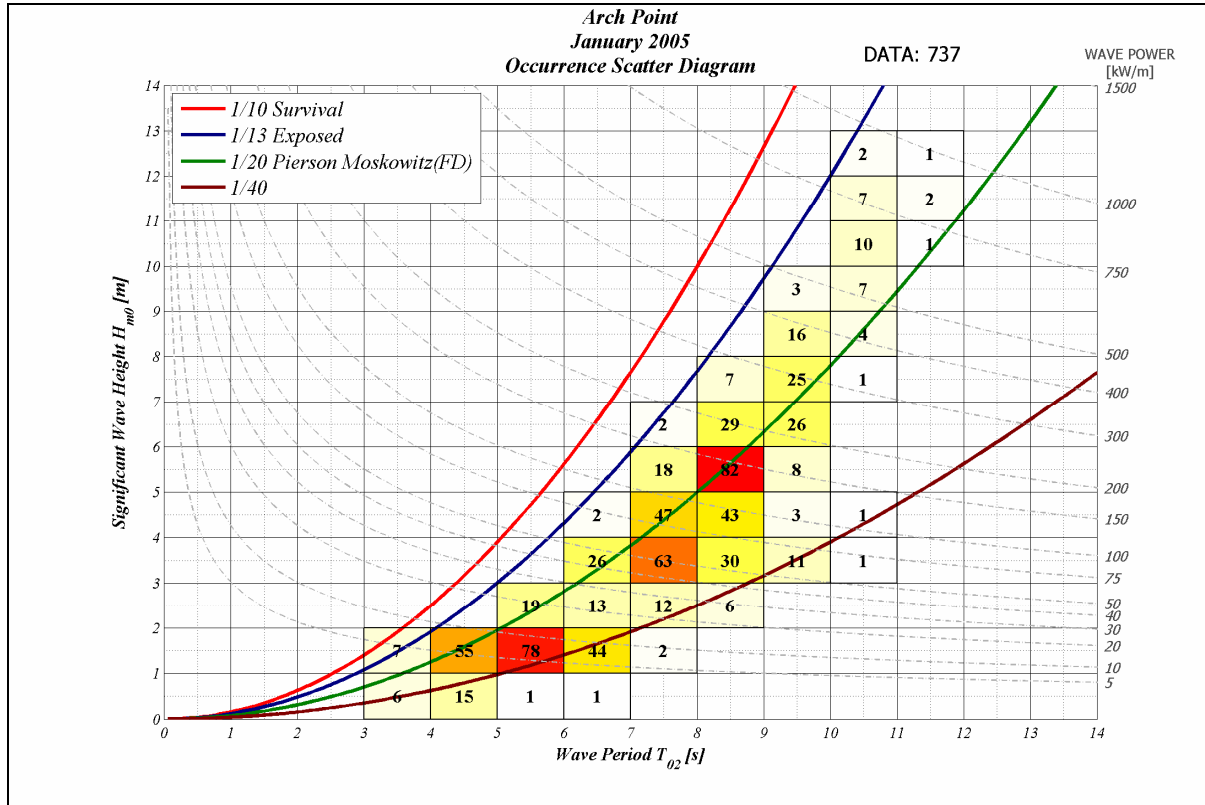
Figure 51. January 2005 bi-variate scatter diagram with selected iso-steepness components.

The average spectra and Bretschneider equivalent for the eight components selected along the iso-steepness line as indicated in Figure 51 are plotted in Figure 52. Six of the eight averaged spectra are in good agreement with the Bretschneider fit, including those sea states of a severe nature. The reason that some of the sea states selected do not conform to the empirically derived spectra in some instanced is due to low levels of occurrence.

Figure 52. Average spectra and Bretschneider fit for iso-steepness scatter elements of Figure 51.

7.3   SYBIL POINT, IRELAND

7.3.1   Measured Seaways

A Datawell non-directional Waverider buoy was deployed at an exposed location 37 nautical miles south west along the western seaboard and in a water depth of approximately 73m at Sybil Point. The data from this location is for a period of 23 days during a winter season from mid-December to mid-January. The data buoy recorded the surface elevation with a sampling frequenc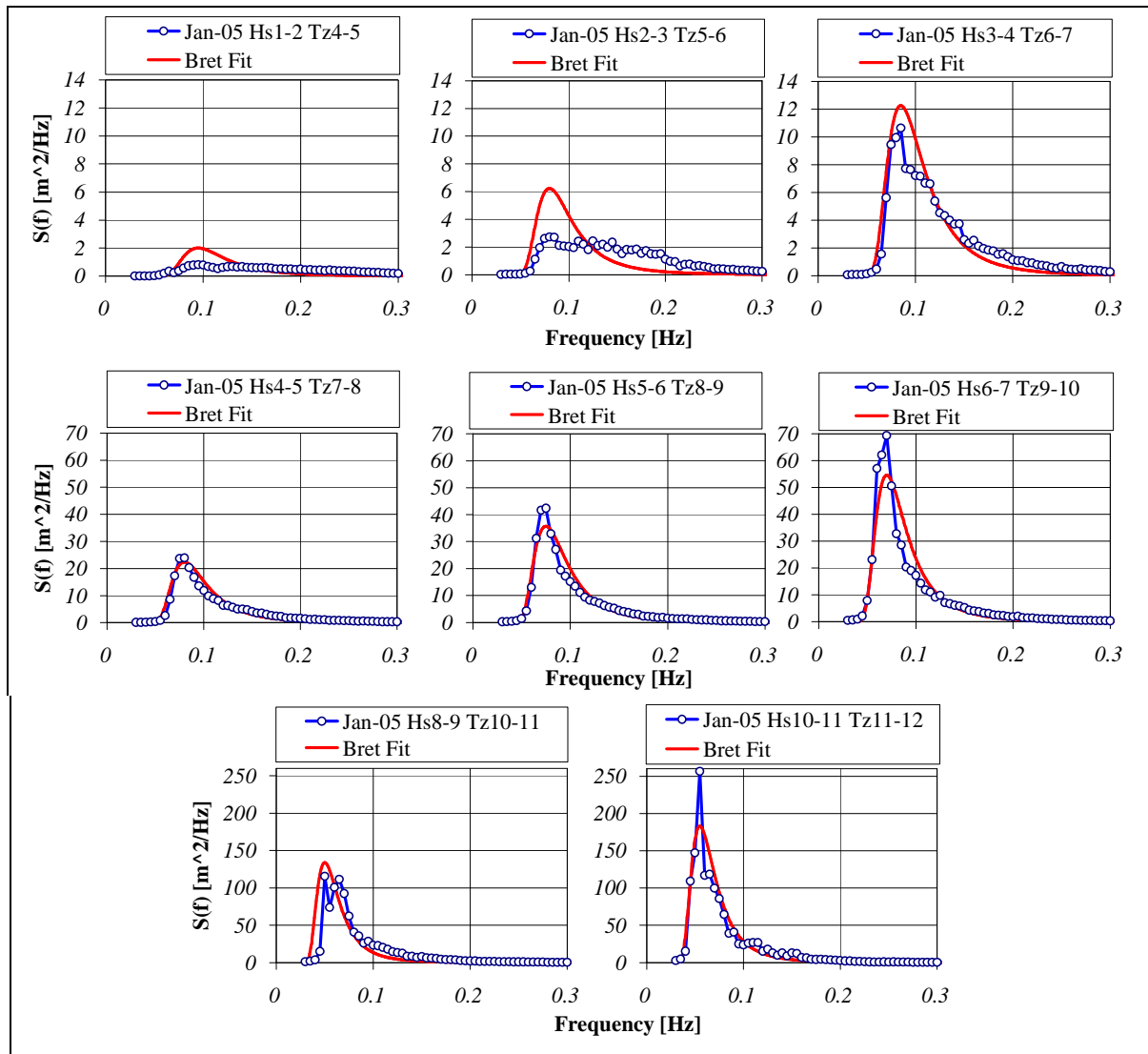y of 2.56Hz, however the receiver at Arch Point used the older Datawell data management system (DIWAR). The data management system (RfBuoy) utilised by the Sybil Point buoy has an extended surface elevation record of 30 minutes, which is subsequently logged ever half hour.

7.3.2   Predicted Seaways

To compliment the Sybil Point measurements, predicted data was made available for a location close to the buoy deployment site. This computed data was provided by the Irish meteorological office, Met Eireann, whose regional WAM model is used for wave forecasting and which extends from 4.75°W to 12.5°W and 50°N to 56°N. It is possible to produce directional spectra for any node point within the regional grid and from these the summary sea state statistics are derived. The WAM model provides a 48 hour forecast updated every 6 hours. The forecast data comprises of a directional spectrum together with the summary statistics. For the comparison study conducted here, the non-directional spectrum of the zero hour analysis with a time interval of 6 hours is derived and compared to the nearest temporal measured spectrum. The location map is shown in Figure 53 which includes the deployment sites of the buoy, the WAM grid at ¼ degree spacing, and the selected WAM data point used for the spectral comparison at Sybil Point.
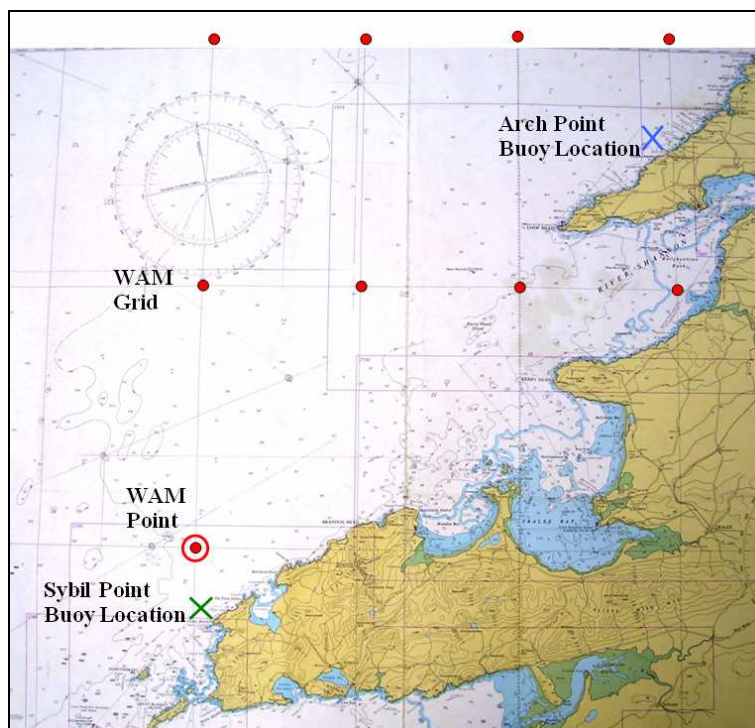
Figure 53. Location map of buoys and WAM grid points.

7.3.3 Predicted Fidelity

This investigation involves evaluating the spatial fidelity by comparison of measured to predicted spectra at the Sybil Point site. A limited dataset is available for comparison but a good range of sea states were recorded, the largest having a significant wave height of 9.97m. Firstly, a regression analysis is done on the concurrent data comparing the summary statistics of the WAM model to the data buoy. This is carried out for the zero hour prediction of the WAM model. It is generally found that the WAM model over predicts in low sea states and under predicts in higher sea states. For selected points in the time history, a comparison is made of the variance density spectrum from the WAM model and the buoy. The directional spectrum is also investigated to better understand the deviation of the WAM model spectral ordinates from the measured spectra.

7.3.4 Forecast Comparison

Previously the summary statistics from regional 3rd generation wave models have been compared to measured values to assess the models accuracy and forecasting ability. In this study, the 2 dimensional spectra from the regional WAM model for Ireland was supplied to the HMRC for investigation. To complement this data set, a data buoy was deployed off the west coast of Ireland. Unfortunately this buoy is non-directional, therefore comparisons of the 1 dimensional frequency spectrum could only by made.

7.3.5 Summary Statistics

The recorded files are of 30 minute duration and were logged every half hour. This measurement process was carried out from 19th December 2007 to 11th January 2008, and resulted in 1,105 files. These files were spectrally analysed to determine the variance density spectrum and associated summary statistics as described in Table 1.1. The bi-variate scatter diagram is shown in Figure 54 which indicates that even though the measurement duration was equivalent to a month's data, a large range of sea states were recorded.
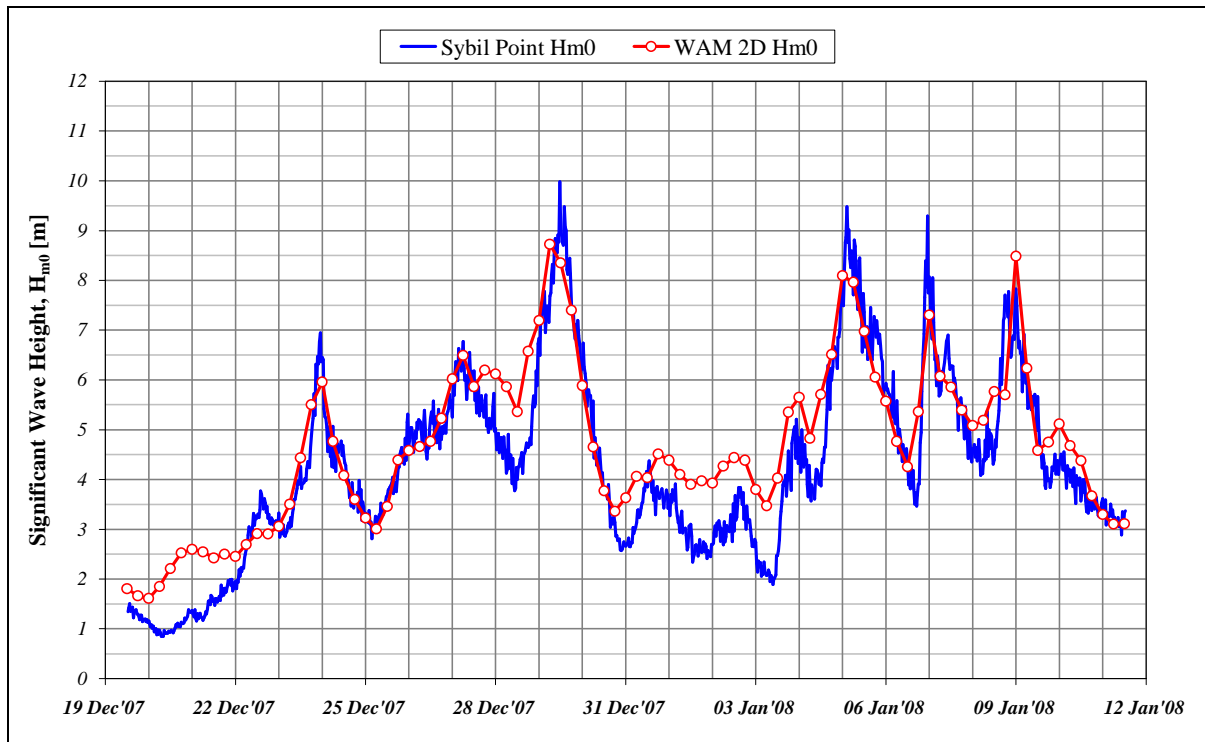
Figure 54. Bi-variate scatter diagram for Sybil Point.

To compliment this measured data, HMRC obtained 3rd generation forecast data which was supplied by Met Eireann, Ireland's meteorological office. The regional WAM model for Ireland has a spatial resolution of a ¼ degree in longitude and latitude, and is nested within the global European model run by the European Centre for Medium Range Forecasts (ECMWF). The regional WAM model provides a 48 hour forecast which is generated every 6 hours. This forecast contains a directional spectrum of 30 frequencies and 24 directional bins. The unit of the variance density is therefore $[m^2/Hz/°]$. By integration across direction, the one dimensional variance spectrum may be obtained. The spectrum in the model is separated with a constant directional resolution ($\Delta\theta$) of 15° and a constant relative frequency resolution ($\Delta f/f$) of 0.1. The frequency resolution is defined by the high and low discrete frequencies and the number of frequencies in this range. The frequency resolution is defined by the equation below, where N is the number of frequencies. This method of discretisation results in a frequency range from 0.0345Hz to 0.5476Hz and $f_{i+1}=1.1f_i$.

$$\Delta f = \left(\left(\frac{f_{high}}{f_{low}} \right)^{1/N-1} - 1 \right) f$$

Figure 55 plots the significant wave height derived from both the measured data and the WAM model. The WAM data used is the zero hour forecast, that is the first forecast value of each 6 hourly 48 hour prediction. In general the WAM data does coincide with the peaks of the storms although the energy contained is either under or over predicted.

Figure 56 shows the relevant wave periods from both data sets for the Sybil Point location, as derived from the spectra. It is clear that there is better agreement between the WAM and measured data for the peak and energy period than for the average period, T_{02}.

Figure 55. Significant wave height, Hm0, of measured buoy data and forecast WAM data from Sybil Point.

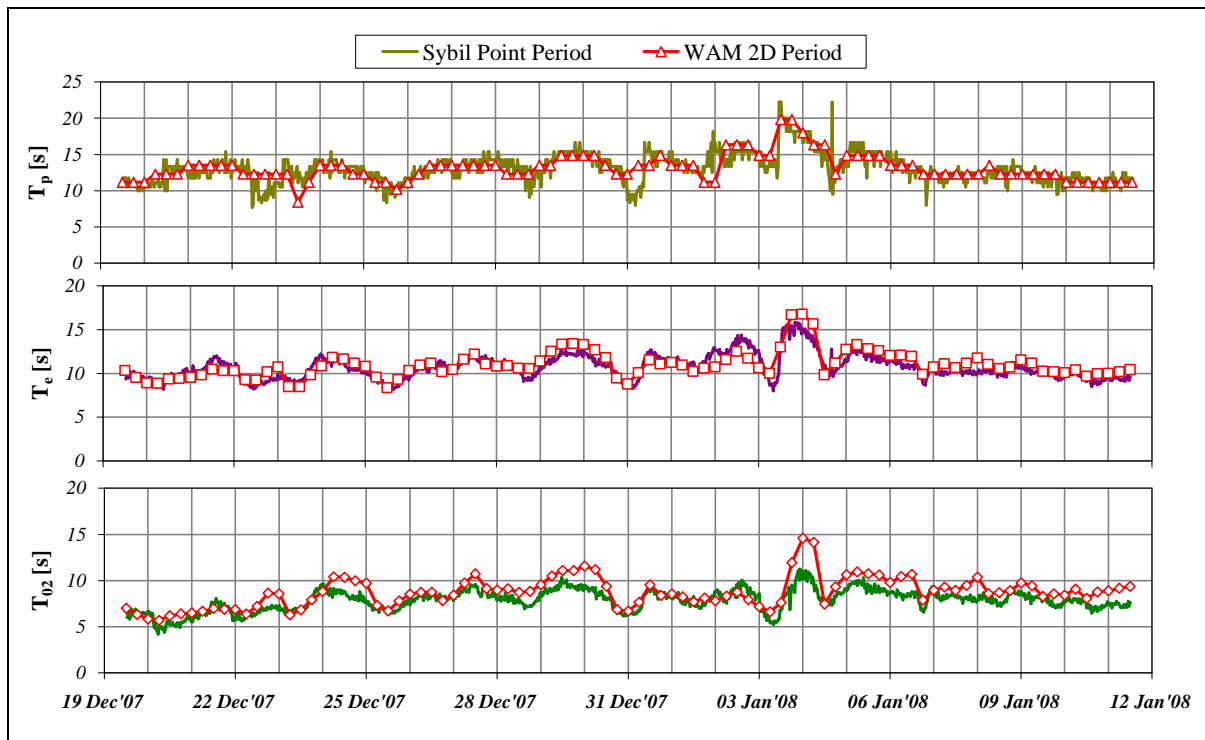**Figure 56. Wave periods, Tp, Te and T02 from measured and forecast data for Sybil Point.**

To better understand the differences from the prediction to the measured data, a regression analysis was conducted on the data. Only those measured data files that were recorded at a time closest to the WAM output were considered, that is every 6 hours. Figure 57 shows the regression plots of the four summary statistics, H_{m0}, T_{02}, T_e and T_p. The trend observed previously of the WAM model over estimating significant wave height at lower levels and under estimating at higher levels is clearly evident in the linear fit. There appears a general over estimation of the average period while the energy period seems to be well predicted. A similar trend to the significant wave height is found with the peak period regression plot as there is some over and under estimation taking place. The correlation coefficient, R^2, in Figure 57 is an indication of the goodness of fit. If the data is a perfect fit then $R^2 = 1$ and if the data sets are completely uncorrelated, then $R^2 \rightarrow 0$.

Table 3.1 presents the percentage difference between the WAM modelled output and the measured summary statistics. A positive percentage difference implies that the WAM data is over predicted. The results of Table 9 below indicate that in general, the WAM model over predicts the four key summary statistics, but especially in relation to significant weave height. It would appear from the mean results that the peak period is the best forecast summary statistics, although there is a large variation in the percentage difference, therefore it is concluded that the energy period, T_e, is the closest forecast result from the WAM model. To draw concrete conclusions from this study however, a greater data set is required to comment on the reliability of the WAM model.
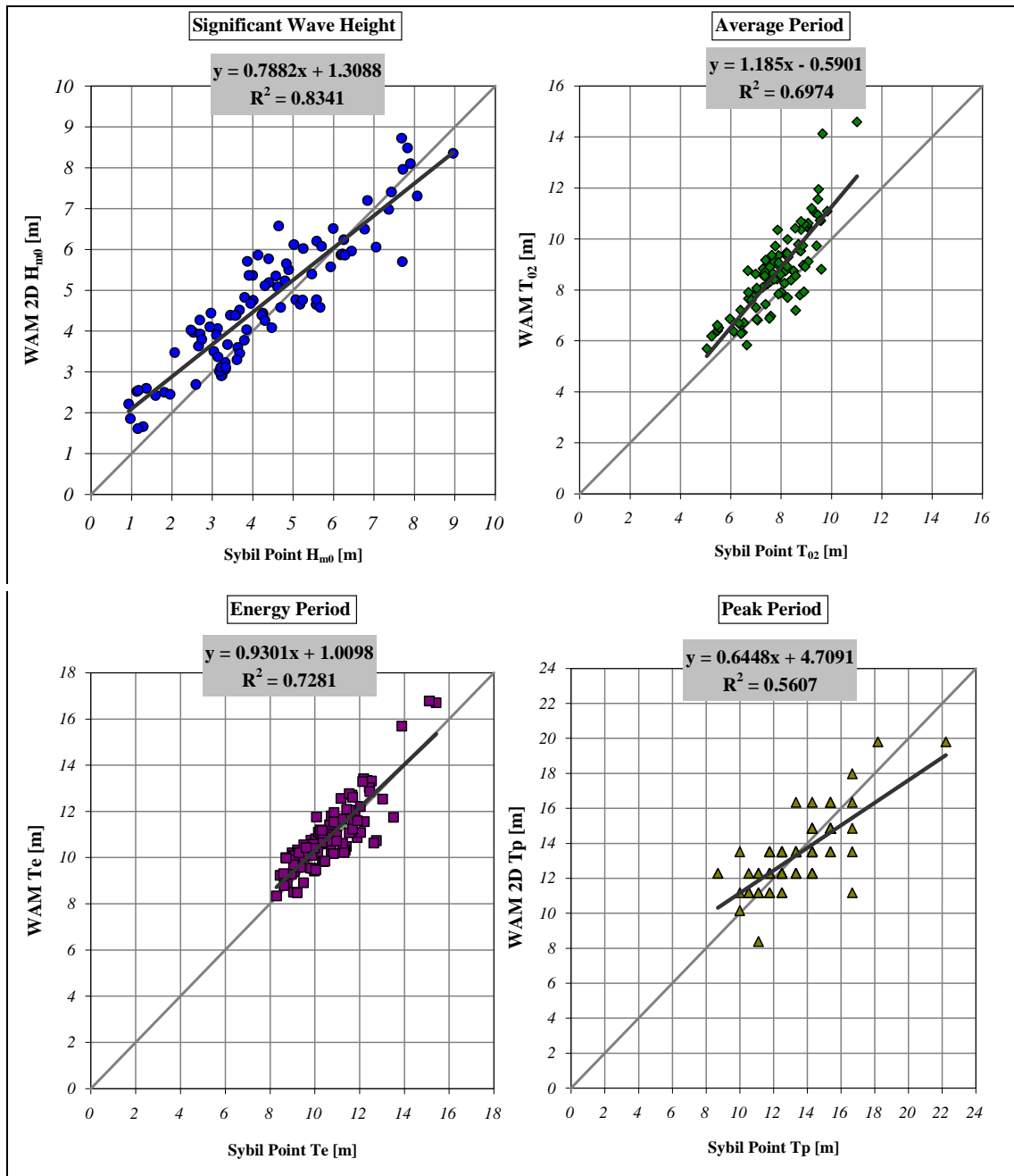
Figure 57. Regression plots of WAM versus measured data, for summary statistics, Hm0, T02, Te and Tp.

Summary Statistics	Mean Percentage Diff [%]	Standard Deviation Percentage Diff [%]	Correlation Coefficient R^2
H_{m0}	10.52	18.65	0.83
T_{02}	9.83	9.34	0.70
T_e	2.06	7.19	0.73
T_p	0.16	11.45	0.56

Table 9. Mean and standard deviation percentage difference and correlation coefficient between WAM and measured summary statistics.

7.3.6   Spectral Comparison

After the regression analysis, it was decided to select certain data points to compare the measured spectral shape with the predicted WAM model output for instances when there was a good match or a large discrepancy. Only a few examples are presented here

for inspection, the details of which are presented in Table 10 and the respective plots of significant wave height, one dimensional spectrum and two dimensional spectrum are shown in Figure 58 to Figure 63.

	WAM Prediction				Measured Data			
	H_{m0}	T_{02}	T_e	T_p	H_{m0}	T_{02}	T_e	T_p
00:00 21/12	2.60	6.51	9.54	13.51	1.37	5.23	9.82	11.76
00:00 25/12	3.23	9.72	10.81	12.29	3.32	7.77	10.03	13.33
12:00 28/12	5.36	8.71	10.59	12.28	4.00	7.61	10.33	14.29
12:00 29/12	8.35	11.09	13.34	14.86	8.96	9.83	12.34	15.38
18:00 30/12	3.36	6.84	9.46	12.29	3.14	7.03	10.04	11.76
06:00 03/01	3.47	6.61	10.00	14.86	2.07	5.49	8.71	14.29

Table 10. Summary statistics of selected spectral comparisons.

Figure 58 and Figure 63 are examples of a large discrepancy between the predicted spectrum from the WAM model to the measured spectrum from the recording buoy. In these plots, the WAM model indicates the presence of a bimodal sea state, both in frequency and direction, with the total energy comprised of wind and swell components approaching from two directions. Although there is an overall over prediction from the WAM model, the buoy data does indicate the existence of a low energy wind sea component.

Figure 59, Figure 61 and Figure 62 signify a reasonable fit between the WAM model and the measured data. Although this might be expected for the uncomplicated spectra of Figure 59 and Figure 61, which are single peaked in both frequency and direction, the WAM model also manages to predict the more complicated spectra that is shown in Figure 62.

Figure 60 indicates that at this location the WAM model does not dissipate the energy after the passage of a storm quickly enough. Further investigation of this would require wind measurements and measurements from a directional buoy in close proximity to the WAM grid node, to fully understand the wave generation mechanics at the chosen location.
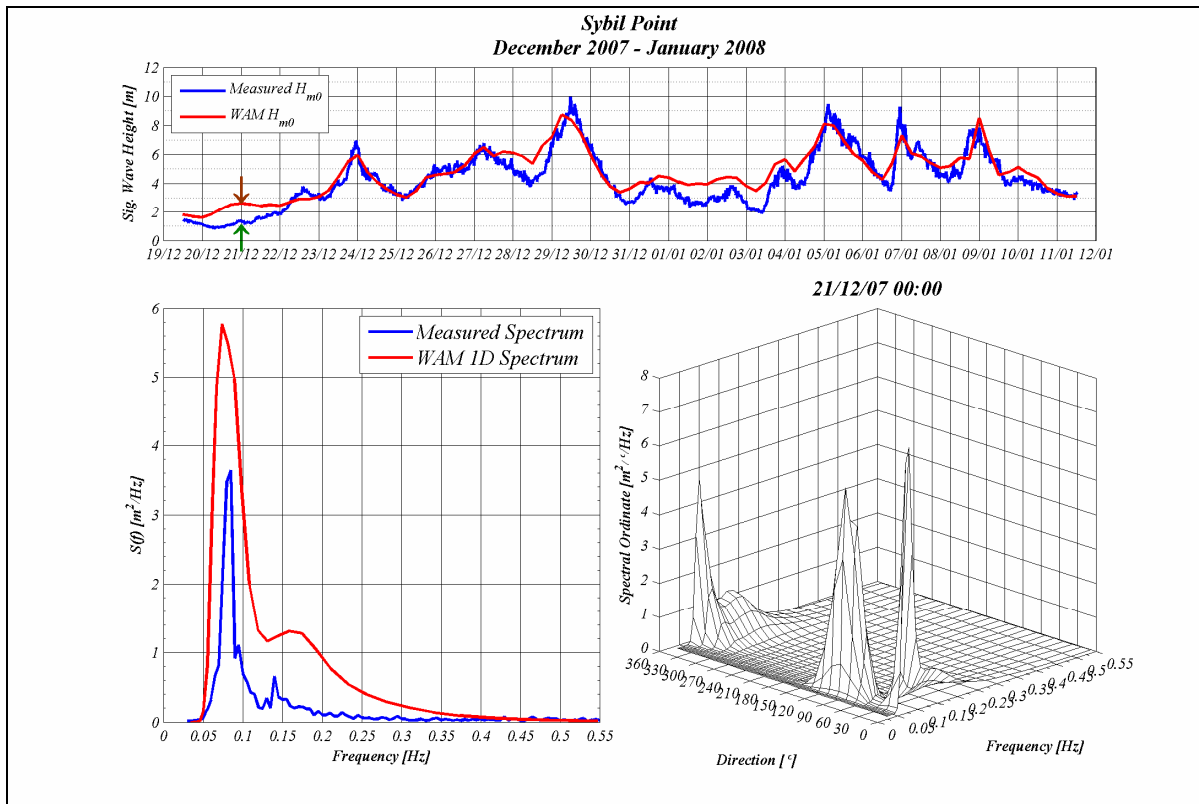

Figure 58. Significant wave height, and two dimensional spectrum for 00:00 21/12/07
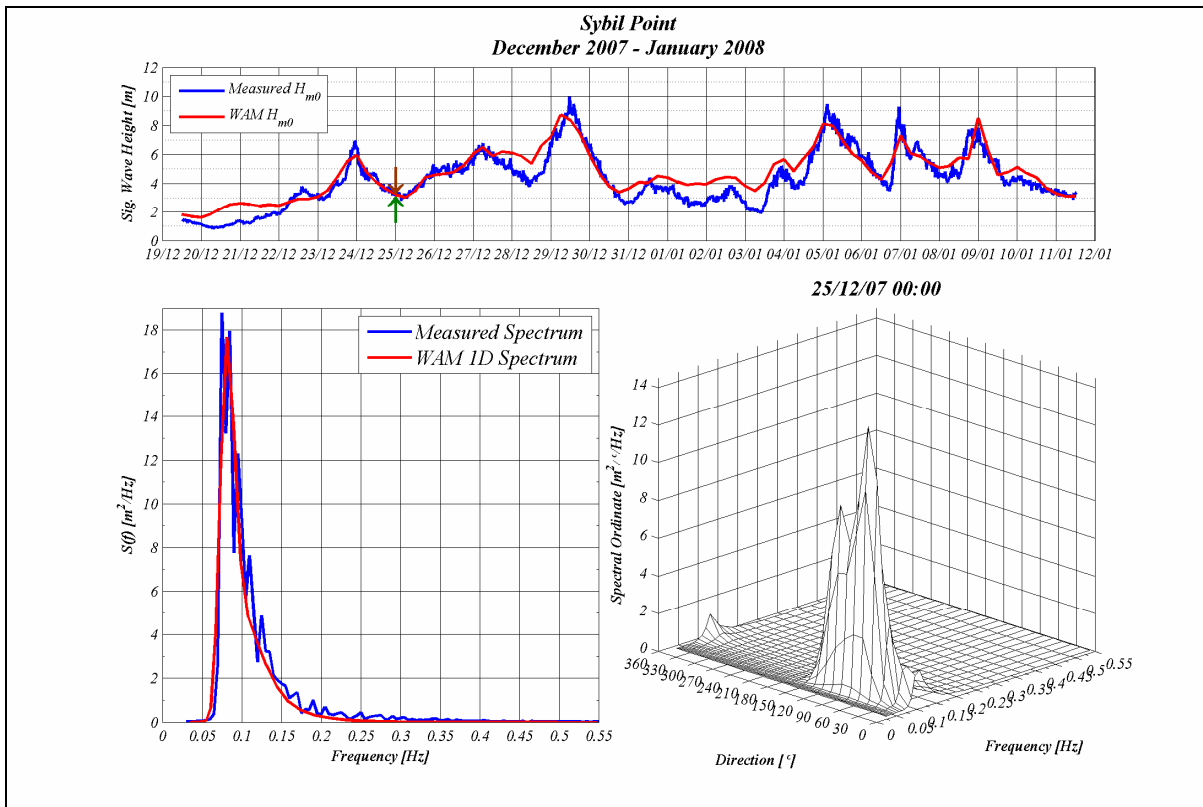
Figure 59. Significant wave height, and two dimensional spectrum for 00:00 25/12/07
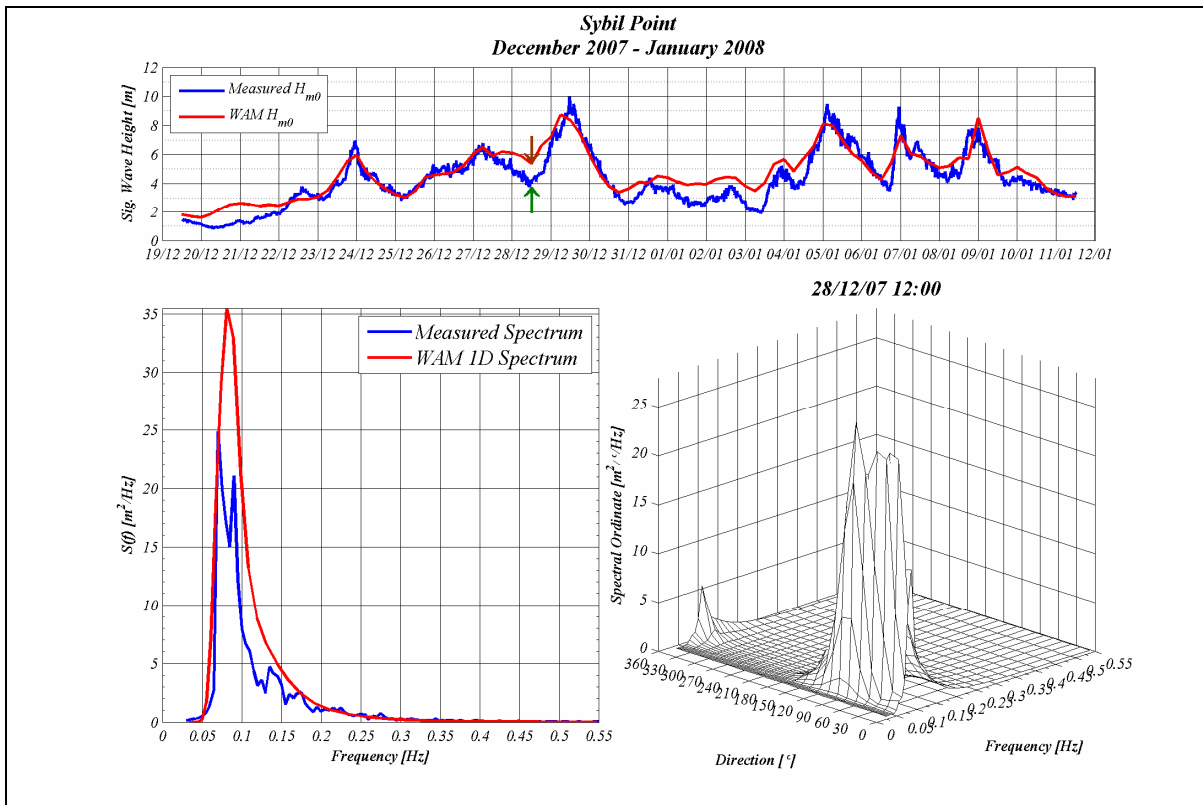

Figure 60. Significant wave height, and two dimensional spectrum for 12:00 28/12/07
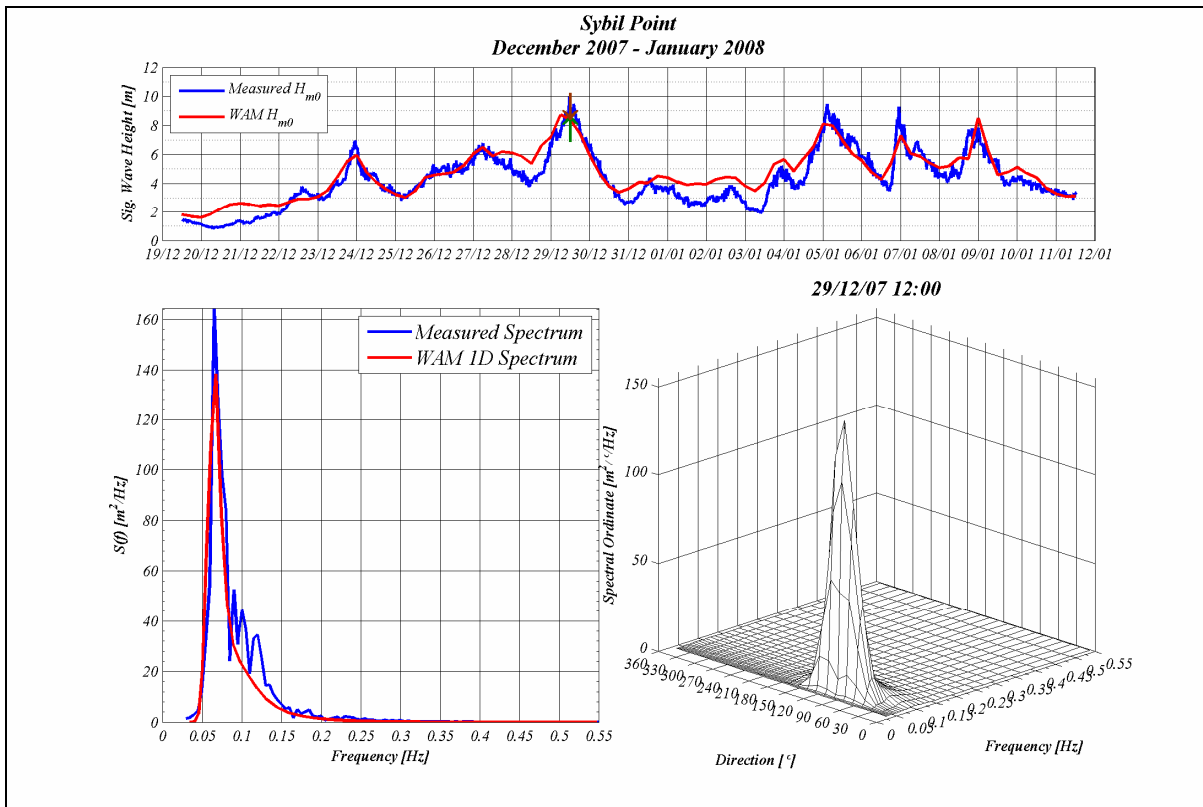
Figure 61. Significant wave height, and two dimensional spectrum for 12:00 29/12/07
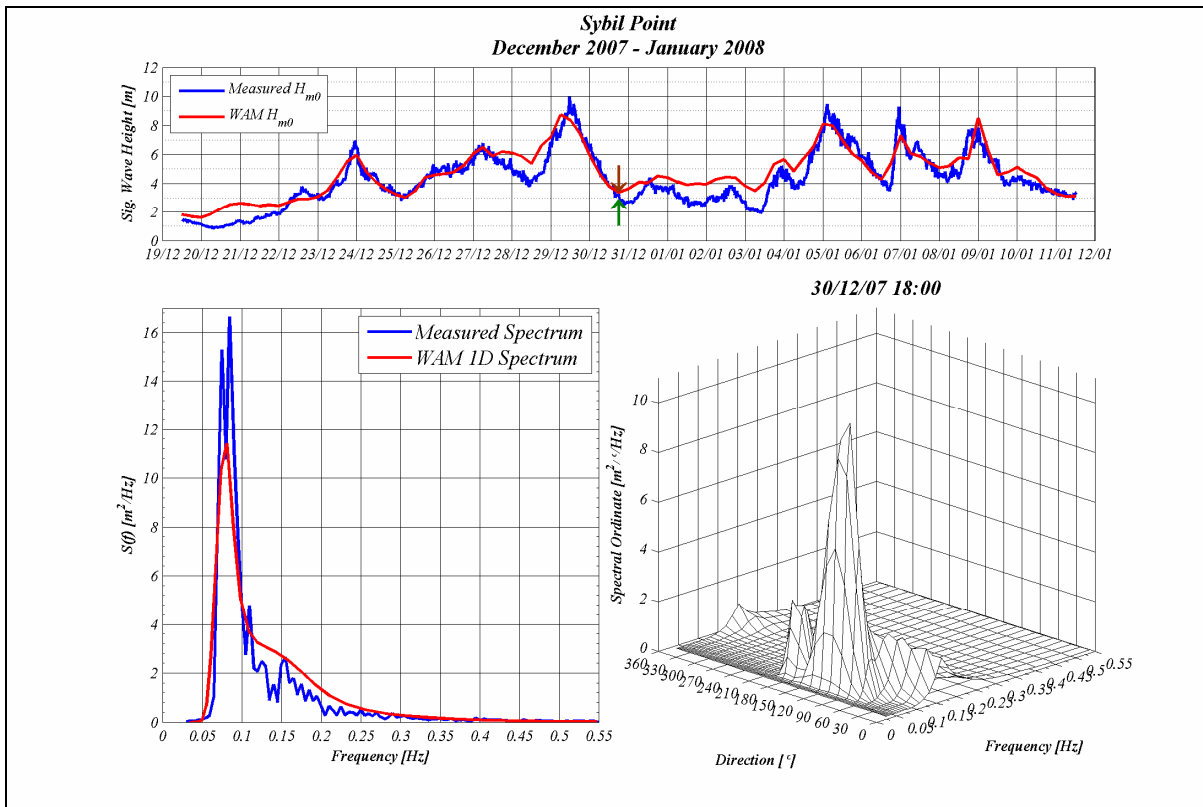

Figure 62. Significant wave height, and two dimensional spectrum for 18:00 30/12/07
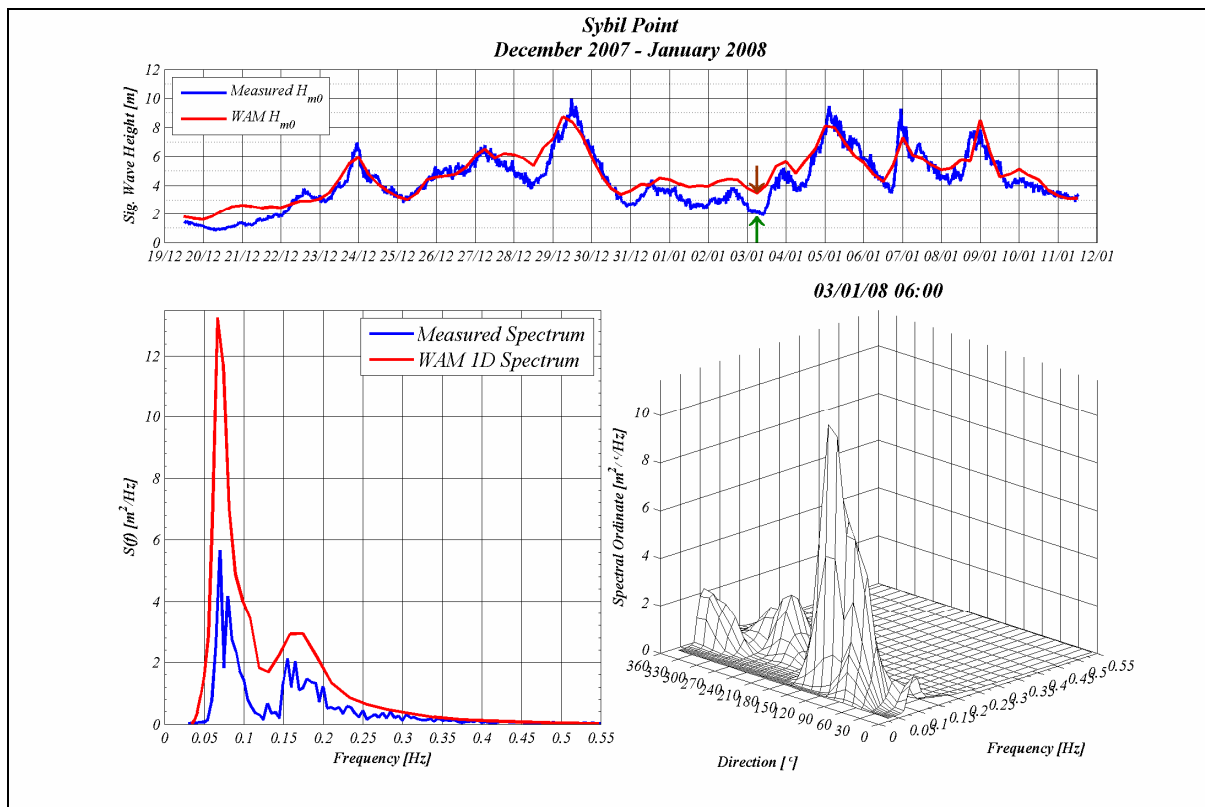
Figure 63. Significant wave height, and two dimensional spectrum for 06:00 03/01/08

REFERENCES

Allender et al, "The Wadic project: a comprehensive field evaluation of directional wave instrumentation", Ocean Engng, Vol. 16, No 5/6, pp. 505-536, 1989.

Altunkaynak, A, "Significant wave height prediction by using a spatial model", Ocean Engineering 32 (2005) 924–936.

Axys Technologies Inc, 2010. TRIAXYS Directional Wave Buoy. [Online] http://www.axystechnologies.com/BusinessUnit/AXYSMarineEnvironmentalMonitoring/WaveCurrentWaterLevelMonitoringSolutions/TRIAXYSDirectionalWaveBuoy/tabid/106/Default.aspx [accessed 20/4/10]

Baxevani A. et al "A New Method for modeling the space variability of significant wave height", Extremes (2005) 8: 267-294.

Baxevani A. et al "Spatio-temporal statistical modeling of significant wave heights", Environmetrics(2009) 20: 14-31.

Bendat and Piersol "Analysis of Random data", Wiley International.

Benoit, M., Frigaard, P., Schaffer, H.A., 1997, "Analysing multidirectional wave spectra: a tentative classification of available methods", IAHR Seminar Multidirectional waves and their interaction with structures, 27th IAHR Congress, San Francisco, 10-15 Aug 1997, pp. 131-158.

Blackman, R. B., Tukey, J. M., 1959. The measurement of power spectra. Dover Publications Inc., New-York, U.S.A., pp. 19-20.

Codar Ocean Sensors, 2010. Seasonde General Specifications. [Online] http://www.codar.com/SeaSonde_gen_specs.shtml [accessed 20/4/10]

Cornett, A.M., 2008. A global wave energy resource assessment. Proc. 18th International Offshore and Polar Ocean Engineering Conference, Vancouver.

Dalrymple, R.A. 1974. A Finite Amplitude Wave on Linear Shear Current, Journal of Geophysical Research, 79, 30, 4498-4504.

Datawell B.V., 2010. Directional Waverider Mk III. [Online] http://www.datawell.nl/inhoud.php?id=3 [accessed 20/4/10]

Dean, R.G. 1965. Stream function representation of nonlinear ocean waves, Journal of Geophysical Research, 70(18), 4561-4572.

Defne, Z., Haas, K.A. & Fritz, H.M., 2009. Wave power potential along the Atlantic coast of the southeastern USA. Renewable Energy. 34 p.2197-2205.

Dodet, G., Bertin, X. & Taborda, R., 2010. Wave climate variability in the North-East Atlantic Ocean over the last six decades. Ocean Modelling. 31, p.120-131.

Fugro Oceanor, 2010. Seawatch Mini II Buoy. [Online] http://www.oceanor.no/products/seawatch%20buoys%20sensors.htm [accessed 20/4/10]

Guinot, F. 2008. Wave-current interaction with Boussinesq approaches, 8th International Conference on Hydrodynamics, Nantes.

Hanson, J. L., Phillips, O. M., 2001. Automated analysis of ocean surface directional wave spectra. Jour. of Atmospheric and Oceanic Technology, vol. 18, pp. 277- 293.

Hasselmann, D.E., Dunckel, M., Ewing, J.A. 1980, "Directional wave spectra observed during JONSWAP 1973", J. Physical Oceanography, 10S, 1264-1280.

Helzel Messtechnik, 2010. WERA specification table. [Online] http://www.helzel.com/de/9307-Features [accessed 20/4/10]

Huang MC "Wave parameters and functions in wavelet analysis", Ocean Engineering 31 (2004) 111–125

Huang, N, Attoh-Okine, N (Eds.), 'The Hilbert-Huang Transform in Engineering' , Taylor and Francis, 2005.

Huang N and Shen S (eds.) 'Hilbert-Huang Transform and Its Application' Interdisciplinary Mathematical Sciences – Vol. 5. , World Scientific, 2008.

Janssen, et al "Error Estimation of Buoy, Satellite, and Model Wave Height Data" – American Meteorological Society

Jonsson, I.G. 1990. Wave-current interactions, in The Sea, B. Le Méhauté and D. Hanes, eds., John Wiley & Sons, New York, 65-120.

Kerbiriou, M.-A., Maisondieu, C., Prevosto, M., Babarit, A., Clement, A. H., 2007. Influence of an improved sea-state description on a wave energy converter production. Proc. Int. Conf. on O.M.A.E.'07, San Diego, USA.

Krogstad H. et al "Method for intercomparison of Wave measurements" Coastal Engineering 37 (1999), 235-257.

Krogstad, H.E. & Barstow, S.F., 1999. Satellite wave measurements for coastal engineering applications. Coastal Engineering, 37, p. 283-307.

Longuet-Higgins, M., Cartwright, D., Smith, N. 1963, 'Observations of the directional spectrum of the sea waves using the motions of a floating buoy", Ocean Wave Spectra, Prentice –Hall.

Lygre, A., Krogstad, H. E., 1986. Maximum entropy estimation of the directional distribution in ocean wave spectra. Jour. of Phys. Ocean., vol. 16, pp. 2052- 2060.

Madsen, P.A., Furhman, D.R. and Wang, B. 2006. A Boussinesq-type method for fully nonlinear waves interacting with a rapidly varying bathymetry, Coastal Engineering, Volume 53, 487-504.

Madsen, P.A. and Schäffer, H.A. 1999. A review of Boussinesq-type equations for surface gravity waves, Advances in Coastal and Ocean Engineering, Vol.5.

Massel SR "Wavelet analysis for processing surface wave records" Ocean Engineering 28 (2001) 957–987

Mitsuyasu, H. et al., 1975, "Observations of the directional spectrum of ocean waves using a clover leaf buoy, J. Physical Oceanography, Vol. 5, 750-760.

Oceanwavedata.com, 2010. [Online].Available at: http://www.oceanwavedata.com/OWD/Products_files/HsPersist_i115j80.csv [accessed 6/4/10]

Neptune Radar, 2010. Pisces at a glance. [Online] http://www.neptuneradar.net/Pisces_aag.html [accessed 20/4/10]

Nortek AS, 2010. AWAC with Acoustic Surface Tracking (AST) [Online] http://www.nortek-as.com/lib/brochures/AWAC.pdf/view [accessed 20/4/10]

Nwogu, O.G. 2009. Interaction of finite-amplitude waves with vertically sheared current fields, Journal of Fluid Mechanics, 627:179-213.

Ortega J and Smith, GHS, 'Hilbert_Huang transform analysis of storm waves', Applied Ocean Research 31 (2009) 212_219.

Priestly, MB 'Non-linear and Non-stationary Time Series Analysis '. Academic Press, 1988

Ryu, S., Kim, M.H. and Lynett, P.J. 2003. Fully nonlinear wave-current interactions and kinematics by a BEM-based numerical wave tank, Computational Mechanics 32, 336–346.

Schlurmann T. 'Spectral analysis of nonlinear water waves based on the Hilbert_Huang Transformation' J Offshore Mech Arctic Eng, Amer Soc Mech Eng (ASME) 2002;124(1):22_7.

Sherman et al 'B-Spline Based Empirical Mode Decomposition' – in Huang and Shen (2008).

Skourup, J., Cheung, K, Bingham, H.and Büchmann, B. 2000. Loads on a 3D body due to second-order waves and a current, Ocean Engineering, 27, 707-727.

Sova M.G.. and Wyatt L.R. "Spatial and Temporal Variability on Ocean Wave Measurement" Internal report, School of Mathematics, University of Sheffield.

Swan, C and James, R.L. 2001. A simple analytical model for surface waves on depth-varying current, Applied Ocean Research, 22, 331-347.

Teledyne RDI, 2010. Workhorse Waves Array. [Online] http://www.rdinstruments.com/waves.aspx [accessed 20/4/10]

Tucker, M.J. & Pitt, E.G., 2001. Waves in Ocean Engineering. Oxford: Elsevier Science Ltd.

Tucker, M. J., 1993. Recommended standard for wave data sampling and near real-time processing. Ocean Engineering 20, 459-474.

Tucker, M.J. and Pitt, E.G. Waves in ocean Engineering, Elsevier Ocean Engineering Book series, Volume 5, 2001, ISBN: 0 08 043566 1.

Tong, H 'Non-linear Time Series Anaysis', Oxford University Press, 1990.

Veltcheva AD, Guedes Soares C. Identification of the components of wave spectra by the Hilbert Huang transform method. Appl Ocean Res. 2004;26: 1_12.

Windrows, B et al ' Adaptive Signal Processing', Prentice Hall, 1985.

Wu, Z and Huang, N 'Statistical Significance Test of Intrinsic Mode Decomposition' - in 'Hilbert-Huang Transform and Its Application' –see above.